Development of optical fiber sensors for selected chemical and physical sensing applications

Thesis to be submitted to

COCHIN UNIVERSITY OF SCIENCE AND TECHNOLOGY

In partial fulfilment of the requirements for the

award of the degree of

DOCTOR OF PHILOSOPHY

Benjamin Varghese P

DEPARTMENT OF INSTRUMENTATION

Cochin University of Science and Technology

Cochin- 682022 Kerala

February 2013

Development of optical fiber sensors for selected chemical and physical sensing applications

Author

Benjamin Varghese P
Department of Instrumentation
Cochin University of Science and Technology
Cochin- 682022 Kerala

Supervising Guide

Dr K.N. Madhusoodanan
Associate Professor
Department of Instrumentation
Cochin University of Science and Technology
Cochin- 682022 Kerala

February 2013

Cover page: Reflection of a FBG

Dedicated to my Parents……

Dr K.N. Madhusoodanan
Associate Professor
Department of Instrumentation
Cochin University of Science and Technology
Cochin- 682022 Kerala
Phone +91 4842575008, Mob: 09349406334
Email : madhu@cusat.ac.in

Certificate

Certified that the Thesis entitled ***"Development of optical fiber sensors for selected chemical and physical sensing applications"*** *submitted by* ***Mr Benjamin Varghese P.*** *is an authentic record of research work carried out by him under my supervision at Department of Instrumentation in partial fulfilment of the requirements for the award of degree of Doctor of Philosophy of Cochin University of Science and Technology and the work embodied in this thesis has not been included in any other thesis submitted previously for the award of any other degree*

Cochin -22
Date : 15-02-2013

Dr K.N. Madhusoodanan
Supervising guide

Declaration

I hereby declare that the thesis entitled ***"Development of optical fiber sensors for selected chemical and physical sensing applications"*** *submitted for the award of degree of Doctor of Philosophy of Cochin University of Science and Technology is based on the original work done by me under the guidance of Dr K.N. Madhusoodanan, Associate Professor, Department of Instrumentation, Cochin University of Science and Technology, Cochin- 682022, Kerala and this work has not been included in any other thesis submitted previously for the award of any other degree*

Cochin 22 ***Benjamin Varghese P.***

Date: 15/02/2013

Acknowledgement

My homage to diseased Colleague Satish John, with whom I started my research work.

I thank my research guide, Dr.K.N. Madhusoodanan for always being so helpful and motivating. His constant guidance, cooperation and support has always kept me going. I owe a lot of gratitude to him for always being there for me and I feel privileged to be associated with a person like him. I shall continue the relation till end of my academic life. He has been supportive and permitted me to pursue various projects.

I express my heart-felt gratitude to Dr P. Radhakrishnan of ISP(CUSAT) for his constant motivation and support during the course of my thesis. He extended all the Lab facilities of ISP during the course of this work.

I extend my sincere word of thanks to Dr Jibukumar, of Electronics Department (Div. of SOE, CUSAT) who has always been there, more as a friend than a scientist. I thank fully acknowledge the Lab facilities offered to me.

I also gratefully acknowledge Dr. Sundarrajan Asokan of Instrumentation Department, Indian Institute of Science for his constant advices, friendship and support.

I extend my sincere thanks to the Department Head, Dr. Stephen Rodriguez for allowing me to use the department facilities. I am thankful to Dr. Jacob Philip, Dr. Jhoney Issac,Dr. K. Rajeev Kumar and all the teachers of the Department of Instrumentation for their help during the research work.

My heartfelt thanks to my fellow lab mates, Ms. Nisha R, Denesh R, Aji Balan Pillai,Ms Mittu Raju, Subin, Anu for always being there and bearing with me through my FIP tenure.

I am grateful to the staff of Instrumentation Department, for their help and cooperation. With utmost love I express my thanks to Mr A V Murali, Joshy, Mr Casmir, Mr Babu Varghese, Mr. Prakash, Mr Fazil, Mr Shaji, Mrs Alikutty Mr Mathew, Mr Antony, for their timely help.

I would like to acknowledge Dr. Kailas Nath, Dr VPN Nampoothiri, and other teachers of ISP and research Scholars Mr Linesh, Mr Libish,Mr Boby Varghese P. Vinod of ISP CUSAT for all their support and motivation during the days of my work.

I acknowledge the University grants Commission (UGC), Government of India for providing fellowship under Faculty Improvement Programe to pursue my research at CUSAT.

I extend my sincere thanks to the Principal, Dr. Sunny Kuriakose, and my colleagues of BPC college for their help during the research work.

Finally, I thank the authorities of NEST &INTPC for extending their lab facilities.

Contents

Preface

The modern age of fiber optic sensors is enabled by the development of extremely low-loss optical fibers in late 1970s. In recent years Fiber optic sensors have developed from the research laboratory to practical applications. Fiber Optic Sensors are immune to radio frequency and Electromagnetic interference hence it can be deployed in electrically and magnetically noisy atmosphere. It can be used in harsh environment and in locations difficult to access. Fiber is made of glass or plastic and offers environmental ruggedness and it can be employed in chemical process industries. Fiber Optic Sensors are small in size, light weighted and flexible. Low loss in optical fibers enables remote in situ monitoring. The measurement of physical or chemical parameter as a function of position along the length of an optical fiber provides a unique capacity to measure different variations. Such distributed sensors are finding applications in industrial and environmental monitoring. Fiber Optic Sensors are highly sensitive and has large band width. The proposed thesis titled **"Development of optical fiber sensors for selected chemical and physical sensing applications"** consists of seven chapters followed by a concluding section. The first Chapter of the thesis provides a general introduction to Fiber Optic Sensors.

The evanescent wave fiber optic sensors reported has a single source, hence the selectivity and sensitivity and repeatability is very poor. In order to improve the performance of the sensor two wavelengths are used; one corresponding to the absorption peak of

the analyte (analytical wavelength), and the second a non -absorbing one. Introduction of analytical wavelength helps to provide selectivity and the use of non absorbing wavelength supports repeatability aspect. The dual wavelength probing scheme, the related theory, verification using $KMnO_4$ and the measurement of traces of silica in water is discussed in chapter 2.

A sensitive and useful design of dual wavelength probing scheme for evanescent wave based fiber optic sensor has been developed and it is extended for the measurement the concentration of Iron, Phosphate and Ammonia in water. Preparation of Reagents, standard solutions, measurement results are described in Chapter 3.

Fiber Bragg Grating (FBG) is an important sensing element for the measurement of several important physical parameters such as strain, temperature. Apart from other fiber sensors the FBG sensors have many advantages like high resolution, insensitivity to fluctuations, multiplexing, distributed sensing etc. So in the present study we have simulated and measured the strain on a cantilever structure made of spring steel using a FBG sensor. The FBG is mounted to the structure using a commercially available fast setting epoxy. The drift of strain due to temperature is also measured and a correction factor due to the temperature drift is suggested. A temperature controlled water bath was used for the measurement of temperature. The measurement of strain, Temperature, cross sensitivity is discussed in Chapter 4.

The main bottle neck in the use of FBG sensors for different applications is the costly demodulation techniques. In this study we

suggest two simple methods for wavelength to intensity conversion. The first method is by selecting a narrow band source, and a FBG with Bragg reflection at trailing edge of the source spectrum. So, as the Bragg reflected wavelength shifts due to strain or temperature the reflected power vary depending on the selection of Bragg wavelength. In the second method two matched FBGs are used. The Bragg reflected signal from the reference FBG is fed in to the FBG in which the measurements are carried out. During the measurement the reflected power varies as the Bragg reflected wavelength shifts. This can be monitored using a power meter. The Simulation of Interrogation technique and the measurements of strain and temperature are discussed in Chapter 5.

Chapter 6 is a study distributed sensing of weight-displacement measurement using optical time domain reflectometry. OTDR has the advantage that the measuring parameter can be monitored continuously along the fiber. A quasi distributed sensing of weight/ displacement realised, in which the parameter is measured at specific locations. Specially made triangular corrugations on Aluminium block are used to create macro bends in a single mode fiber, which measures weight/ displacement. Distributed study, measurement of displacement and weight, study of variation in number of corrugation, size of corrugation etc are discussed in this chapter.

Chapter 7 is a demonstration of simultaneous measurement of strain, weight and temperature using wavelength division multiplexed, quasi-distributed FBG sensors.

The summary of research work and the relevant results obtained from the present study are outlined in the concluding section. The scope of future work is also presented.

Part of the thesis has been published in the following journals:

[1] P.Benjamin Varghese, Satish John and K.N. Madhusoodanan, Fibre optic sensor for the measurement of concentration of silica in water with dual wavelength probing, Rev. Sci. Instrum., **81**,035111, 2010.

[2] P.Benjamin Varghese, P.Vinod, Jibukumar, K. N.Madhusoodanan and P. Radhakrishnan, A quasi distributed fiber optic weight-displacement sensor using macro bends, Opt. Fiber Technol., **18**, (4), 215, 2012.

[3] P. Benjamin Varghese, P. Vinod , K. N. Madhusoodanan and P.Radhakrishnan, Development of a strain sensor using Fiber Bragg Grating and its effect on temperature variation, Jl. of the Instrum. Soc. of India, **41**, (4), 197, 2011.

[4] P.Benjamin Varghese, K.N.Madhusoodanan, P.Vinod and P. Radhakrishnan, A Novel Fiber Bragg Grating Sensor for Measuring Weight, IEEE Xplore Digital Library, 6139568, DOI : 10.1109/INDICON, 2011.

[5] P.Benjamin Varghese, R.Dinesh, MittuRaju, Jose J.Edathala and K. N.Madhusoodanan, Fiber Bragg grating interrogator for temperature measurement, Jl. of the Instrum. Soc.of India, **42**, 4, 2012.

[6] Benjamin P. Varghese, Aji Balan Pillai and Madhusoodanan Kottarathil Naduvil, Fiber optic sensor for the detection of Ammonia, Phosphate, Iron in water, J. Opt., DOI 10.1007/s12596-013-0121-5, 2013.

[7] P. Benjamin Varghese, R. Dinesh, MittuRaju, Jose J.Edathala, K. N.Madhusoodanan, A Simple Interrogator for FBG Sensors, International Journal of Advanced Electrical and Electronics Engineering,**1**, (3), 17, 2012

[8] Benjamin Varghese P, Dinesh Kumar R, Mittu Raju, K N Madhusoodanan, P Radhakrishnan. Wavelength division multiplexed FBG sensors for the simultaneous measurement of strain, weight and temperature, J.of Instrum. Technol. and Innovations **3**, 3, 2013.

[9] Benjamin Varghese P, Denesh R, Mittu Raju, K N Madhusoodanan Implementation of Interrogation systems for Fiber Bragg Grating sensors, Photonic Sensors 3, 3, 283, 2013.

Chapter 1

INTRODUCTION

Contents

1.1 A brief overview of Fiber Optic Sensors

In the 1970's during the early stages of development of fiber optic technology, the changes in the transmission characteristics due to external perturbations such as bends, pressure, temperature etc were investigated extensively. The exceptional sensitivity of optical fibers to external perturbations led to the development of large variety of sensors. The sensors were developed based on the modulation of amplitude, phase, frequency, polarization, wavelength etc of light. These sensors are finding extensive applications in varies fields such as process industry, research laboratories, structural engineering, Biomedical engineering etc. The inherent advantages of Fiber Optic Sensors (FOS) over the conventional electronic sensors attracted great deal of interest and activities in this field.

1.2 Advantages of Fiber Optic Sensors

FOS are immune to Electromagnetic interference and it can be deployed in electrically and magnetically noisy atmosphere. These

sensors are safe to use in Oil refineries and other explosive atmosphere, offer environmental ruggedness and can be employed in chemical process industries. FOS are small in size, light weighted and flexible. Low loss in optical fibers enables remote in situ monitoring. The measurement of physical or chemical parameter as a function of position along the length of an optical fiber provides a unique capacity to measure spatial variations. Such distributed sensors are finding applications in industrial and environmental monitoring. FOS are highly sensitive and has large bandwidth [1-2].

1.3 Light propagation in an optical fiber

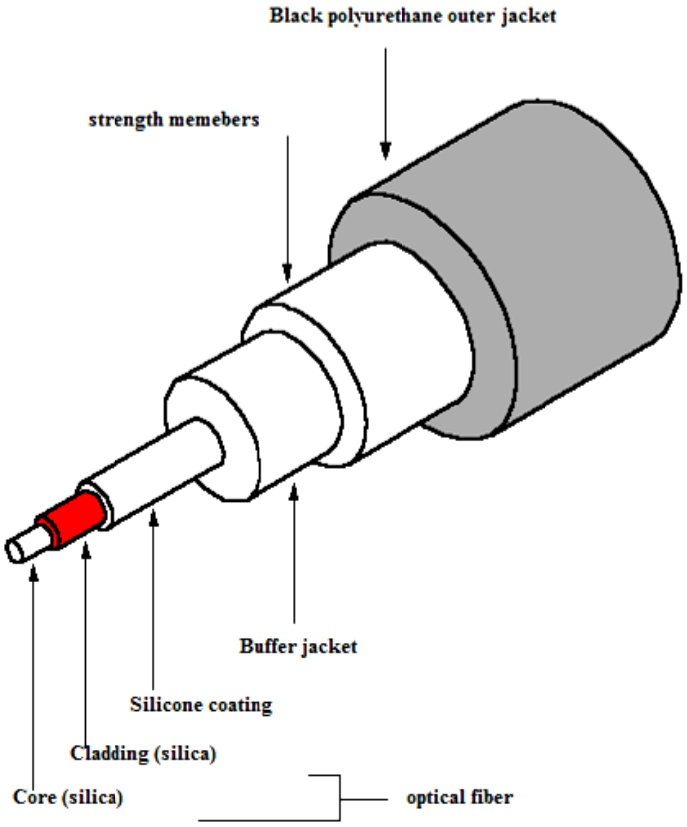

Figure 1.1 Schematic cross section of Optical Fiber, showing various layers

An optical fiber along with different protective coatings is depicted in figure 1.1. It is a cylindrical dielectric wave guide having central 'core' of uniform refractive index with a diameter of 4-1000μm. It is surrounded by cladding of slightly lower refractive index. The cladding is also covered with additional plastic coating for the mechanical support and environmental protection. The light ray, launched at one end of the fiber propagates down to the other end. The two kinds of rays propagated through the fiber are, skew rays and meridional rays. The rays passing through the axis of the fiber are meridional rays and the other rays are skew rays. When light travels from high refractive index medium to low refractive index medium, the total internal reflection takes place if the angle of incidence is greater than critical angle. Due to the cylindrical symmetry of the structure the ray would suffer repeated total internal reflections at the lower and upper interfaces and thus gets guided. If 'θ_i' is the maximum angle of the ray with the fiber axis that is guided by the fiber, the angle '$2\theta_i$' is the acceptance angle of the fiber then '$\sin\theta_i$' is called the numerical aperture of the fiber. The acceptance angle of an optical fiber is illustrated in the figure 1.2.

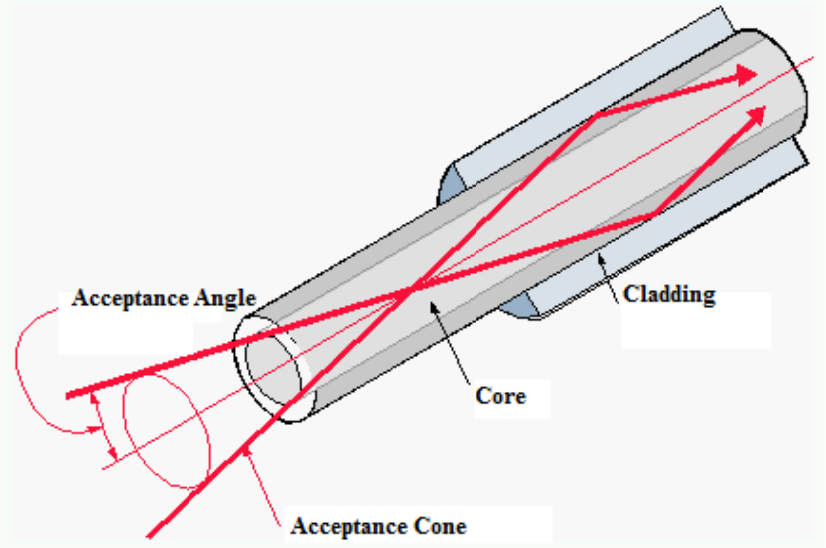

Figure1.2 Acceptance angle of an Optical fiber

1.4 Modes in optical fiber

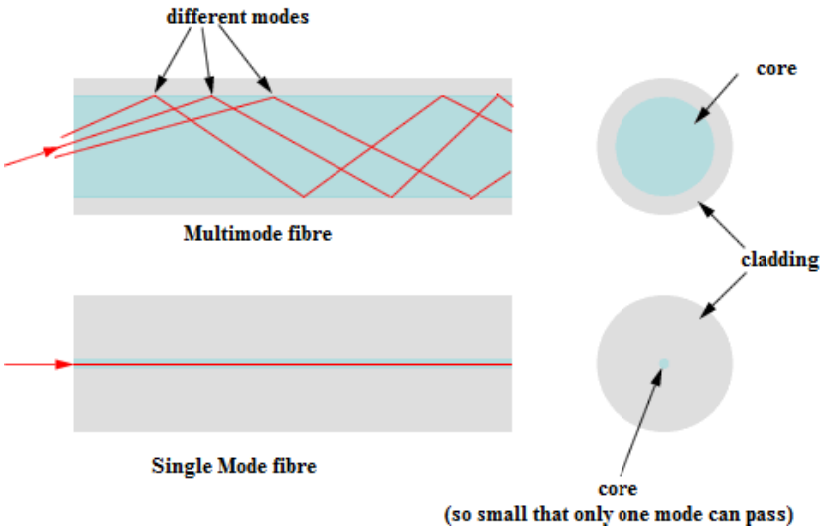

Figure 1.3 Schematic representation of ray transmission in step index Multimode and single mode fibers

A mode is the specific electromagnetic field distribution that propagates through the fiber without any change in its amplitude

distribution. The exact nature of distribution is determined by boundary condition imposed by the fiber. The 'V' number of the fiber decides the number of modes that can propagate through the fiber

$$V = \frac{2\pi a}{\lambda}(n_1 - n_2)^{\frac{1}{2}} \qquad (1.1)$$

where 'a' is the core radius of the fiber, n_1 and n_2 are the refractive index of core and cladding. For a step index fiber, if V-number is less than 2.405, the fiber will support only one mode and it is called single mode fiber. If the V-number is greater than 2.405, then the fiber supports more than one mode and it is called a multimode fiber [3]. Figure 1.3 illustrates the schematic of single and multimode step index fibers with the ray transmission.

1.5 Fiber optic cable termination

The connector is a mechanical device mounted at the end of a fiber optic cable, light source, receiver etc. The connector must direct light, collect light and must be easily attached and detached from the equipment. We have used FC/APC, FC/PC [figure 1.4], SC/APC, SC/PC [figure 1.5] connectors in our experiments. FC connectors feature a position locatable notch and a threaded receptacle. FC connectors are constructed with a metal housing and they are nickel plated. They are rated for 500 mating with a mating loss of 0.25dB. SC connectors provide accurate alignment via their ceramic ferrules and connector is a push –on pull off connector with a locking tab. SC connectors are rated for 100 mating cycles and have an insertion loss of 0.25dB. The SC/FC adapters are shown in figure 1.6.

Figure 1.4 FC connectors (a) FC/APC (b) FC/PC

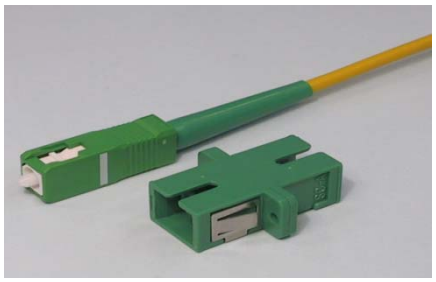

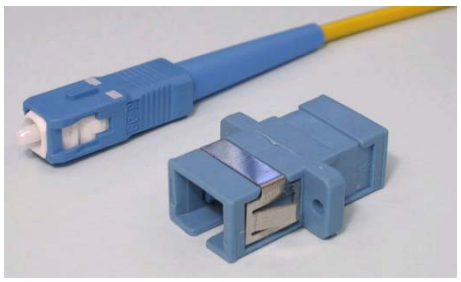

Figure 1.5 SC connectors (a) SC/APC (b) SC/PC

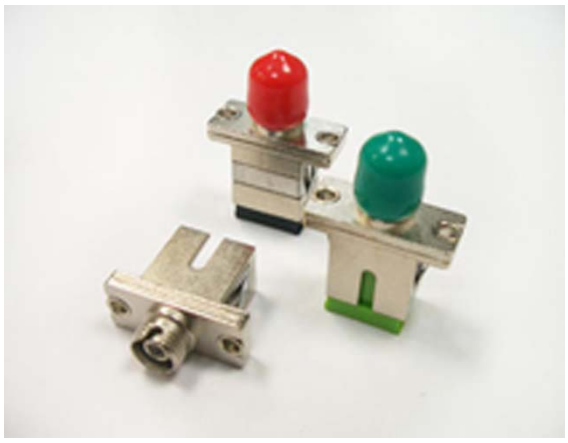

Figure 1.6 SC/FC Adapters

1.5.1 Fiber splicing

Connecting two fibers requires precise alignment of mated fiber cores. There are two types of splicing, fusion and mechanical. Fusion splice uses an electric arc in order to fuse two fiber optic

cables together. The fusion splicing uses localised heat to melt or fuse the ends of two optical fibers together. The splicing process begins by preparing each fiber end for fusion. Fusion splicing requires all protective coatings to be removed from the ends of the fiber, then it is cleaved using score and break method. The quality of each fiber end is inspected using a built in microscope. In fusion splicing, splice loss is a direct function of the angles and quality of the two fiber end faces. Fusion-splicing apparatus consists of two fixtures on which fibers are mounted with two electrodes. An inspection microscope assists in the placement of prepared fiber into the fusion splicing apparatus. The fibers are placed into the apparatus, aligned, and then fused together. The splices offer sophisticated, computer controlled alignment of fiber optic cables to achieve losses as low as 0.02 dB. Figure 1.7 shows splicing of an optical fiber using splicing machine.

Figure 1.7 Splicing machine

1.5.2 Fiber coupler

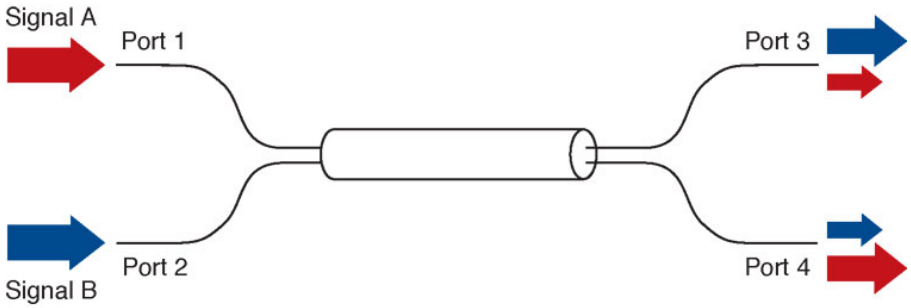

Figure 1.8 Schematic of fiber coupler

The schematic of Fiber couplers, or splitters is shown in figure 1.8, are special optical fiber devices with one or more input fibers for distributing optical signals into two or more output fibers. Optical energy is passively split into multiple output signals (fibers), each containing light with properties identical to the original except for reduced amplitude. Because the splitter is a passive device it is immune to electromagnetic interference, consumes no electrical power and does not add noise to system design. Fiber couplers have input and output configurations defined as M x N. M is the number of input ports (one or more). N is the number of output ports. When there are multiple inputs, output signals are always a combination of the input signals. Fiber optic couplers or splitters are available in a range of styles and sizes to split or combine light with minimal loss.

1.5.3 Optical Circulators

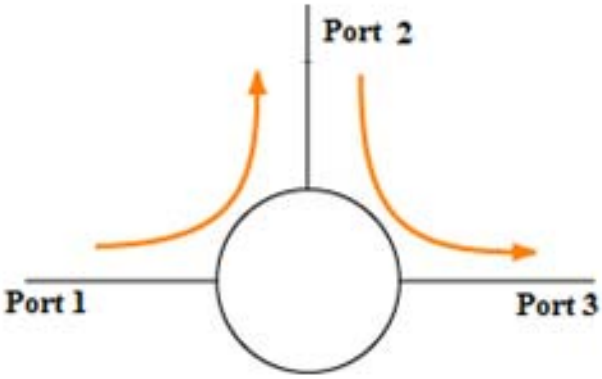

Figure 1.9 Schematic of optical circulator

An optical circulator is a multi-port (minimum three ports) nonreciprocal passive component. The function of an optical circulator is similar to that of a microwave circulator—to transmit a light wave from one port to the next sequential port with a maximum intensity, but at the same time to block any light transmission from one port to the previous port, as illustrated in figure 1.9.

Optical circulators can be divided into polarization-dependent optical circulator and polarization-independent optical circulator. Polarization-dependent optical circulator is functional only for light with a particular polarization state. The polarization-dependent circulators are only used in limited applications such as free-space communications between satellites, and optical sensing. Polarization-independent optical circulator functions independent of the polarization state of a light. It is known that the state of polarization of a light is not maintained and varies during the propagation in a standard optical fiber, due to the birefringence caused by the

imperfection of the fiber. Therefore, the majority of optical circulators used in fiber optic communication systems are designed for polarization-independent operation.

Optical circulators can be further divided into two, namely full circulator and quasi-circulator based on their functionality. In Full circulator light passes through all ports in a complete circle (i.e., light from the last port is transmitted back to the first port). In the case of a full three-port circulator, light passes through from port 1 to port 2, port 2 to port 3, and port 3 back to port 1. In Quasi-circulator light passes through all ports sequentially but light from the last port is lost and cannot be transmitted back to the first port. In a quasi-three-port circulator, light passes through from port 1 to port 2 and port 2 to port 3, but any light from port 3 is lost and cannot be propagated back to port 1. In most applications only a quasi-circulator is required. Photograph of an optical circulator is given in figure 1.10.

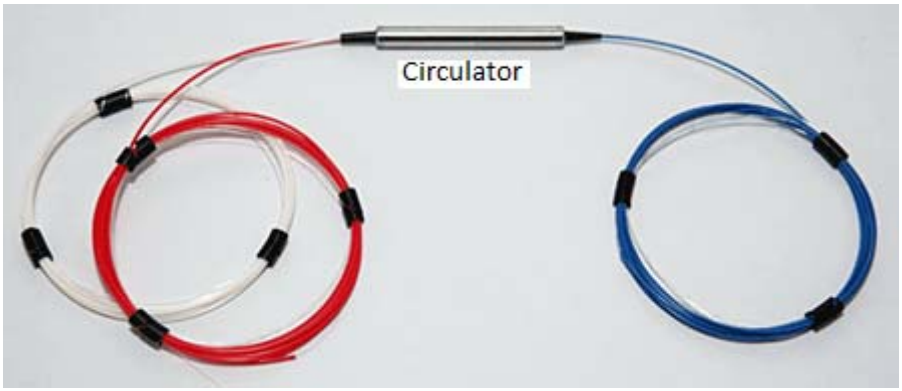

Figure 1.10. Optical fiber configuration with circulator

1.6 Attenuation in optical fiber

Absorption, scattering and bending are three major loss mechanisms in fused silica glass (SiO_2) fibers [4, 5]. The attenuation in the fiber can be either intrinsic or extrinsic. Intrinsic attenuation is caused by substances inherently present in the fiber, whereas extrinsic attenuation is caused by external forces such as bending or tension etc. Intrinsic absorption is very low in the wavelength-window used for communication. Above 1700nm, glass starts absorbing light energy because of vibrational transistions of Si-O bond.

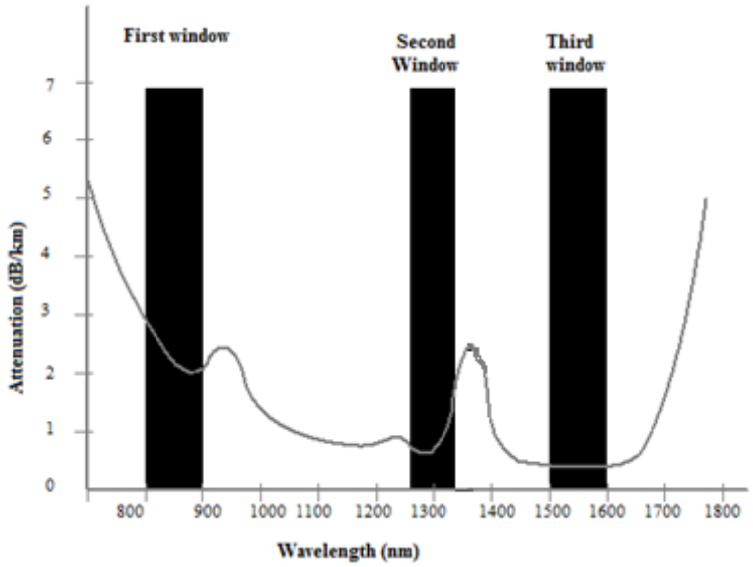

Figure 1.11 Transmission window of Silica

Intrinsic attenuation is due to impurities in the glass introduced during manufacturing process. When light passes through the fiber it could be either absorbed or scattered. So the intrinsic losses are further categorised as material absorption and Rayleigh scattering. Absorption

losses are associated with absorption due to metal ions and hydroxyl ions. The most common impurity is the hydroxyl ion. The studies reveal that there are three principle windows at 850, 1310 and 1550nm wavelength bands as shown in 1.11. The third transmission window at 1.55μm shows the minimum fiber attenuation of approximately 0.2dB/km

Rayleigh scattering losses in glass arise from light interacting with density fluctuation in the fiber. Variations in material density and compositional fluctuation occurring during fiber manufacturing create random inhomogenities that give rise to refractive index variation. The refractive index variation leads to Rayleigh scattering, if the size of the defect is less than one –tenth of the wavelength of the incident light. This mechanism does not cause elimination or conversion of optical energy but simply forces a part of the optical wave to escape from the wave guide. The scattering intensity is proportional to $1/\lambda^4$ so that longer wavelengths in the standard transmission windows exhibit lower attenuation losses than shorter wavelengths.

Brillouin and Raman scattering are other two types of scattering that can cause additional loss because of interaction between incident photons and phonons of the material. Phonons, the quantized energy of vibrations, behave like particles and therefore can interact with photons. Because of the Doppler effect, a frequency shift occurs during the collision. Brillouin scattering is induced by acoustic waves and shows a frequency shift in the order of 100 GHz which

depend upon the angle under which scattering is measured. This Doppler frequency shift is maximized in the backward direction. Different methods have been proposed for optical fiber sensors based on this effect. Brillouin frequency shift increases linearly with (longitudinal) strain and temperature. The effect of the brillouin scattering can be reduced by using short coherent length light sources.

Raman scattering on the other hand, is caused by molecular vibrations of 'optical' phonons which is generated by the interaction of a strong electric field of the optical wave and quartz molecules. The resulting non-uniform spectrum exhibits the so called Stokes –lines. These lines extend at low temperatures chiefly to longer wavelengths and approach a symmetrical shape with increasing temperature. The spectral width increases to more than 10 THz. A description on how to take advantage of the Raman effect for distributed temperature sensing can be found in Dakin and co-workers [6]. Both the Brillouin and Raman scattering phenomena are nonlinear effects that occur only at higher power levels.

The extrinsic losses are mainly due to the radiative losses occur whenever an optical fiber under goes a bend of finite radius of curvature. Micro bending is due to the tiny imperfections in the geometry of the fiber caused by manufacturing process or by mechanical stress, such as pressure, tension, and twist as depicted in figure 1.12 .To overcome this problem, fibers are protected by a buffer.

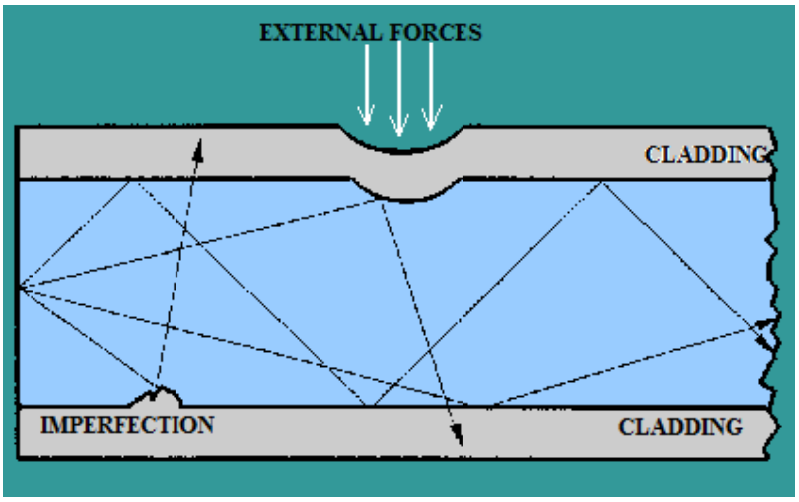

Figure1.12 Micro bends in optical fiber

Macro bend occurs when the fiber is formed to a curvature with diameters of the order of centimeters [6]. In the figure1.13 the period of corrugation of the order of centimeters as in the case of a micro bend deformer. When the angles of the ray with normal to the core cladding interface inside a fiber are greater than or equal to the critical angle, they are confined within the core. At a macro bend the angle of the ray with the normal to the core cladding interface decreases in the bent region. If the angle is less than the critical angle then the higher order modes radiate out of the fiber core, thus the power transmitted through the fiber will decrease.

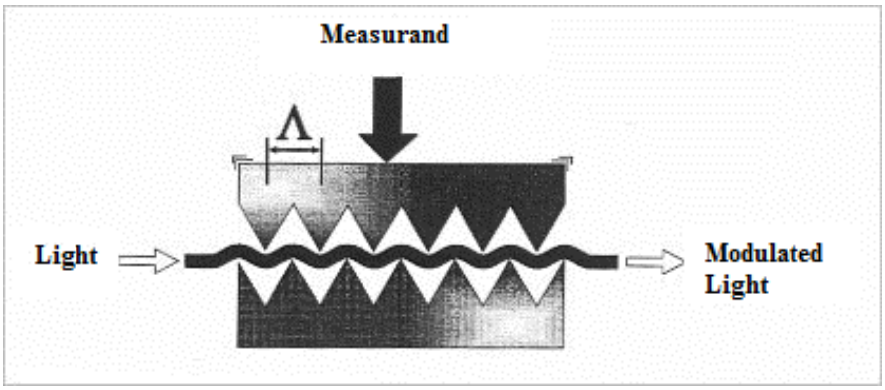

Figure 1.13 Macro bends in optical fiber

1.7 Dispersion

The dispersion reduces the information carrying capacity of an optical fiber through pulse broadening in a digital network. Three basic forms of dispersions are intermodal dispersion, chromatic dispersion and polarisation mode dispersion. Intermodal dispersion which limits the data rates in a multimode fiber, results from splitting of the signals in to multiple modes that travel at slightly different distances. Chromatic dispersion occurs in both single and multimode fibers, due to variation in propagation delay with wavelength. Polarisation mode dispersion is caused by the splitting of a polarised signal in to orthogonal polarisation modes with different speeds of propagation. Figure 1.14 is the pictorial representation of different types of dispersion in optical fibers.

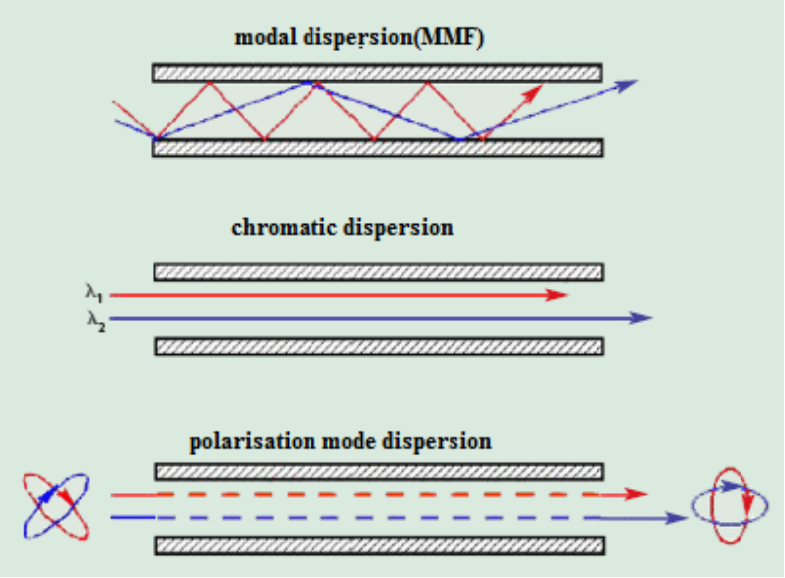

Figure 1.14 Different types of Dispersion in an Optical fiber

1.8 Fiber optic sensors

FOS can be classified into intrinsic and extrinsic sensors. In an intrinsic sensor the measurand modifies the light propagating in the fiber. In an extrinsic sensor, fiber is used to transmit light from the source to the optical sensing head attached to the other end of the fiber. FOS can be further classified in terms of modulation scheme used. They are intensity modulated, phase modulated, polarisation modulated, frequency modulated and wavelength modulated sensors.

1.8.1 Intensity modulated Sensors

Intensity modulated FOS are the simplest and widely used ones. The intensity modulation can be achieved by displacement of one fiber relative to the other. Shutter type, misalignment, lateral displacement, and collection of modulated light reflected from a target using a Y coupler, macro bending and evanescent wave coupling to another medium are intensity modulated sensors [7]. In intensity modulation by displacement, the light coupled to a fiber joint is varied through transverse, longitudinal, and angular displacements as shown in figure 1.15. The transmitting and receiving fibers are aligned along the same axis to receive maximum power. Any axial, angular, or transverse misalignments can cause the received power to vary and it can be calibrated to measure the displacement.

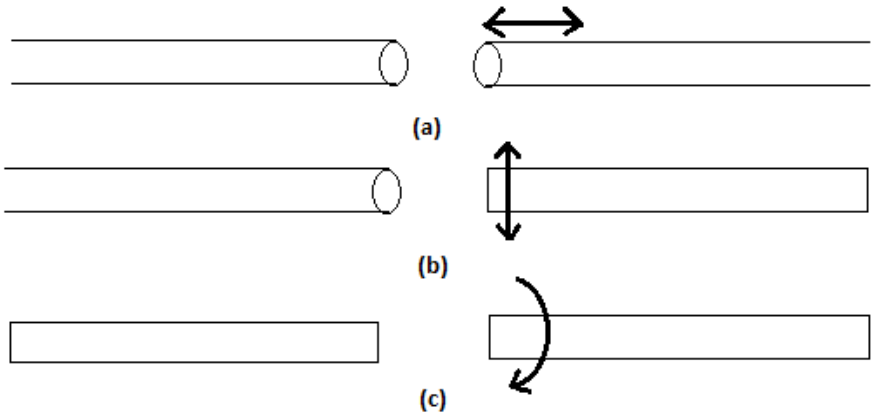

Figure 1.15 Intensity modulations by displacement (a) axial (b) lateral (c) angular

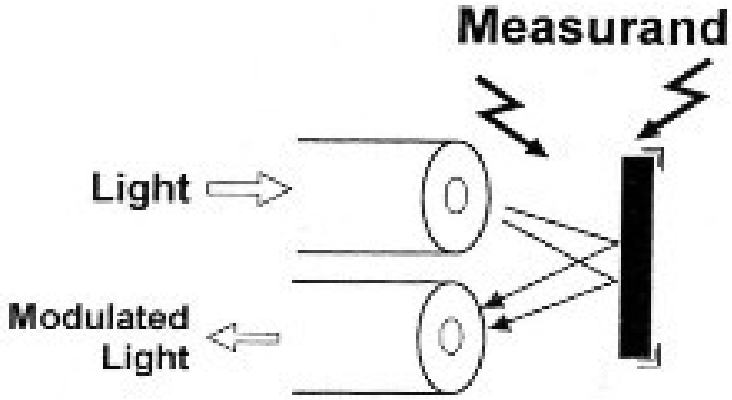

Figure1.16 Intensity modulation by reflection

The arrangement of an intensity modulation by Reflection method is depicted in figure 1.16. The light emitted from a fiber is reflected from a mirror and it is collected by another fiber. The displacement of the mirror can be precisely measured using such an arrangement. In shutter type arrangement, there are two fibers having the same axis one is transmitting and the other one is receiving fiber. A shutter is used in between the fibers and the measurand actuates the shutter, causing the optical power to decrease.

1.8.2 Evanescent wave Fiber Optic Sensors

Another important type of FOS based on intensity modulation method is evanescent wave fiber optic sensors. When the light travels from denser to rarer medium, if the angle of incidence is greater than the critical angle, the light is reflected back to the denser medium. The light is not reflected back from the interface, it travels slightly inside; transmitted and reflected light forms a standing wave where the wave front is perpendicular to the interface. The major part of the energy distribution is confined within the fiber core. The energy in the cladding decreases exponentially [8-12]. The figure 1.17 illustrates the evanescent in optical fiber, where the cladding is replaced with the sample.

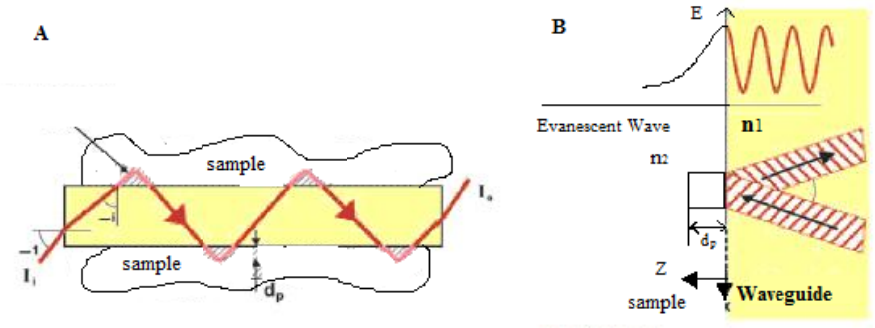

(A)Evanescent wave in a waveguide ,in contact with a sample.(B)Evanescent at the interface between two media,under total internal reflection

Figure1.17 Evanescent wave in a Waveguide

When the cladding is replaced by an absorbing fluid, a part of the signal is absorbed and the power transmitted will decreases. This absorption of evanescent field in an optical fiber is used to develop a variety of sensors [13]. There are two approaches in this method. If the wavelength of light propagating coincides with absorption band of

the fluid, then it is direct spectroscopic arrangement. If an intermediate reagent which responds optically by absorption is employed, then it is called reagent mediated sensors [14].

1.8.3 Interferometric sensors

Interferometric sensors or phase modulated sensors consist of a coherent light source such as a laser. The light from the source is split and then coupled into two single mode optical fibers. A phase shift occurs when the measurand perturb the optical properties of one of the fibers relative to the other. This change in phase is measured precisely. The advantage of Interferometric sensors over intensity modulated sensors is their higher sensitivity and larger dynamic range. However Interferometric sensors are expensive due to the sophisticated electronic processing equipment used for measurement.

Interference pattern is the intensity distribution obtained when two or more waves superimpose. To observe the interference pattern it is necessary that the interfering waves originate from a single source. Two coherent beams are obtained using division of wave front from a source. When these waves are superimposed interference phenomenon is obtained. Let E_1 and E_2 represent two monochromatic waves propagating in the same direction. The amplitudes can be written as

$$E_1 = a_1 \ \exp\left[i(\omega t - \Phi_1)\right] \tag{1.2}$$

and

$$E_2 = a_2 \ \exp\left[i(\omega t - \Phi_2)\right] \tag{1.3}$$

where ω is the angular frequency, a_1 and a_2 are the peak amplitudes and Φ_1 and Φ_2 are the phases. On superimposing these two waves at a point we get

$$E = E_1 + E_2 \tag{1.4}$$

Intensity at a point is given by I,

$$I = I_1 + I_2 + 2 * \sqrt{I_1 I_2} \cos \emptyset \tag{1.5}$$

where $\emptyset = \emptyset_1 - \emptyset_2$, is the phase difference between two waves at the point of observation. I_1 and I_2 are the intensities at the point due to two waves acting separately. Constructive interference will take place when $\cos \emptyset = 1 \ or \ \emptyset = 2k\pi$

where k=0, 1, 2, 3 and the intensity is given by

$$I_{max} = I_1 + I_2 + 2 * \sqrt{I_1 I_2} \tag{1.6}$$

On the other hand when $\cos \emptyset = -1 \ or \ \emptyset = (2k+1)\pi$, the destructive interference will take place and the intensity is given by

$$I_{min} = I_1 + I_2 - 2 * \sqrt{I_1 I_2} \tag{1.7}$$

If $I_1 = I_2 = I_0$ then,

$$I_{max} = 4I_0 \tag{1.8}$$

$$I_{min} = 0 \tag{1.9}$$

There are four kinds of interferometer configurations, namely Mach –Zehnder, Michelson, Fabry-Perot and Sagnac interferometers.

Mach-Zehnder interferometer

Mach-Zehnder and Michelson Interferometers have flexible geometry and highly sensitive to different measurands [15]. Mach-Zehnder (MZ) interferometer uses two fibers, one is sensing fiber and the other is reference fiber as in figure 1.18. Using a 3 dB coupler the laser light is split into two equal intensities and injected to the two fibers. The two light beams are recombined using a 3 dB fiber coupler. The combined beam is detected and phase shift is measured. The phase shift occurs due to change in total physical length, refractive index, or the transverse dimensions of the fiber. Change in total physical length of an optical fiber occurs due to the application of longitudinal strain or thermal expansion. Temperature or pressure and longitudinal strain cause variation in refractive index. Transverse dimensions of the fiber changes due to radial strain or longitudinal strain through Poisson's ratio or thermal expansion

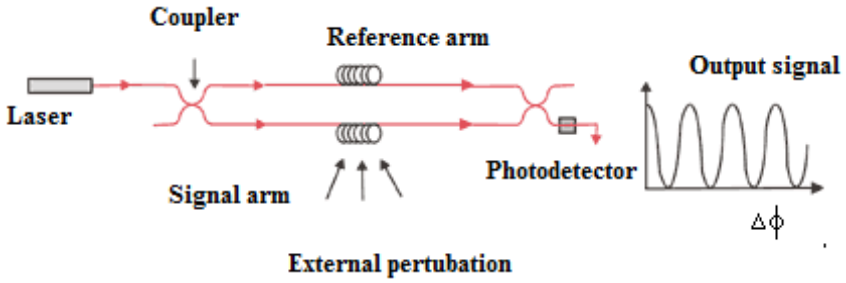

Figure1.18 Schematic of Mach-Zehnder interferometer

The recombined beams are exactly in phase and the beam intensity is maximum when the total lengths of sensing and reference fibers are exactly the same or differ by an even multiple of λ/2. If the difference in total length is an odd multiple of λ/2 then the intensity of the

recombined beam will be minimum. Thus a 100% modulation occurs over a change of λ/2 in the fiber length and hence it is very sensitive.

Michelson Interferometer

Michelson interferometer also employs a reference fiber and sensing fiber with reflective coatings at the ends. A 3 dB coupler is used for coupling light in to the fibers. The light reflected from fiber end return to the detector through the 3 dB coupler as shown in figure 1.19. Michelson Interferometer is similar to MZ interferometer except for the use of two mirrors and single coupler instead of two in MZ.

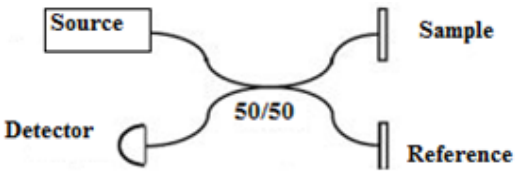

Figure1.19 Schematic of Michelson Interferometer

Sagnac Interferometer

Sagnac interferometer is used to measure angular displacement [16-18]. In this configuration light from laser is split into two by the 3 dB coupler. The light is injected into a loop as shown in figure 1.20. Thus the light travels in opposite directions. When loop is stationary there is no phase shift since both beams takes same time to travel in clockwise and anticlockwise direction. When the fiber loop rotates about an axis perpendicular to the plane of loop, a phase shift occurs between two light beams depending on the number of turns in the loop, rotation rate and area enclosed by the loop.

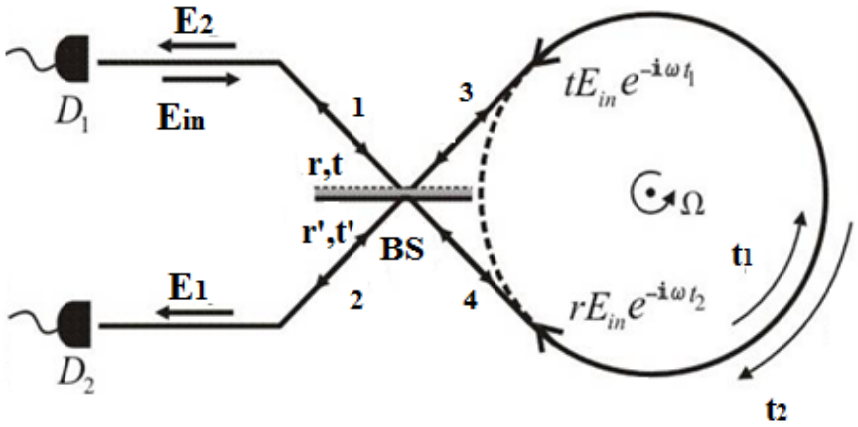

Figure 1.20 Schematic of Sagnac Interferometer

Fabry Perot Interferometer

This interferometer is used to sense different physical and chemical quantities. The configuration is as shown in figure 1.21. It uses two partially transmitting mirrors [19]. Light from laser is injected into fiber through mirror 1. Mirror 2 partially reflects and transmits this light. The reflected light again falls on mirror 1 and gets partially reflected. The process continues and intensity decreases after each reflection. The beam transmitted through mirror 2 undergoes interference. The multiple reflections magnify the phase differences resulting in high sensitivity [20].

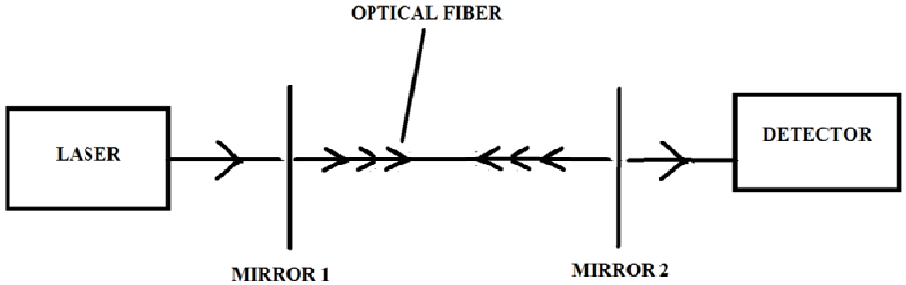

Figure 1.21 Schematic of Fabry Perot Interferometer

1.8.4 Fiber Bragg grating based sensing

Fiber Bragg Grating (FBG) sensors are wavelength modulated sensors. FBG based sensing has many advantages compared to other type of sensing [21-23]. The signal obtained from FBG sensors is monitored in wavelength domain hence the source fluctuations will not affect the performance of the measurement. Linear output, high resolution are the other advantages. Few problems in these sensors are cross sensitivity between temperature and strain. Demodulation is by using a costly high resolution spectrum analyser. The pictorial representation of FBG in an optical fiber is shown in figure 1.22.

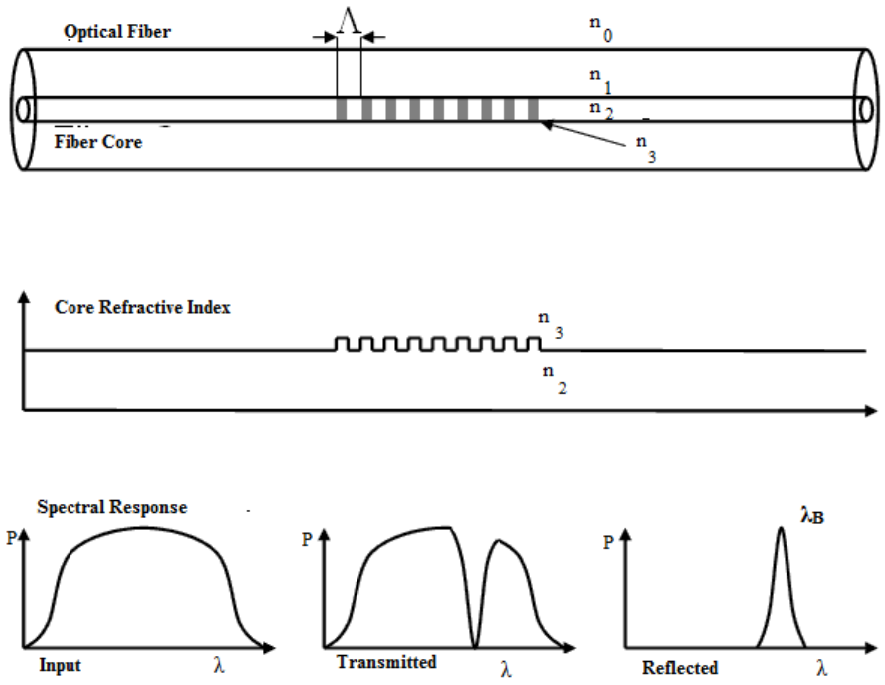

Figure1. 22 (a) FBG in an optical fiber (b) Refractive index profile of the core (c) Spectral response

Theory

A fiber Bragg grating consists of a longitudinal, periodic variation in the refractive index of a single mode fiber. When light from a broad band source is launched into the fiber, FBG reflects one wavelength which satisfies the Bragg's condition.

According to Bragg's law

$$\lambda_B = 2n_{eff}\Lambda \qquad (1.10)$$

Where 'λ_B' is the Bragg wavelength, 'n_{eff}' is the refractive index of the fiber core and 'Λ' Bragg grating period .The strain measurement is based on the physical elongation of optical fiber which corresponds to change in grating pitch and refractive index of the fiber due to photo elastic effect. At constant temperature shift in Bragg wavelength can be expressed as [14]

$$\Delta\lambda_B = (1 - p_e)\lambda_B\varepsilon \qquad (1.11)$$

where 'ε' is the applied strain and 'p_e' the effective photo elastic coefficient and it is expressed as

$$p_e = \left(\frac{n^2}{2}\right)[P_{12} - \mu(P_{11} + P_{12})] \qquad (1.12)$$

'P_{ij}' is the Pockel's coefficients of the strain optic tensor and 'μ' is the Poisson's ratio of the optical fiber.

Bragg wavelength shift due to temperature accounts for temperature dependence of the refractive index of silica and thermal expansion of glass. Major contribution is due to temperature

dependence of the refractive index of silica. The shift in Bragg wavelength can be expressed as

$$\Delta\lambda_B = [\frac{1}{\Lambda}(\frac{\delta\Lambda}{\delta T}) + \frac{1}{n}(\frac{\delta n}{\delta T})]\lambda_B \Delta T \quad (1.13)$$

The first term relates to thermal expansion of fiber and second term to the temperature dependence of refractive index. This makes the FBG a good sensor for strain and temperature [24-29]. These measurements require a broad band source, a high resolution spectrum analyser and a 3dB coupler.

Fabrication of FBG sensors

FBG is fabricated on a photosensitive step index single mode silica fiber. The krypton fluoride excimer laser at 248nm is normally used for this purpose. The absorption of UV light creates permanent damage in the fiber. The three techniques used for the fabrication of FBG are interferometric, phase mask and point by point method. In interferometric method a laser beam is split into two, using Beam splitter and it is recombined to form the interference pattern [30]. The photosensitive fiber is removed of its protective plastic coating and placed across the interference region. The absorption of UV changes the linkages between the Ge-oxygen links and causes permanent change in the refractive index of the fiber. The pitch of grating is given by,

$$\Lambda = \frac{\lambda}{2}\sin\left(\frac{\theta}{2}\right) \quad (1.14)$$

The optical alignment is very critical in this arrangement. In phase mask method a diffraction grating is used to split the laser beam in to several orders and the interference between various orders producers the required pattern in the fiber [31, 32] .This technique is widely used for the fabrication of FBG. In point by point method, each grating plane is produced separately by a focused single pulse from excimer laser [33]. A single pulse of UV light from an excimer laser passes through a mask containing slit. A focusing lens images the slit into the core of the fiber and refractive index of the core in the irradiated fiber section increases locally. The fiber is translated through a distance 'Λ' corresponding to the grating pitch. The fabrication methods are detailed in Chapter 4.

1.8.5 Polarimetric sensors:

Many parameters like pressure, temperature, electric current, magnetic field, and voltage can be measured using Polarimetric sensors [34-39]. The state of polarisation of light is modulated by Faraday Effect, electro-optic effect, photo elastic effect. In 1845 Michel Faraday found that when a beam of plane polarised light passes through a substance subjected to a magnetic field, its plane of polarisation rotates by an angle depending on the magnetic field component parallel to the direction of propagation. This effect is known as magneto-optic effect. When the propagation of light is reversed the direction of rotation is not reversed. Longer light path is possible by the use of optical fiber, the increase in light path increases the angle of rotation hence the sensitivity of fiber sensor. Similarly the

Electro-optic effect (Kerr effect) is also used for the measurement in Polarimetric sensors. In short, to measure current in a conductor a linearly polarised laser beam is launched in to a single mode fiber that loops the current carrying conductor. When current flows through the conductor the magnetic field produced by the current rotates the plane of polarisation of light .The magnitude of rotation is proportional to the current and also the number of turns of the fiber.

1.8.6 Frequency modulated sensors

Frequency modulated sensors are based on Doppler Effect, Raman scattering, luminance etc. The change in frequency with velocity is called Doppler Effect [40, 41]. This effect has been successfully used to measure blood flow velocity in artery. The Raman Effect is the inelastic scattering of photons by matter. When a monochromatic light beam propagates in an optical fibre, spontaneous Raman scattering transfers some of the photons to new frequencies, due to the exchange of electronic, vibrational or rotational molecular energy levels of material [42]. The scattered photons may lose energy (Stokes) or gain energy (anti-Stokes). If the pump beam is linearly polarized, then the polarization of scattered photons may be the same (parallel scattering) or orthogonal (perpendicular scattering). This effect is very weak and it requires sophisticated instrumentation to get desired signal level.

1.9 Distributed fiber optic sensors

Distributed fiber optic sensors can monitor single or multiple measurands at large number of locations continuously, over the path

of an optical fiber [43-45]. A distributed FOS generally consists of a light source, optical fiber, circulator, photo detector and signal processing devices. Reduced number of components, lower cost, reduced weight and cabling are the few advantages of distributed sensing. If the measurand can be monitored continuously along the fiber, then it is termed as intrinsically distributed sensor. If the measurand is measured at finite number of locations along the fiber, then it is termed as quasi-distributed sensor. The main methods are based on time domain reflectrometry, frequency domain reflectrometry and wavelength division multiplexing.

1.9.1 Optical time domain reflectrometry

Transmission loss in the fiber is mainly due to the random microscopic variation in the refractive index of the fiber core namely Rayleigh scattering. A fraction of light is returned towards light source. As the optical pulse is launched in to the fiber and the back scattered intensity is monitored with respect to time, we can derive the loss of the fiber along its length. This technique is called Optical time domain reflectometry [46]. The Optical Time Domain Reflectometer (OTDR) can be employed to detect the measurand induced variations in the fiber [47-55]. A typical arrangement is shown below in the figure 1.23.

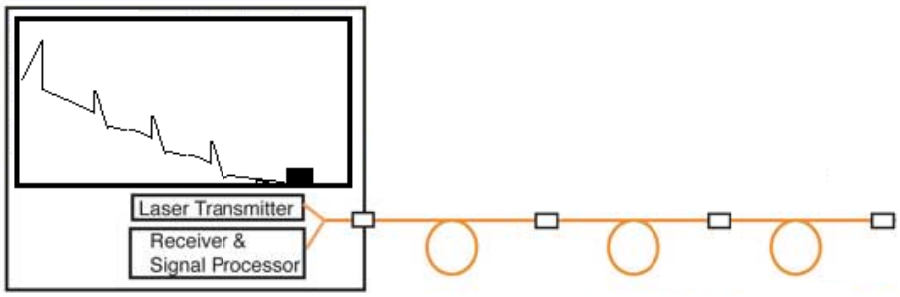

Figure1.23 Schematic of Optical time domain reflectrometry

An intrinsically distributed FOS sense the measurand continuously along the fiber. It has wide range of applications in power supply industry, oil and gas industry, process industries, buildings, tunnels etc. An intrinsically distributed temperature sensor can monitor the windings of power transformers and turbines. In cooling pipes and transmission lines, temperature is monitored using an intrinsically distributed FOS. In petrochemical industry such sensors are used for sensing pipeline temperature and leakage. In process industries sensors are used for monitoring the drying and curing process. Intrinsically distributed sensors are widely used for structural health monitoring. An OTDR with optimum resolution can be used to monitor the process parameters.

In quasi-distributed FOS, the measurand is monitored only at finite locations [56]. Micro or macro bending in the fiber is one of the loss mechanisms and it can be used for quasi-distributed sensing of various parameters such as force, pressure and displacement. In a quasi-distributed sensing the spatial resolution is not very important provided the individual sensing points are clearly resolved. In Quasi distributed

sensing the sensing elements can be modified to meet the sensitivity and range. A typical OTDR trace signal is shown in figure 1.24.

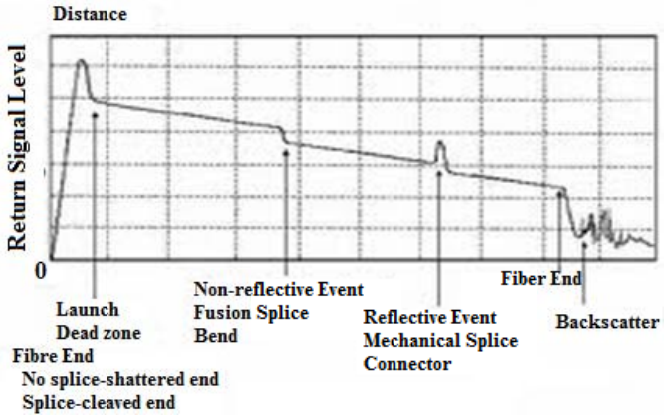

Figure1.24. Signature of an OTDR

1.9.2 Optical frequency domain reflectrometry

Stimulated Raman scattering in optical fibers is an important nonlinear phenomena which arises from the interaction of an intense light beam with the vibrational modes of the fiber silica molecules, when such high pump power levels propagate throughout the fiber. During the scattering process, an optical phonon induces the molecule to make a transition to an excited vibrational state of energy. As a consequence the scattered photon of energy is red shifted with respect to the pump energy by an amount equals to the difference between the pump energy and the excited vibrational state energy. The scattered light is also called as Stokes light frequency. An Optical Frequency Domain Reflectometer is used for the detection of frequency and corresponding distance of such signals.

1.9.3 Wavelength division multiplexing

Distributed fiber optic sensing with Wavelength Division Multiplexing (WDM) can be accomplished using FBG sensors. FBG sensors are widely used for the measurement of strain and temperature. In order to measure these parameters at different locations a number of Bragg gratings are written on the same fiber. Bragg wavelength is selected in such a way that one may not interfere with the other. When a broad band source is focused to the fiber depending upon the Bragg wavelength of FBG, light is reflected back. Hence it can be effectively configured for the quasi distributed measurement of different parameters. A typical arrangement is as shown in figure 1.25. The typical source, reflected and transmitted spectrum is also as shown. Such wavelength division multiplexed FBG sensors are effectively used for quasi distributed sensing of different parameters [57, 58].

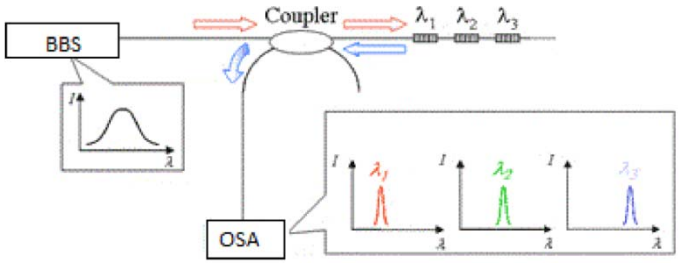

Figure1.25 Distributed sensing using FBG

1.10 A Review of the Related Work

1.10.1 Fiber optic sensors for Chemical Sensing.

The evanescent wave fiber optic chemical sensing has been reported extensively in literature [59-63]. The fiber-optic chemical

sensor used for the determination of pollutants in water was developed by Kathleen M. Leonard in 1995 [59]. The indicator, PRODAN, bounded to optical fiber is found to fluoresce at varying wavelengths for an array of anthropogenic organics like acetone, cyclohexane, chloroform, toluene, and cyclohexane etc. A high power UV source is used for the excitation and high resolution spectrum analyser is used for detection of varies pollutants. Thomas Lee S et.al [60] suggested the possibility of using a permanently micro bent bare optical fiber for detecting chemical species in water. Further P. Suresh Kumar et.al [61] suggested a fibre optic technique for detecting trace amounts of nitrite compounds in water. The fibre optic sensor described is based on evanescent field absorption in solution formed by the reaction of nitrite compounds in water with suitable chemical reagents. A short unclad portion of a plastic clad silica fiber acted as the sensing region. The experimental result showed the detection of very low concentrations of the order of 1 ppb of nitrite compounds with a large dynamic range of 1–1000 ppb and makes it suitable for the measurement of nitrites in drinking water.

M Sheeba in 2005 [62]suggested the design, development of a fibre optic evanescent wave refractometer for the detection of trace amounts of paraffin oil and palm oil in coconut oil. This sensor is based on a side-polished plastic optical fibre. The sensing region is developed by removing the cladding and a small portion of the core. A powerful source of wavelength 670 nm was used for probing. Later in 2009, Pabitra Nath [63] suggested better sensitivity of evanescent wave fiber optic sensor with double pass evanescent field absorption

from an unclad U-bent multimode optical fiber. One end of the fiber is polished to form an angled-tip, whereas the other end is flat polished. Evanescent field absorption in the bending region undergoes further absorption as it reflects back from the fiber tip-air interface, which is reported to have higher sensitivity of the sensor. B.D Gupta et al [64] evaluated optical fiber evanescent field absorption sensors, based on attenuated total reflections spectroscopy. The technique relies on the penetration of the evanescent wave of a totally internally reflected ray into an absorbing medium surrounding the core of the fiber. The amount of absorption depends on both the amplitude of the evanescent field in the absorbing medium and the number of reflections within the sensing region. The light of wavelength close to the peak absorption wave length of the fluid is coupled into one of the ends of the fiber, while the other end is connected to a power meter. As the concentration of the fluid around the unclad region of the fiber increases, the output power received by the detector decreases. This loss in power is used as a criterion for detecting and determining the concentration of the fluid. This has been further supported by the empirical relation determined to fit the experimental data on the response curve. Fiber optic chemical sensors with analytic sensitive coatings are also reported. Humidity sensor proposed by Jinesh Mathew et al [65] has hygroscopic coating on the fiber. The Gas sensing is also reported based on the sensitive coating on the fiber [66-69]. Most of all these sensors require an OSA and a broad band source for the measurements. In this thesis, a reagent mediated, dual wavelength evanescent wave fiber optic sensor is discussed in order to

enhance the selectivity, sensitivity and repeatability in chemical sensing and it is used for the measurement of traces of certain chemical contaminants in water.

1.10.2 Sensors based on Fiber Bragg gratings

Hill *et al* fabricated the first FBG [70]. Intensive study on fiber gratings began after a controllable and effective method for their fabrication was devised in 1989 [71]. Fiber gratings have been applied in add/drop filters, amplifier gain flattening filters, dispersion compensators, fiber lasers and hence in optical fiber communications [72]. Under phase matching conditions, a fiber Bragg Grating (FBG) couples the forward propagating core mode to the backward propagating core mode. An FBG can be written into a segment of a single-mode fiber in which a periodic modulation of the core refractive index is formed by exposure to a spatial pattern of ultraviolet light. The spatial pattern can be created by using an appropriate phase mask.

FBGs respond to both strain and temperature. Hence their effects need to be separated from each other, in order to measure each physical parameter or to measure both simultaneously. Considerable effort has been focused on this topic and various solutions have been proposed. A straight forward and very practical approach is to use a reference grating, a FBG, which is isolated from one parameter. Fiber Bragg grating (FBG) sensor-based systems have been widely used for many engineering applications [73-79]. Application reported includes structural monitoring. The evaluation results of the use of FBG strain

sensors incorporated in CFRP (carbon fibre reinforcement polymer) rods and tubes helps in monitoring the performance of the NSMR (near surface mounted reinforcement) which is an essential part of the repair and strengthening of any bridges. In geotechnical structures, the fiber Bragg grating sensing technology is used to measure strains along a standard inclinometer casing. These are then utilised to calculate the lateral or horizontal deflections of the casing using the measurement of tilts and displacements of geotechnical structures.

Ki-Sun Choi et al in 2012[76] reported the health and damage assessment of wind turbine blades using the FBG sensors. Sensors attached on or embedded into the blade structures of wind turbine would make it possible to analyze not only non-destructively, but also without the need to implant intrusive electrical devices. Similarly a number of applications in structural health monitoring are also reported in literature. Fiber Bragg grating-based sensor systems have been used for structural monitoring for several years. Those systems have been employed in tests carried out over a long period and have showed high-quality performance in laboratory as well as in field tests. These monitoring systems are used to determine the data from the FBGs, have proved to take measurement in harsh environments under static and dynamic load conditions. Extensive studies were performed on fiber grating sensors and few of them have now reached commercialization stages. In this thesis theoretical evaluation of FBG sensors using MATLAB for strain and temperature measurement is carried out and then the results are compared with experimental results.

1.10.3 Interrogators for FBG Sensors

The signal obtained from FBG sensor is usually encoded directly in wavelength domain and hence it is insensitive to source fluctuations. The main drawbacks in the use of FBG sensors for different applications are the costly demodulation techniques. Optical spectrum analyzers are not suitable for real sensor systems because they are expensive and their wavelength scanning speed is too slow. Hence interrogators are required for FBG sensors. Their roles are to extract measurand information from the light signals coming from the sensor heads. The measurand is typically encoded in the form of a Bragg wavelength change, and hence, the interrogators are typically expected to read the wavelength shift and provide measurand data. In the literature, many optical wavelength-intensity demodulation techniques have been discussed. Some are quite simple but are more limited in measurement resolution, dynamic range or multiplexing, and some are more complicated and provide better resolution but are more expensive or need stabilization.

The interrogators are mainly based on long period grating, FBG filter, chirped fiber grating etc. [78-82]. A key interrogating component in the case of long period grating technique is a long-period grating which acts as an edge filter converting strain-induced wavelength variation into optical power measurement. The transmission profile of the long-period grating is shown to be nearly linear over a sufficiently wide range, yielding a linear relationship between the resultant intensity and applied strain using a standard

lock-in technique. The interrogator is based on FBG filter has two feedback control loops, a PZT-driven fiber stretcher, optical fibers embedded with the sensor and filter gratings, and a string resonator. Light from a super luminescent LED (SLED) given through a 3-dB coupler and is transmitted into the sensor fiber. A narrow band of the transmitted light, whose wavelength is centred at the Bragg wavelength of the sensor FBG, will be reflected, depending on the strain condition of the sensor FBG. Part of the reflected light then enters the filter fiber embedding the filter FBG via the coupler. The optical power transmitted through the filter FBG is measured with a photodiode. When the resonance wavelengths of the sensor and filter FBGs are matched, the reflection of the incident light by the filter FBG would become maximum, resulting in the minimum measured power on the photodiode. The optical fiber embedding the filter FBG is attached to a PZT-driven stretcher and controlled with a feedback loop so that the strain on the filter FBG can be continuously adjusted to match that of the sensor FBG. Because the strain on the filter FBG is controlled to match that of the sensor FBG, the strain condition on the sensor FBG can be monitored from that of the filter FBG. The strain on the filter FBG may be determined from the strain-voltage relation of the PZT-driven fiber stretcher. However, as a general piezo material exhibits large hysteresis and nonlinear characteristics, the accuracy of the measured strain degrades if the PZT-driving-voltage is chosen as a method to determine the strain of the filter FBG. In C. Song et al.[81] introduced a string resonator that measures absolute strain of the filter fiber to solve the above stated problem.

In the case of Chirped Fiber bragg Grating (CFG) interrogator, a broad-band light source (BBS) is transmitted to a circulator and fed to a sensor FBG. Then, the reflected light from the sensor head is returned to the circulator and enters the demodulator. The unpolarized light reflected from the sensor FBG is divided into two orthogonal polarized lights through the polarizing beam splitter (PBS). The parallel (to the paper sheet plane) polarized light at back end of the PBS is coupled to a single-mode fiber (SMF), and the other polarization component is discarded. With the help of the polarization controller, the parallel polarized light is set to excite both orthogonally polarized lights in the SMF. After the unpolarized light (which has both orthogonal polarization components) reflects from the CFG, it returns to the PBS and is divided into two polarized lights, and finally detected at photo detectors. The polarization controller was used to make linear relation between the wavelength and the optical power. This interrogator configuration is bit complex and difficult.

The interrogator reported includes Mach–Zehnder interferometer (MZI) based system also [83]. Light from a broadband source is coupled into the fiber which transmits the light to the grating element. The wavelength component reflected hack along the fibre towards the source is tapped off using a coupler and fed to an unbalanced MZI. This light effectively becomes the source light into the interferometer; wavelength shifts induced by perturbation of the grating resemble a wavelength modulated source. This unbalanced interferometer behaves as a spectral filter with a raised cosine transfer

function, and the wavelength dependence on the interferometer output is observed using power meter with differential input.

Depending upon the application, sensitivity and accuracy required, different types of interrogators are designed. In the present thesis an attempt is made to make the interrogators with simple components. Theoretical evaluations of the interrogator are carried out using MATLAB. The experimental data also showed linear results with good repeatability as expected.

1.10.4 OTDR Based Distributed Sensing.

Distributed fiber optic sensors have proven to be an efficient means for interrogating a large number of points along a single optical fibre, a capability which has attracted substantial interest from industries involved in oil, gas and structural health monitoring. The majority of distributed optical fibre sensors have utilized Raman scattering [84, 85], Brillouin scattering [86–89], Rayleigh scattering [90], etc. In Raman scattering and Brillouin scattering, the technique is based on optical time-domain reflectometry that uses a single pulsed light source and on spatially resolving both the Brillouin anti-Stokes frequency shift at 1533 nm and the intensity of the Raman anti-Stokes signal at, 1450 nm. The Raman signal is sensitive to temperature but not to strain. With knowledge of the temperature of the fiber, one can then compute the strain from the Brillouin frequency shift information. The intensity of the anti- Stokes Raman signal exhibits more sensitivity to temperature, than does the anti- Stokes Brillouin signal. To predict the temperature changes accurately, the Raman

signal be referenced to a temperature independent signal measured with the same spatial resolution.

Analysis on Raman Stokes lines with an OTDR allows the assessment of distributed temperature sensing in a fiber, since Stokes intensities are dependent on the fiber temperature due to the change in phonon distribution. A coded, Raman-based distributed temperature sensor system using 255-bit Simplex coded optical time domain reflectometry (OTDR) and optimized sensing link composed of cascaded fibers with different Raman coefficients is also reported.

The fiber optic micro bend sensor is based on the phenomena of optical fiber micro bend loss, where an optical fiber is placed between a pair of corrugated plates with teeth. When the light wave propagates along the fiber, local light loss will occur at the bent region of the optical fiber due to the mode coupling between guided modes and radiation modes. The higher-order modes in a multimode optical fiber will be most easily coupled out from the fiber at small bends. The microbend loss of the fiber is a function of the fiber bending amplitude and its sinusoidal tooth spacing or mechanical wavelength. The induced perturbations causes a change in the Rayleigh backscattered trace and the change is detected and spatially located. Multiple disturbances can be detected simultaneously allowing a moving disturbance to be tracked, such systems also provide a measure of the magnitude of perturbation. An optical time domain reflectometry (OTDR) system based on the Rayleigh noise is used for the weight and displacement study.

The studies reported earlier have a destructive nature of testing [91-94], and lacks repeatability. The sensing head mechanism reported by N.M.P. Pinto et al. [95] consists of a fibre tied in the shape of an eight number figure on a single mode optical fibre. When a displacement occurs, the sensing head size decreases and power loss is induced through the decrease of the loop radius. The sensor does not require an external mechanism to increase or decrease the bend radius. To implement a quasi-distributed sensor, four displacement sensing heads were constructed in a continuous optical fibre. A commercial OTDR connected to a personal computer (PC) for data display, processing and storage was used for the measurement. The OTDR locates the position of each sensing head and measures the induced displacement loss through the Rayleigh backscatter light signal.

The sensing mechanism reported by X. Guangping et al. [94] is based on the principle of additional losses produced by a series of micro bend on the optical fiber. The mechanical sensing element of the micro bend sensors is a pair of groove plates. One of the plates is fixed by epoxy on the complex material frame that has a very perfect elasticity. Both ends of an elastic diaphragm are fixed to the frame of micro bend sensor that is firmly bonded on the measured structure and suffer the same strain with the measured structure. The mechanical transducers used are actually several standard paper clips, which are fixed to the elastic frame of complex material. Under the action of structure strain, the two ends of the elastic diaphragm will displace along the strain direction, thus lowering the arched height of the diaphragm. This action causes the diaphragm to press against the paper clips, causing the paper

clips to move downwards and subsequently, causes the optical fiber to suffer from the modulation of micro bend. The extent of micro bend loss depends on the gap between the paper clips and the extent of the paper clips motion. A commercial OTDR measures the strain and deformation and its position of the structure. The proposed configuration supports non- destructive weight and displacement sensing using triangular corrugations with proper springs and guides and ensures repeatability also.

1.10.5 FBG Based Distributed Sensing

The FBG's Bragg wavelength has the property to shift linearly with temperature or strain, without any hysteresis. Today, FBG represent an important part of the fiber optic sensing and cover various kinds of applications [96–99]. Qiying Chen et al.[100] used FBG sensors for temperature and humidity measurement. The polymer-coated FBGs indicate linear shifts in the Bragg resonance wavelengths of the gratings with the temperature changes. The polyimide-coated FBG was placed in the environmental chamber where the temperature was kept constant. The data shows the behaviour of the FBG spectral characteristics when the grating was exposed to different humidity conditions. The Bragg wavelength shifted when the humidity in the test environment was varied from 13 %RH to 91 %RH. As the humidity level increased, the wavelength was found to shift toward the longer wavelength, which is consistent with the elongation of the FBG caused by the expansion of the polymer coating. Tjin S C et.al. [98] has used an array of FBG sensors

for structural health monitoring. Multiplexed FBG-based strain sensors were fixed onto the reinforced bars in concrete structures to determine the strain changes at different locations within the structures during loading and unloading tests. A similar set of FBG-based strain sensor arrays was also mounted onto the surface of the structures for the purpose of comparison. At the same time an FBG-based sensor array optimized for temperature measurement was also distributed alongside the strain sensors to obtain the temperature information, as well as to compensate for the temperature-induced wavelength shifts on those FBG strain sensors.

Caucheteur C[99] reported the Catalytic fiber Bragg grating sensor for hydrogen leak detection in air. The explosion risk linked to the use of hydrogen as fuel requires low-cost and efficient sensors hence they suggested a multipoint in-fiber sensor capable of hydrogen leak detection in air as low as 1% concentration with a response time smaller than a few seconds. Their solution makes use of fiber Bragg gratings (FBGs) covered by a catalytic sensitive layer made of a ceramic doped with noble metal which, in turn, induces a temperature elevation around the FBGs in the presence of hydrogen in air. FBGs have the advantage of allowing multiplexing schemes, enabling quasi-distributed sensing. With a large number of FBGs interrogated by one single device, the cost per sensor unit drastically decreases and becomes even more competitive with electrical sensors.

FBG supports both time division and wavelength division multiplexing [81, 99-109] configurations. Luiz Carlos Guedes Valente

et al. [102] suggested a combined time and wavelength multiplexing technique of optical fiber grating sensor arrays using commercial OTDR equipment. The experimental arrangement consists of OTDR, a spectral band pass filter, and a serial connection of several arrays of FBG sensors. Typical OTDR devices use a Fabry–Perot laser source of 10-20nm band width. An optical band-pass filter transmitting only a few laser modes is introduced between the OTDR and the fiber. A FBG with its reflection peak coincides with the filter is present in the fiber. The FBG will generate an easily detectable signal due to its reflection. For a fixed filter spectrum, the reflected power will depend on the FBG peak reflection. FBGs at same nominal wavelength can be accessed along the fiber with delay times corresponding to their spatial position along the fiber. Y.J. *Rao et* al.[105] reported a simultaneous spatial, time and wavelength division multiplexing topology, with a tuneable wavelength filter and an interferometric wavelength scanner. This configuration is used to interrogate a range of in-fibre Bragg grating (FBG) sensors.

The straight forward multiplexing technique of the FBG system is the wavelength division multiplexed (WDM) mode, where each FBG in a fiber has its own characteristic wavelength range that is different from others in the same fiber, allowing for easy identification of the FBG corresponding to a particular signal. This scheme of sensing can accommodate a large number of sensors on the same fiber per channel of an interrogator, limited only by the specifications of the FBG interrogator. The development of FBG based distributed sensor systems has been studied for various applications. The present study is

about the simulation, experimental evaluation of simultaneous measurement of strain, Temperature, Weight in a Wavelength division multiplexed FBG sensors.

1.11 The present Work

The present work is on the development of fiber optic sensors for chemical and physical sensing. For chemical sensing a dual wavelength evanescent wave fiber optic sensor with good selectivity, sensitivity, portability and repeatability is developed. The sensor is used for the measurement of Silica, Iron, Phosphate and Ammonia in water. These sensors can be used for water quality analysis. The performance of the sensor is evaluated with the water samples from different locations. Physical parameters like strain and temperature are measured using FBG based sensors. The reflected spectrum of FBG during strain and temperature variation is simulated using MATLAB. For strain measurement the FBG is pasted on a cantilever structure and strain induced shift of reflected spectrum is estimated. Apart from this the temperature drift of the reflected spectrum during strain measurement is determined. The reflected spectral shift of FBG up to 100^0C is observed. Interrogation system for FBG sensors has to be designed for better dynamic response, portability and affordability. The performance of the interrogation systems are evaluated using MATLAB. Two different approaches for the interrogation of FBG sensors are discussed. The first method employs a narrow band source and an FBG with Bragg reflection at trailing edge of the source spectrum. Power reflected from a matched reference FBG is fed into the measuring FBG in the second method.

The performance of the two interrogation methods is evaluated through strain and temperature measurements. Distributed measurements of fiber optic sensors based on optical time domain reflectometry and wavelength division multiplexed FBG sensors are realised. In time domain reflectometry, spring loaded triangular corrugations are used for creating macro bends in the fiber, which is used for the measurement of weight and displacement. Three FBG sensors along a fiber with different resonant wavelengths are used for the simultaneous measurement of Strain, Weight and Temperature.

References

[1] B. D. Gupta, Fiber optic sensors principles and applications, New India Publications, New Delhi, Ch. 1, p 2, 2006.

[2] Bishnu P. Pal, Fundamentals of fiber optics in Telecommunication and Sensor systems, New Age International, New Delhi, Ch. 22, p 548, 1997.

[3] G. Keiser, Optical fiber communications, Mc-Graw-Hill International Editions, New York ,Ch. 2, p 46, 1991.

[4] S. C. Guptha, Optoelectronic devices and systems, Prentice-Hall of India, New Delhi, Ch. 1, p 40, 2005.

[5] H. Kolimbiris, Fiber Optics Communications, Pearson Education, Delhi, Ch. 9, p 300, 2004.

[6] Dennis Derickson, Fiber optic test and measurement, H. P., Prentice Hall, New Jersey, Ch. 11, p 449, 1998.

[7] Bishnu P. Pal, Fundamentals of fiber optics in telecommunication and sensor systems, New Age International, New Delhi, Ch. 23, p 552, 1997.

[8] B. D. Gupta and S. K. Khijwania, Experimental studies on the response of the fibre optic evanescent field absorption sensor, Fibre Integr. Opt., **17**, 63, 1998.

[9] G. Z. Wang, K. A. Murphy and R. O. Claus, Effect of external index of refraction on multimode fiber couplers, Appl Opt., **34**, (36), 8289, 1995.

[10] Jianqing Lu, Zhenyi Chen, Fufei Pang and Tingyun Wang, Theoretical Analysis of Fiber-Optic Evanescent Wave Sensors, Microwave Conference, DOI: 10.1109 / CJMW. 2008. 4772500, IEEE Xplore, 2008.

[11] Yasser Chiniforooshan, Jianjun Ma and Wojtek J. Bock, Evanescent-Wave Fiber-Optic Sensor: On Power Transfer From Core-Cladding Interface to Fiber End-Face, J. Lightwave. Technol., **30**, 8, 2012.

[12] S. Thomas Lee, P. Suresh Kumar, K. P. Unnikrishnan, V. P. N. Nampoori, C. P. G. Vallabhan, S. Sugunan and P. Radhakrishnan, Evanescent wave fibre optic sensors for trace analysis of Fe3+ in water, Meas. Sci. Technol., **14**, 858, 2003.

[13] V. Ruddy, B. D. Maccraith and J. A. Murphy, Evanescent wave absorption spectroscopy using multimode fibers, J. Appl. Phys., **67**, 6070, 1990.

[14] B. D. Gupta, Fiber optic sensors principles and applications, New India publications, New Delhi, Ch. 5, p 62, 2006.

[15] A. Dandridge, Fiber optic sensors based on the Mach-Zehnder and Michelson interferometers, Fiber optic Sensors: An Introduction for Engineers and Scientists, E. Udd, ed., Weily, New York, 1991.

[16] H. Lefevre, The Fiber optic Gyroscope, Artech, Norwood, M.A, 1993.

[17] W. K. Burns, Optical rotation sensing, Academic Press, San Diego, 1994.

[18] R. B. Smith, Selected Papers on Fiber optic Gyroscopes, SPIE Milestone series, MS 8, 1989.

[19] C. E. Lee and H. F. Taylor, Sensors for Smart Structures based upon the Fabry-Perot interferometer, Fiber optic Smart Structures, E. Udd, ed., Wiley, New York, 249, 1995.

[20] B. D. Gupta, Fiber optic sensors principles and applications, New India Publications, New Delhi. Ch. 8, p 169, 2006.

[21] Y. J. Rao, In fiber Bragg grating sensors, Meas. Sci. Technol., **15**, (8), 1442, 1997.

[22] A. D. Kersey, M. A. Davis, J. Patrik, M. LeBlanc, K. P. Koo, C. G. Askins, M. A. Putnam and E. J. Friebele, Fiber grating sensors, J. Lightwave Technol., **15**, (8), 1442, 1997.

[23] K. T. V. Grattan and B. T. Meggitt, Optical Fiber Sensor technology, Kluwer Academic Publishers, Boston, Ch. 2, p 157, 2000.

[24] S. M. Melle, T. Alavic, S. Karr, T. Coroy, K. Lui and R.M. Measures, A Bragg grating-tuned fiber laser strain sensor system, IEEE Photon. Tech. Lett., **5**, 516, 1992.

[25] Y. J. Rao, In fiber Bragg grating sensors, Meas. Sci. Tech., **8,** 355, 1997.

[26] W. W. Morey, G. Meltz and W. H. Glenn, Fiber grating sensors, SPIE, **1169**, 98, 1989.

[27] R. T. Jones, T. A. Berkoff, D. G. Bellemore, D. A. Early, J. S. Sirkis, M. A. Putnam, E. J. Friebele and A. D. Kersey, Cantilever plate deformation monitoring using wavelength Division Multiplexed fiber Bragg grating sensor, SPIE, **2718,** 258, 1996.

[28] S. Triollet, L. Robert, E. Marin and Y. Ouerdane, Discriminated measures of strain and temperature in metallic specimen with embedded superimposed long and short fibre Bragg gratings, Meas. Sci. Technol., **22**, 015202, 2011.

[29] Xuewen Shu, Kate Sugden and Ian Bennion, Single uniform FBG for simultaneous measurement of liquid level and temperature, Meas. Sci. Technol., **21**, 094003, 2010.

[30] G. Meltz, W. W. Morey and W. H. Glenn, Formation of Fiber Bragg gratings in optical fibers by transverse holographic method, Opt. Lett., **14**, 823,1989.

[31] Hill, K. O., Malo, B., Bilodeau, F., Johnson, D. C , Albert, and J., Bragg gratings fabricated in monomode photosensitive optical fiber by UV exposure through a phase mask, Appl. Phys. Lett., **62**, 1035, 1993.

[32] A. Othonos and X. Lee, Novel, improved methods for writing Bragg gratings with Phase masks, IEEE Photonic Tech. L., **7**, 1183, 1995.

[33] B. Malo, K. O. Hill, F Bilodeau, D. C. Johnson and J. Albert , Point by point Fabrication of micro- Bragg gratings in photosensitive fiber using single excimer pulse refractive index modification techniques, Electron. Lett., **29**, 1668, 1993.

[34] Shizhuo Yin, B. Paul, Ruffin Francis and T.S. Yu, Fiber Optic sensors, CRC Press, New York, Ch. 3, p 74, 2008.

[35] W. Eickhoff, Temperature sensing by mode-mode interference in birefringence optical fibers, Opt. Lett., **6**, 204, 1981.

[36] M. Mondanos, M., Lloyd, P. A., Giles, I. P., Badcock R., Weir and K., Damage detection in composites using Polarimetric low coherence polarimetry, Proc. SPIE Int. Soc. Opt. Eng., **4185**, 276, 2000.

[37] M. N. Charasse, M. Turpin and J. P. Le Pesant, Dynamic pressure sensing with side hole birefringent optical fiber, Opt. Lett., **16**, 1043, 1991.

[38] Y. N. Ning, Z. P. Wang, A. W. Palmer, K. T. V. Grattan and D. A. Jackson, Recent progress in optical current sensing techniques, Rev. Sci. Instrum., **66**, (5), 3097, 1995.

[39] S. C. Rashleigh, Magnetic field sensing with single mode fiber, Opt. Lett., **6**,133, 1981.

[40] C. Riva, B. Ross and Bendek, Laser-Doppler measurements of blood flow in capillary tubes and retinal arteries, Invest. Opthalmol, **11**, 936, 1972.

[41] B. D. Gupta, Fiber optic sensors principles and applications, New India publications, New Delhi, Ch. 10, p 195, 2006.

[42] Dennis Dericckson, Fiber optic test and measurement, H. P., Prentice Hall, New Jersey, Ch. 11, p 448, 1998.

[43] A. D. Kersey, Distributed and multiplexed fiber optic sensors, In fiber optic Sensors: An introduction for engineers and scientists, E Udd, ed., Wiely, New York, 1991.

[44] Shizhuo Yin, B. Paul, Ruffin Francis and T.S. Yu, Fiber Optic sensors, CRC Press, Ch. 1, p 24, 2008.

[45] K. T. V. Grattan and B. T. Meggitt, Optical Fiber Sensor Technology, Kluwer Academic Publishers, Boston, Ch. 4 , p 241, 2000.

[46] Dennis Dericckson, Fiber optic test and measurement, H. P., Prentice Hall, New Jersey, Ch.11, p 435, 1998.

[47] Fei Luo, Jingyuan Liu, Naibing Ma and T. F.Morse, A fiber optic microbend sensor for distributed sensing application in the structural strain monitoring, Sensors and Actuators, 75, 41, 1999.

[48] Xie Guangping, Seah Leong Keey and Anand Asundi, Optical time-domain reflectometry for distributed sensing of structural strain and deformation, Opt. Laser Eng., **32**, 437, 2000.

[49] N. M. P. Pinto, O. Frazao, J. M. Baptista and J. L. Santos, Quasi-Distributed displacement sensor for structural monitoring using a commercial OTDR, Opt. Laser Eng., **44**, 771, 2006.

[50] Tang Tian Guo, Wang Qing Yuan and Liu Hao Wu, Experimental Research on distributed fiber sensor for sliding damage monitoring, Opt. Laser Eng., **47**, 156, 2009.

[51] Gunes Yilmaz and Sait Eser Karlik, A distributed optical fiber sensor for temperature detection in power cables, Sensor. Actuat. A, **125**, 148, 2006.

[52] Kai Tai Wan and Christopher K. Y. Leung, Applications of a distributed fiber optic crack sensor for concrete structures, Sensor. Actuat. A, **135**, 458, 2007.

[53] S. F. Knowles, B. E. Jones, S. Purdy and C. M. France, Multiple micro bending optical-fiber sensors for measurement of fuel quantity in aircraft fuel tanks, Sensor. Actuat. A, **68,** 320, 1998.

[54] Chuan Li, Yi-MoZhang, Hui Liu, Sheng Wu and Cai-Wen Huang, Distributed fiber optic bidirectional strain-displacement sensor modulated by fiber bending loss, Sensor. Actuat. A, **111**, 236, 2004.

[55] Kazuro Kageyama, Isao Kimpara, Toshio Suzuki, Isamu Ohsawa and Hideaki Murayama kengo Ito, Smart marine structures: an approach to the monitoring of ship structures with fiber optic sensors, Smart Mater. Struct., **7**, 472, 1998.

[56] B. D. Gupta, Fiber Optic Sensors principles and applications, New India Publications, New Delhi, Ch.13, p 239, 2006.

[57] Majumder M. , Gangopadhyay T. K., Chakraborty A. K., Dasgupta K. and Bhattacharya D. K, Fibre Bragg gratings in structural health monitoring-Present status and applications, Sensor. Actuat. A, **147**, (1), 15, 150, 2008.

[58] Yun-Jiang Rao, In-fibre Bragg grating sensors, Meas. Sci. Technol., **8**, 355, 1997.

[59] K. M. Leonard, Development of a fiber optic chemical sensor for multi contaminant monitoring of environmental systems, Sensor. Actuat. B, **24**, 458, 1995.

[60] T. Lee, A. G. Nibu, P. Suresh kumar, P. Radhakrishnan, C. P. G. Vallabhan and V. P. N. Nampoori, Chemical sensing with micro bend optical fibers, Opt. Lett., **26**, 1541, 2001.

[61] P. Suresh Kumar, C. P. G. Vallabhan, V. P. G. Nampoori and V. N. Sivasankara Pliiai, A fiber optic evanescent wave sensor used for the detection of trace nitrites in water, J. Opt. A: Pure. Appl. Opt., **4**, 247, 2002.

[62] M. Sheeba and P. Radhakrishnan, Fiber optic sensor for detection of adulterant traces in coconut oil, Meas. Sci. Technol, **16**, 2247, 2005.

[63] Pabitha Nath, Enhanced sensitive fiber optic sensor with double pass evanescent field absorption, Microw. Opt. Techn. Let., **51**, 12, 2009.

[64] B. D. Guptha and S. K. Khijwania, Experimental studies on the response of the fiber optic evanescent field absorption sensor, Fiber Integr. Opt., **17**, 63, 1998.

[65] Jinesh Mathew, YuliyaSemenova, GinuRajan, PengfeiWang, GeraldFarrell, Improving the sensitivity of a humidity sensor based on fiber bend coated with a hygroscopic coating, Opt Laser Technol. **43,** 1301, 2011.

[66] Renganathan B, Gobi G, Sastikumar D, Srinivasan R, Chandra bose A. Optical fiber coated with nanocrystalline tin oxide for ammonia vapor sensing. Sensor Lett **8**, 1, 2010.

[67] DikovskaAO,AtanasovPA, AndreevAT, ZafirovaBS, KarakolevaEI, StoyanchovTR ZnO thin film on side polished optical fiber for gas sensing applications. Appl.Surf Sci.**254**, 1087, 2007.

[68] TaoS,FanguyJC, SarmaTVS A fiber-optic sensor for monitoring trace ammonia in high-temperature gas samples with a CuCl2-doped porous silica optical fiber as a transducer.IEEE Sens J. **8,**12,2000 2008.

[69] Dikovska AO, Atanasova GB, Nedyalkov NN, Stefanov PK, Atanasov PA, Karakoleva EI, et al. Optical sensing of ammonia using ZnO nanostructure grown on a side-polished optical-fiber. Sens. Actuat. B, **146,**331,2010.

[70] Hill K O, Fujii F, Johnson D C and Kawasaki B S Photosensitivity on optical fiber waveguides: application to reflection filter fabrication. Appl. Phys. Lett. **32,**647,1978.

[71] G. Meltz, W.W. Morey, W.H. Glenn, Formation of Bragg gratings in optical fibers by a transverse holographic method, Opt. Lett. 14 p 823, 1989.

[72] A.Othonos, K.Kalli, FiberBraggGratings—Fundamentals and Applications in Telecommunications and Sensing, Artech House, Boston, 1999.

[73] A. Kerrouche,W.J.O. Boyle, Y.M. Gebremichael, T. Sun, K.T.V. Grattan, B. Täljsten, A. Bennitz, Field tests of Fibre Bragg Grating sensors incorporated into CFRP for railway bridge strengthening condition monitoring, Sens. and Actuat. A: Physical **148 (1)** 68, 2008.

[74] Y.M. Gebremichael, W. Li, B.T. Meggitt, W.J.O. Boyle, K.T.V. Grattan, B. Mckinley, F. Boswell, K.A. Arnes, S.E.

Aasen, B. Tynes, Y. Fonjallaz, T. Triantafillou, A Field deployable, multiplexed Bragg grating sensor system used in an extensive highway bridge monitoring evaluation tests, IEEE Sens. J. **5**,3,2005.

[75] Y.M. Gebremichael, W. Li, B.T. Meggitt, W.J.O. Boyle, Bragg-grating-based multisensor system for structural integrity monitoring of a large civil engineering a road bridge in Norway, Proced. of SPIE 4596, 343, 2001.

[76] Ki-Sun Choi, Yong-Hak Huh, Il-Bum Kwon and Dong-Jin Yoon A tip deflection calculation method for a wind turbine blade using temperature compensated FBG sensors Smart Mater. Struct. **21**,025008,2012.

[77] Abdelfateh Kerrouche,W.J.O. Boyle, Tong Sun, K.T.V. Grattan, J.W. Schmidt, B. Täljsten, Enhanced FBG sensor-based system performance assessment for monitoring strain along a prestressed CFRP rod in structural monitoring Sens. and Actuat. *A* **151,** 127, 2009

[78] Tyler J Arsenault, Ajit Achuthan, Pier Marzocca, Chiara Grappasonni and Giuliano Coppotelli, Development of a FBG based distributed strain sensor system for wind turbine structural health monitoring, Smart Mater. Struct. **22,** 075027,2013.

[79] A S Guru Prasad, U Sharath, V Nagarjun, G M Hegde and S Asokan, Measurement of temperature and pressure on the

surface of a blunt cone using FBG sensor in hypersonic wind tunnel Meas. Sci. Technol. **24,** 095302, 2013

[80] R. W. Fallon, L. Zhang, L. A. Everall, J. A. R .Williams and I. Bennion, All-fiber optical sensing system: Bragg grating sensor interrogated by a long period grating, Meas. Sci. Technol., **9**, 12, 1969, 1998.

[81] I. C. Song, S. K. Lee, S. H. Jeong and B. H. Lee, Absolute strain measurement made with fiber Bragg grating sensors, Appl.Opt., **43**, (6), 1337, 2004.

[82] S. Kim, S. Kim, J. Kwon and B. Lee, Fiber Bragg grating strain sensor demodulator using a chirped fiber grating, IEEE Photon. Technol. Lett., **13**, 8, 839, 2001.

[83] A. D. Kersey, T. A. Berkoff, and W. W. Morey, High-resolution fiber grating based strain sensor with interferometric wavelength-shift detection, Electron. Lett.,. **28**, 3, p 236, 1992.

[84] Luiz C.S. Nunes , Bruno S. Olivieri, Carla C. Kato, Luiz C.G. Valente, Arthur M.B. Braga, FBG sensor multiplexing system based on the TDM and fixed filters approach Sens. and Actuat. A **138**,341, 2007.

[85] Alahbabi M N, Cho Y T and Newson T P Simultaneous temperature and strain measurement with combined spontaneous Raman and Brillouin scattering Opt. Lett. **30** 1276, 2005.

[86] Kee H H, Lees G P and Newson T P , 1.65μm Raman-based distributed temperature sensor Electron. Lett. **35** 1869, 1999

[87] Belal M, Cho Y T, Ibsen M and Newson T P, A temperature-compensated high spatial resolution distributed strain sensor Meas. Sci. Technol. **21,** 015204, 2010.

[88] Song K Y, He Z and Hotate K, Distributed strain measurement with millimeter-order spatial resolution based on Brillouin optical correlation domain analysis Opt. Lett. **31** 2526, 2006

[89] Alahbabi M N, Cho Y T and Newson T P , Long-range distributed temperature and strain optical fibre sensor based on the coherent detection of spontaneous Brillouin scattering with in-line Raman amplification Meas. Sci. Technol. **17** 1082, 2006.

[90] Alahbabi M N, Cho Y T and Newson T P 100 km distributed temperature sensor based on coherent detection of spontaneous Brillouin backscatter Meas. Sci. Technol. **15** 1544,2004.

[91] Posey R J, Johnson G A and Vohra S T Strain sensing based on coherent Rayleigh scattering in an optical fibre Electron. Lett. **36** 1688, 2000.

[92] Z. B. Ren and Ph. Robert, Polarization multiplexing applied to a fiber current sensor, Opt. Lett., **14**, (21), 1, 1989.

[93] Fei Luo, Jingyuan Liu, Naibing Ma and T. F. Morse, A fiber optic microbend sensor for distributed sensing application in the structural strain monitoring, Sensor. Actuat., **75**, 41, 1999.

[94] Xie Guangping, Seah Leong Keey and Anand Asundi, Optical time-domain reflectometry for distributed sensing of structural strain and deformation, Opt. Laser. Eng., **32**, 437, 2000.

[95] N. M. P. Pinto, O. Frazao, J. M. Baptista and J. L. Santos, Quasi-Distributed displacement sensor for structural monitoring using a commercial OTDR, Opt. Laser. Eng., **44**, 771**,** 2006.

[96] Othonos A and Kalli K Fiber Bragg Gratings, Fundamentals and Applications in Telecommunications and Sensing, London: Artech House,1999.

[97] Rao Y J Recent progress in application of in-fibre Bragg grating sensors Opt. Lasers Eng.**31** 297, 1999.

[98] Tjin S C, Wang Y, Moyo P and Brownjohn J M W Application of quasi-distributed fibre Bragg grating sensors in reinforced concrete structures Meas. Sci. Technol.**13** 583, 2002.

[99] Caucheteur C, Debliquy M, Lahem D and M´egret P Catalytic fiber Bragg grating sensor for hydrogen leak detection in air IEEE Photon. Technol. Lett. **20** 96, 2008.

[100] Qiying Chena, Ping Lu, Fiber Bragg Gratings and their applications as Temperature and Humidity Sensors, Atomic, Molecular and Optical Physics, 6, p235,2008

[101] Crunelle C, Wuilpart M, Caucheteur C and M´egret P 2007 Fast demodulation technique for a quasi-distributed temperature sensor SPIE European Symp. Optical Metrology, **6616,** 2007.

[102] Valente L C G, Braga A M B, Ribeiro A S, Regazzi R D, Ecke W, Chojetzki C and Willsch R Combined time and wavelength multiplexing technique of optical fiber grating sensor arrays using commercial OTDR equipment IEEE Sensors J. **3,** 31, 2003.

[103] Y. Sano, T. Yoshino, Fast optical wavelength interrogator employing arrayed Waveguide grating for distributed fiber Bragg grating sensors, J. of Lightwave Technol. **21,** 1, 2003.

[104] G.Z. Xiao, P. Zhao, F.G. Sun, Z.G. Lu, Z. Zhang, C.P. Grover, Interrogating fiber Bragg grating sensors by thermally scanning a demultiplexer based on arrayed waveguide gratings, Optics lett. **29,** 19, 2004.

[105] Y.J. Rao, A.B. Lobo Ribeiro, D.A. Jackson, L. Zhang, I. Bennion, Simultaneous spatial,time and wavelength division multiplexed in-fibre grating sensing network, Optics Commun. **125**, 53 1996.

[106] H. Gao, H. Li, B. Liu, H. Zhang, J. Luo, Y. Cao, S. Yuan,W. Zhang, G. Kai, X. Dong, Anovel fiber Bragg grating sensors multiplexing technique, Optics Commun. **251**, 361, 2005.

[107] A.D. Kersey, T.A. Berkoff, W.W. Morey, Multiplexed fiber Bragg grating strain sensor system with a fiber Fabry-Perot wavelength filter, Optics Lett. **18,** 16, 1993.

[108] D.A. Jackson, A.B. Lobo Ribeiro, L. Reekie, J.L. Archambault, Simple multiplexing scheme for a fiber-optic grating sensor network, Optics Lett. **18**, 14, 1993.

[109] R.S. Weis, A.D. Kersey, T.A. Berkoff, A four-element fiber grating sensor array with phase-sensitive detection, IEEE Photonics Technol. Lett**. 6** 12, 1994.

****

Chapter 2

DUAL WAVELENGTH EVANESCENT WAVE SENSOR FOR THE DETERMINATION OF SILICA IN WATER

Contents

Implementation of Dual wavelength evanescent wave fiber optic sensor is discussed in this chapter. The performance is evaluated using $KMnO_4$ solution and it is employed for the measurement of traces of silica in water.

2.1 Introduction

Evanescent field absorption is a powerful well established laboratory technique for chemical analysis [1]. In order to achieve maximum evanescent wave penetration, the boundary of an uncladed optical fiber is well suited. The narrow core diameter of the fiber provides large number of reflections per unit length hence more interaction with the analyte. Evanescent wave sensors offer remote sensing, in line analysis together with benefits of simplicity,

reliability, flexibility, and relatively low cost [2,3]. All these have motivated the interest to investigate evanescent wave spectroscopy.

In recent years there has been significant progress in the field of fiber optic sensors, for the detection of various chemical species [4-8]. The most attractive feature of a fiber optic sensor is that whenever an integral study is necessary, they are able to serve as both the sensing element and the signal transmission medium, allowing the electronic instrumentation part to be located remotely from the measurement site [9]. Compared to other sensing methods, evanescent wave sensing technique provides several advantages, especially in chemical sensing applications [10-14].

2.2 Motivation in developing Dual wavelength evanescent wave sensor

Among the fiber optic sensors reported in literature, refractive index variation based ones are the earliest and the basic type [14-20]. The major limitation of this class of sensors is that fluctuations in the optical source will greatly affect the output intensity, which will ultimately lead to undesirable results. So the use of low cost LED sources in fiber optic sensors leads to inconsistent results. A remedy for this problem is the use of a constant current drive for the sources, reference signal and a differential amplifier. Use of a 3 dB fiber optic coupler will help in obtaining the reference signal and hence the output can be made stable even with low cost LED sources. Chemical content detection is an area of interest for industry, where the level of various chemicals in the raw water and effluent water has to be closely

monitored. Intensity based fiber optic sensors can be utilized for chemical content detection with little effort, but the major drawback in this case is the poor selectivity and repeatability. Poor selectivity is due to the fact that intensity based measurements simply rely on the refractive index variation of the sample solution, so any other solution having refractive index in the same range can give the same result. In evanescent wave based FOS, the analyte comes into direct contact with fiber core, so that a small fraction of the sample may get adhered to the core surface. This small fraction of the analyte may lead to erroneous output when a new sample is introduced into the sensor. This leads to poor repeatability of the sensor.

In order to make the evanescent wave based fiber optic sensor more reliable, an experimental set up is developed. Here instead of a single source, two wavelengths are used, one corresponding to the absorption peak of the analyte (analytical wavelength), and the second a non-absorbing one. Introduction of analytical wavelength helps to provide selectivity and the use of non-absorbing wavelength supports repeatability aspect. The sources employed are LEDs, hence the system is cost effective but they have the inherent drawback of intensity fluctuations. Use of a 3 dB coupler and differential detection arrangement cancels the problem of source fluctuations. The mechanical problem of aligning two optical sources to a common fiber is also solved by the 3 dB coupler. The sensing head is a multimode plastic fiber which is having a small length of its core being exposed by removing the cladding. This class of fibers has the advantage of cost effectiveness, higher flexibility and tensile strength. The sensing

region is bent in U shape so that more number of modes will interact with the analyte, hence the sensitivity of the fiber optic sensor increases. Use of plastic fiber makes the system inexpensive, rugged and reusable.

2.3 Evanescent Wave in optical fibers

Optical fiber consists of a core with refractive index n_1 surrounded by cladding of lower refractive index n_2. The light transmission in optical fiber is based on the principle of total internal reflection. When the incident light is reflected from an interface at an angle greater than critical angle, the total internal reflection takes place. The intensity of light does not abruptly decay to zero at the interface; a small portion of light penetrates in to the reflecting medium. The electric field amplitude is maximum at the interface but decays exponentially outward [21]. This penetrated electromagnetic field is called the evanescent wave.

The Electric Field amplitude, E at a distance x along the normal is

$$E = E_0 \exp(-x/d_p) \qquad (2.1)$$

where E_0 is the electric field intensity at the interface, d_p is the penetration depth.

$$d_p = \frac{\lambda}{2\Pi n_1 \sqrt{\sin^2 \Theta - (n_2/n_1)2}} \qquad (2.2)$$

where 'λ' is the wavelength of light. n_1 and n_2 are the refractive indices of denser and rarer media. θ is the angle of incidence with normal to the interface.

2.4 Theory of dual wavelength probing

The relative amount of power flowing in the core and cladding can be obtained by integrating the Poynting Vector within suitable limits along the axial direction [22].

We have

$$P_{core} + P_{cladding} = P_T \tag{2.3}$$

Here P_{core} and $P_{cladding}$ are the power flowing through the core and cladding of the fiber respectively. P_T is the total power flowing in the fiber.

$$\frac{P_{cladding}}{P_T} = 1 - \frac{P_{core}}{P_T} \tag{2.4}$$

If a non-coherent source like a LED or a tungsten filament lamp is used, it will excite all fiber modes with the same power. The total average cladding power is given by the relation [22].

$$\frac{P_{cladding}}{P_T} = \frac{4}{3} M^{-1/2} \tag{2.5}$$

where 'M' is the total number of modes exited in the fiber.

The number of modes is related to the normalized frequency parameter V number, as

$$M = \frac{V^2}{2} \text{ ,} \tag{2.6}$$

and the expression for V number is

$$V = \frac{2\pi}{\lambda} a\left(n_1^2 - n_2^2\right)^{1/2} \quad , \tag{2.7}$$

where 'a' is the core radius and n_1, n_2 are the refractive indices of core and cladding respectively.

So expression (2.5) becomes

$$\frac{P_{cladding}}{P_T} = \frac{4}{3}\left(\frac{V^2}{2}\right)^{-1/2} = \frac{4\sqrt{2}}{3\ V} = \frac{0.3\ \lambda}{a(n_1^2 - n_2^2)} \quad , \tag{2.8}$$

From this expression it is clear that the value of 'V' decreases for a given set up and wavelength, as the cladding index increases. As V decreases the average power through the cladding increases and hence the power coupled to the detector through the fiber core will decrease. This is the basis of all fiber optic evanescent wave intensity based sensors.

Since the number of modes is proportional to the square of the V number [23], we can relate as

$$M \propto V^2 = K\left(n_1^2 - n_2^2\right) \tag{2.9}$$

So, even a small change in the value of cladding index will produce a large change in M value, and this accounts for the higher sensitivity of evanescent wave based fiber optic sensors. The method detailed above has a major drawback of poor selectivity, since the

change in index can be brought about by any species that has an index in the range of the cladding. When evanescent wave based sensors are employed for concentration measurements or adulteration level measurements in liquid or gaseous medium, apart from sensitivity, selectivity is of prime importance. In evanescent wave based sensors the sensing region is developed by removing the cladding either completely or partly for a short length. Then light intensity carried by the fiber from the source to the detector gets modulated by the refractive index of the surrounding medium at the sensing location.

Now the light radiation that leaves the core at the sensing region can undergo several modifications. One of them is to produce attenuated total internal reflection (ATIR) depending on the refractive index of the medium surrounding the exposed region. The radiation may also get absorbed by the surrounding species, if the operating wavelength is same as that of the analytical wavelength of the species. Above effects are responsible for the modulation of light intensity propagating through an evanescent wave sensor. The first effect is present in all evanescent wave sensors and the second effect will come into play only if the operating wavelength is the analytical wavelength of the given species.

So whenever an evanescent wave based fiber optic sensor is employed for concentration / chemical content measurement, it is always advisable to use an analytical wavelength as the probing tool. Considering the above description, the expression for average power in the cladding can be modified as

$$\frac{P_{cladding}}{P_T} = index\,based\,losses + Absorption losses\,(A) \tag{2.10}$$

$$\frac{P_{cladding}}{P_T} = \frac{0.3\ \lambda}{a(n_1^2 - n_2^2)} + A \tag{2.11}$$

From 2.4 the power flow through the core will be

$$\frac{P_{core}}{P_T} = 1 - \frac{0.3\ \lambda}{a(n_1^2 - n_2^2)} - A \tag{2.12}$$

'A' is the absorbance of the species surrounding the exposed region of the sensor, which can be explained with the help of Beer's law for absorbing solutions. It states that the absorbance is directly proportional to concentration of the solution and the path length for light travelling through the species as given in equation

$$A \propto b.C \tag{2.13}$$

where 'b' is the path length of light travel and C is the concentration of the species [24]. Absorbance can be written as

$$A = \varepsilon.b.C\,, \tag{2.14}$$

ε is the absorptivity and expressed in terms of $Lmol^{-1}cm^{-1}$,a constant that does not depend on concentration.

In fiber optic sensor the path length 'b' can be kept constant, hence the contribution of absorbance in cladding power as in equation (2.11) reduces to the concentration of the species surrounding the exposed area.

Hence the equation (2.12) can be further modified as

$$P_{core} = P_T - P_T \frac{0.3\ \lambda}{a(n_1^2 - n_2^2)} - P_T.A \tag{2.15}$$

By taking the differential signal of the same source, source fluctuations can be eliminated. Here P_{core} is the power that is coupled to the detector after passing through the sensing region and P_T is the total power injected into all modes of the fiber. In the expression (2.15), the second term corresponds to the contribution of index dependant power variation and the third term depends solely on the concentration of the solution. The third term is negligibly small for a non-absorbing wavelength. For a non-absorbing wavelength the equation becomes

$$P_{core} = P_T - P_T \frac{0.3\ \lambda}{a(n_1^2 - n_2^2)} \tag{2.16}$$

To have a quantitative analysis of concentration / chemical content level, it is better to have a system capable of dual wavelength probing arrangement. In this scheme, one wavelength should be the analytical wavelength for the species under consideration and the second wavelength should be a non-absorbing one. The difference of output power for absorbing and non-absorbing wavelengths will be the contribution due to the absorption taking place in the solution.

2.5 Experimental Details

The concepts discussed above is utilised for the measurement of traces of silica in water. An intermediate reagent which reacts with

the analyte is used to form an absorbing solution. The preparation of the reagent is detailed below.

2.5.1 Preparation of reagent and standard solutions.

One of the important aspects of analysis is the reagent grade water, which is to be used for preparation and dilution of reagents and for the blank analysis. The water used for the preparation of reagents should not have detectable concentration of the element to be analysed. Water should be free of substances that interfere with analytical methods. As the apparatus and reagents may contribute silica, it is important to avoid glassware and to use reagents low in silica. A blank determination can also correct the silica so introduced. The dual wavelength probing can also cancel the interference like turbidity and other interferences to a great extent.

The common aqueous forms of silica are H_4SiO_4 and H_3SiO_4-. In the presence of magnesium it can form scale deposits in boilers and steam turbines. Analysis is carried out by preparing a solution of test water with the following reagents [25]. The sample containing silica is reacted with molybdate ion in an acidic medium (pH 1.2 to 1.5) and the resulting green yellow coloured complex is reduced to a blue complex with 1-amino -2-napthol -4-sulphonic acid.

Procedure for the preparation of reagents and standard solutions is given below

Amino- Naptol- Sulphonic acid solution: Dissolve 0.5g of 1- amino-2- napthol-4-sulphonic acid in 50ml of a solution containing 1g of

sodium sulphite Na_2SO_3. Add the solution to 100ml of a solution containing 30g of sodium hydrogen sulphide NaHSO3. Make up to 200ml and store in a dark plastic bottle. This solution has a shelf-life of 14 days.

Ammonium Molybdate solution : Dissolve 10 g of ammonium Molybdate [$(NH_4)6.MO_7O_{24}.4H_2O$] in water and dilute to 100ml with water.

Hydrochloric acid: Mix equal volumes of hydrochloric acid with specific gravity 1.19 and water.

Oxalic acid solution (10%): Dissolve 10 g of oxalic acid ($H_2C_2O_4.2H_2O$) in water and dilute to 100ml**.**

Silica stock solution: (1 ml=1mgSiO_2) Dissolve 4.732g of sodium meta silicate ($Na_2SiO_3.9H_2O$) in water and dilute to 1 litre. Standardise the solution by acid dehydration procedure.

Silica standard solution: 1ml=1mg of SiO_2 dilute 10.0ml of silica stock solution to 1 litre with water, again dilute 100ml of this diluted solution to 1 litre.

Calibration: Solutions were prepared with 15 different concentrations to cover the range 0-1ppm by diluting the appropriate volumes of silica standard solution in 100ml polythene bottles. The calibration curve is prepared by plotting absorbance versus concentration.

Transfer 50 ml. of the sample in to 100 ml polythene bottle and mix 1.0 ml of hydrochloric acid. Then add 2.0 ml of ammonium molybdate solution and mix well. After 5minutes, add 1.5 ml of oxalic

acid solution and shake well. Add 2.0 ml of amino-napthol-suphonic acid solution to the prepared solution. Mix well and allow standing for 10 minutes for the colour development.

2.5.2 Experimental setup for dual wavelength probing

The experimental setup for dual wavelength is depicted in figure 2.1. It has two LED sources, one corresponds to the absorption peak of the analyte and a non absorbing wavelength as reference. A standard 3dB multimode fiber optic coupler [26] in the visible range is used for splitting the absorbing and reference wavelengths to the sensor head and reference arm. Microscope objectives and XYZ positioner is used to focus the light from LED to the fiber. The experimental configuration is adjusted to have identical optical coupling at the reference and sample arm. XY positioner is used at the detector end of the fiber for aligning the fiber to the detector. The output of the detectors are differentially amplified and given to the analog to digital converter**.** The reference arm compensates for any intensity fluctuation of the source. The intensity fluctuation is minimised with help of constant current drives also**.** A microcontroller based system is developed for controlling the process. For quantitative analysis, the source corresponding to analytical wavelength is switched on and $(PD_1 - PD_2)_{abs}$ is obtained. The analytical wavelength is switched off and then the reference wavelength is switched, $(PD_1 - PD_2)_{ref}$ is also determined. The difference, $(PD_1 - PD_2)_{abs} - (PD_1 - PD_2)_{ref}$ is calculated and displayed in terms of concentration. The sensor cell is filled with concentration of unknown sample, the output of the sensor at absorbing

wavelength is attenuated due to refractive index, spectral absorption, and other contributing losses. The power loss due to refractive index, turbidity and other contributing losses will be almost the same for both reference and absorbing wavelengths. So the difference of these two signals will be the absorbance of the given species in the solution. Since low concentrations are measured, the results are found linear. The reagents and standard solutions are prepared using standard procedures [24, 25]**.** The exposed area of the sensor fiber is 2 cm long. A plastic multimode step index fiber with core diameter of 980 μm and NA of 0.5 used to make the sensor. The refractive indices of the core and the cladding are 1.49 and 1.41 respectively. The core is made up of polymethacrylate and a thin layer of fluorinated polymer serves as the cladding material [27]. To prepare the sensor head, a 2 cm of the jacket of a plastic fiber is removed and the cladding from exposed region is removed using a blade. Finally the sensor head is washed thoroughly in water and inserted into a glass vessel having inlet and outlet provisions. The sensor is glued to a vessel so that the sensor remains intact inside the vessel and becomes immune to physical vibrations.

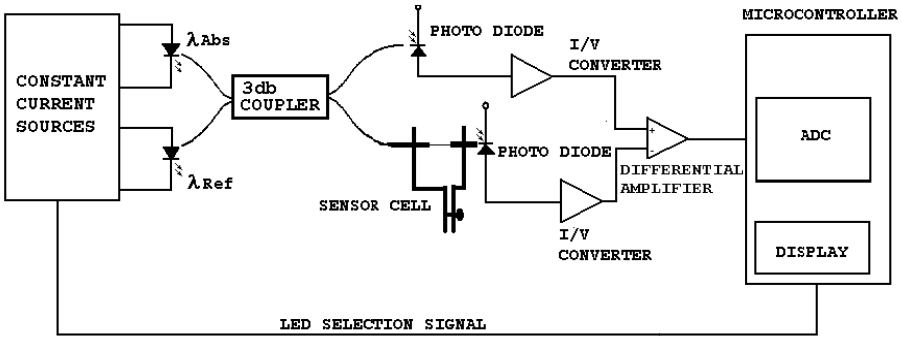

Figure 2.1 Experimental setup for dual wavelength probing

2.6 Results and discussions

In order to validate the dual wavelength probing scheme, measurements are carried out initially with $KMnO_4$ solution. Then it is used for the determination of silica traces in water.

2.6.1 Evaluation of dual wavelength probing with $KMnO_4$ solution

Sample solution aqueous $KMnO_4$ solution is prepared from 2ppm to 20 ppm. The absorption spectrum of $KMnO_4$ solution is shown in figure 2.2, which is determined with the help of spectrophotometer (Carry5000) and it is compatible with that of literature [28]. The solution has five absorption peaks with in this range, which accounts for the undulations in the spectrum. The suitable analytical wavelength and non absorbing wavelengths are determined from this spectrum. The analytical wavelength is chosen as 538nm since it corresponds to the absorption peak and non absorbing wavelengths chosen are 640nm or 426 nm.

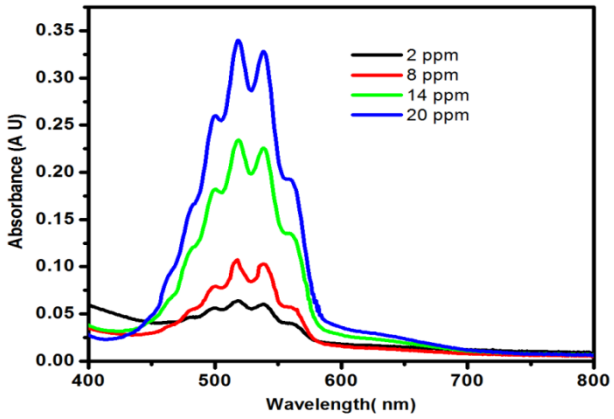

Fig 2.2 Absorption of $KMnO_4$ for different concentrations

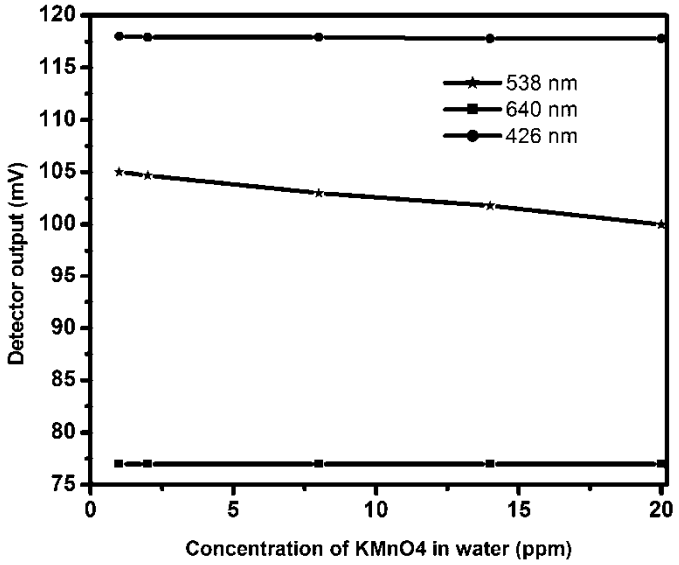

Figure 2.3 Response of the Detector for different wavelengths

The LED corresponding to the wavelength discussed above are identified and it is used for the experiment. All the three LEDs are connected separately and the transmitted power at PD_1 is measured. The response of PD_1 is plotted in figure 2.3. Initially the lowest concentration of $KMnO_4$ is filled in the sensor cell and the digital read out for analytical (538 nm) and non absorbing wavelength (640 nm) is measured. Then the cell is emptied and the next higher concentration is filled in the cell and the experiment is repeated for all available concentrations. The same experiment is repeated with the other non absorbing wavelength (426 nm). In figure 2.3 as the concentration of $KMnO_4$ increases from 2ppm to 20ppm the detector output power decreases for all the three probing wavelengths (523nm, 426 nm & 640nm). This is due the change in refractive index of the solution, as

in equation (2.15) & (2.16). A closer analysis of the graph reveals that the decrement in output power is significant in the case of 538nm, which is the analytical wavelength for $KMnO_4$ solution. At the same time the change in the output power for non-absorbing wavelength, 640 and 420nm is very small. As the concentration of KMnO4 increases the output power decreases due to absorbance and refractive index variation. This response of the sensor supports the proposed theory of utilizing dual wavelength probing.

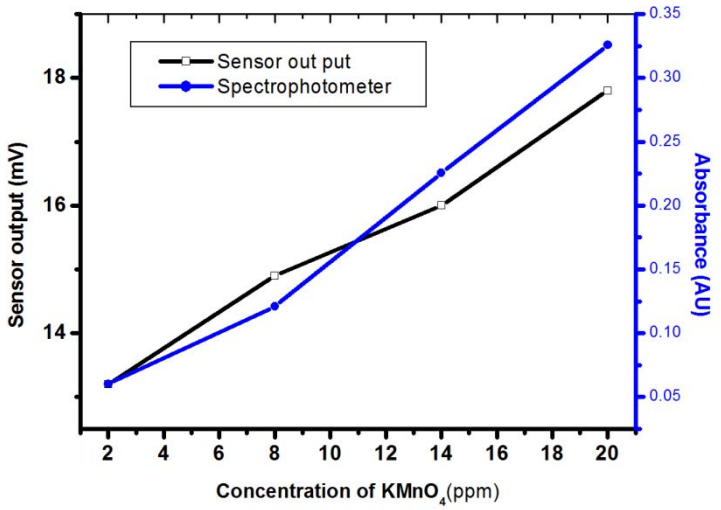

Figure 2.4 Response of the Spectrophotometer and sensor for different concentrations of $KMnO_4$

The dual wavelength probing scheme is connected and the concentration of $KMnO_4$ is estimated for concentration ranging from 2 ppm to 20 ppm and it is plotted in figure 2.4. The response of the dual wavelength sensor is linear and power increases from13.5mV to 18mV.The absorbance of the solution determined with spectrophotometer (Cary 5000), is also plotted. The sensor output and

the absorbance of the solution vary linearly with concentration of $KMnO_4$. The experiment is repeated many times and the same results are observed. This result also supports dual wavelength probing.

2.6.2 Trace analysis of silica in water

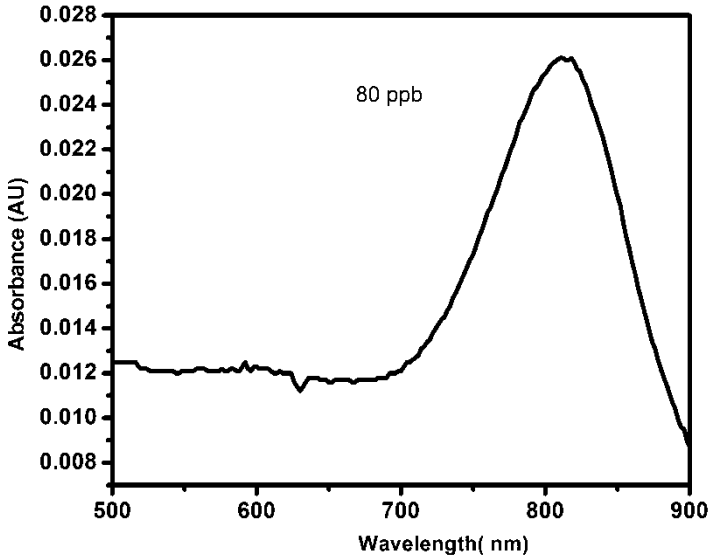

Figure 2.5 Absorption of Silica in water (80 ppb)

The absorption spectrum of silica in water is measured and it is depicted in figure 2.5. For determining the concentration of silica in water, the wavelengths are selected from absorption spectrum. The absorbing wavelength corresponding to the absorption peak is 815 nm and non absorbing wavelength can be from 700 nm to 500 nm. Red LED which has emission peak at 640nm is selected as non absorbing wavelength. The sample solutions of silica are prepared from 20 ppb to 1000 ppb. The measurements are carried out using the dual wavelength probing scheme and it is plotted in figure 2.6. The linear results in the measurement of silica concentration in water are

observed in this range and the sensitivity is 0.05 mV/ppb. The concentration is estimated with spectrophotometer and the results are found to be matching and it is also shown in figure 2.6. A photograph of the experimental set up is shown in figure 2.7.

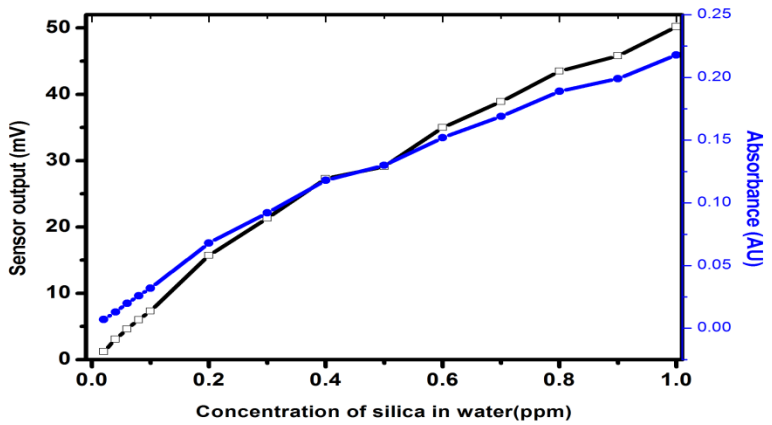

Fig 2.6 Response of the sensor and spectrophotometer for different concentrations of silica

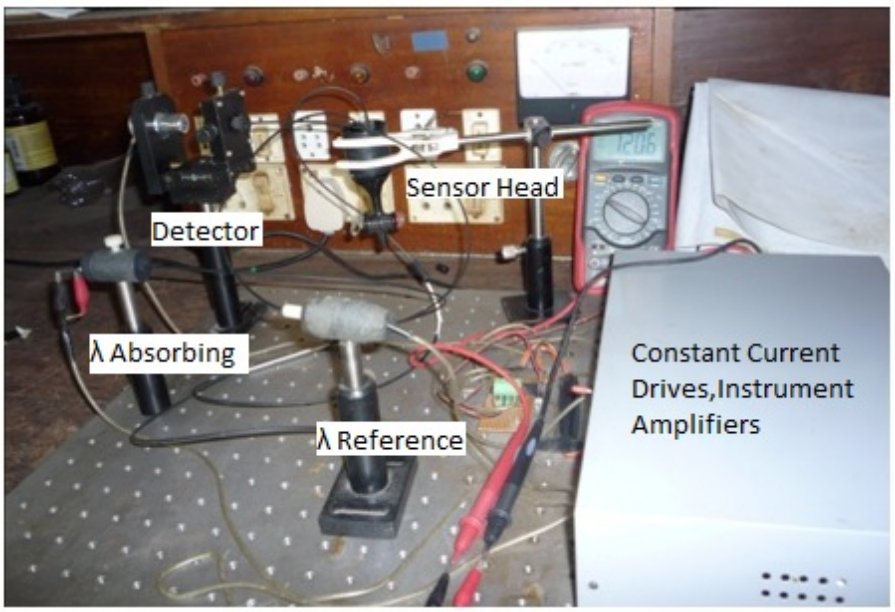

Figure 2.7 The photograph of the experimental set up

The water samples from the low pressure drum and high pressure drum of a power plant is collected, mixed with reagent and its photograph is given in figure 2.8 (a) & (b). The performance of the developed sensor is compared with that of spectrophotometer in the table 1.

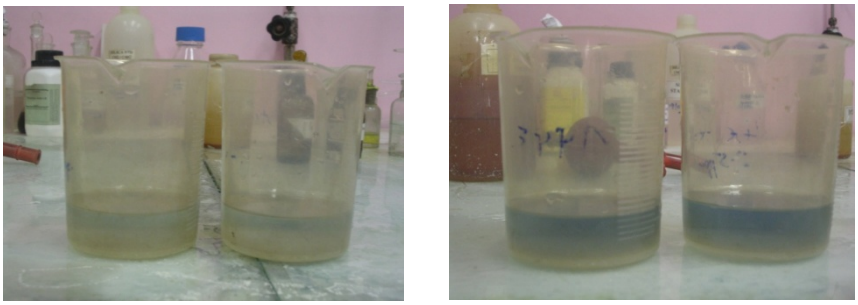

Figure 2.8 (a) Silica Sample of LP drum 1&2 (b) Silica Sample of HP drum 1&2

Table: 1 Comparison of spectrophotometer and the device output

Silica Sample location	Concentration estimated using Spectrophotometer (ppm)	Concentration estimated using dual wavelength sensor (ppm)
Lp drum 1	0.9	0.91
Lp drum 2	0.8	0.84
Hp drum 1	0.3	0.28
Hp drum 2	0.2	0.24

2.7 Conclusion

A sensitive and useful design of dual wavelength probing scheme for evanescent wave based fiber optic sensor has been developed and used to measure the concentration of silica in water. Dual wavelength probing makes the design more reliable, repeatable and portable. This design makes the sensor employable for

concentration, chemical content and adulteration level monitoring in industries or any such needy environments. Use of low cost components makes the system cost effective and simple.

References

[1] B. D. Gupta, Fiber optic sensors principles and applications, New India publications, New Delhi, Ch. 5, p 59, 2006.

[2] Shizhuo Yin, B. Paul, Ruffin Francis and T. S. Yu, Fiber Optic sensors, CRC Press, New York, Ch.1, p 2, 2008.

[3] Bishnu P. Pal, Fundamentals of fiber optics in Telecommunication and Sensor systems, New age International, New Delhi, Ch. 22, p 548, 1997.

[4] W. R. Seitz, Chemical sensors based on fiber optics, Anal. Chem., **56**, 16, 1984.

[5] K. M. Leonard, Development of a fiber optic chemical sensor for multi contaminant monitoring of environmental systems, Sensor. Actuat. B, **24**, 458, 1995.

[6] J. Burck, J. P. Conzen, B. Beckhaus and H. J. Ache, Fiber optic evanescent wave sensor for in situ determination of non polar organic compound in water, Sensor. Actuat. B, **18**, 291, 1994.

[7] A. Rogers, Distributed optical –fiber sensing, Meas. Sci. Technol., **10**, 75, 1999.

[8] S. M. Klainer, J. R. Thomas and J. C. Francis, Fiber–Optical sensors offer a realistic solution to environmental monitoring needs, Sensor. Actuat. B, **11**, 81, 1993.

[9] S. Thomas Lee, P. Suresh Kumar, K. P. Unnikrishnan, V. P. N. Nampoori and C. P. G. Vallabhan, Evanescent wave fiber optic sensor for trace analysis of Fe^{3+} in water, Measurement Science and Technology, **14**, 858, 2003.

[10] T. Lee, A. G. Nibu, P. Suresh kumar, P. Radhakrishnan, C. P. G. Vallabhan and V. P. N. Nampoori, Chemical sensing with micro bend optical fibers, Opt. Lett., **26**, 1541, 2001.

[11] B. D. Guptha and S. K. Khijwania, Experimental studies on the response of the fiber optic evanescent field absorption sensor, Fiber Integr. Opt., **17**, 63, 1998.

[12] J. Mendham, R. C. Denny, J. D. Barns and M. J. K. Thomas, VOGEL'S Text Book of Quantitative Chemical Analysis, Pearson Education, London, Sixth Edition, 2007.

[13] K. T. V. Grattan and B. T. Meggitt, Optical Fiber Sensor Technology, Kluwer Academic Publishers, London, Ch. 6, p 338, 2000.

[14] Ramakant Srivastava, Carmen Bao and Carls Gomez- Reino, Planar-surface-waveguide evanescent-wave chemical sensors, Sensor. Actuat. A, **51**, 165, 1996.

[15] P. Suresh Kumar, C. P. G. Vallabhan, V. P. G. Nampoori and V. N. Sivasankara Pliiai, A fiber optic evanescent wave

sensor used for the detection of trace nitrites in water, J. Opt. A: Pure. Appl. Opt., **4**, 247, 2002.

[16] V Ruddy, B. D MacCraith and J. A. Murphya, Evanescent wave absorption spectroscopy using multimode fibers, J. Appl. Phys., **67**, 10, 1990.

[17] Pabitha Nath, Enhanced sensitive fiber optic sensor with double pass evanescent field absorption, Microw. Opt. Techn. Let., **51**, 12, 2009.

[18] B. Culshaw, F. Muhammad, G. Stewart,S. Murray, D. Pinchbeck, J. Norris, S. Cassidy, M. Wilkinson, D. Williams, I. Crisp, R. Van Ewyk and A. McChee, Evanescent wave methane detection using optical fibers, Electron. Lett., **28**, 2232, 1992.

[19] K. Taga, B. Mizaikoff and R. Kellner, Fiber optic evanescent field sensors for gaseous species MIR transparent fibers, J. Anal. Chem., **348**, 556, 1994.

[20] J. Heo, Monica Rodrigues, Steven J. Saggese, George H. Sigel and Jr., Remote fiber optic chemical sensing using evanescent wave interactions in chalcogenide glass fibers, Appl. Opt., **30**, 3944, 1991.

[21] B. D. Gupta, Fiber optic sensors principles and applications, New India publications, New Delhi, Ch.5, p 60, 2006.

[22] Gerd Keiser, Optical fiber Communications, McGraw Hill, Ch. 2, p 61 2003.

[23] S.C. Guptha, Optoelectronic devices and systems, Prentice-Hall of India, Ch. 1, p 20, 2005.

[24] J. Mendham, R. C. Denny, J. D. Barns and M. J. K. Thomas, VOGEL'S Text Book of Quantitative Chemical Analysis, Pearson Education, New Delhi, Sixth Edition, 2007.

[25] American Public Health Association, A W W A and W E F, Standard methods for the Examination of water and waste water, 21st Edition, Ch. 4, p 122, 2005.

[26] Joseph C. Palais, Fiber Optic Communications, Pearson Education Asia, Ch 8, p 209, 2001.

[27] M. Sheeba and P. Radhakrishnan, Fiber optic sensor for detection of adulterant traces in coconut oil, Meas. Sci. Technol, **16**, 2247, 2005.

[28] A. M. Taylor, Band Spectrum of $KMnO_4$ in the crystalline state and in solution, Transactions of Faraday Science, **25.** p860,1929

****

Chapter 3

CONCENTRATION MEASUREMENTS OF AMMONIA, PHOSPHATE AND IRON IN WATER

Contents

The developed dual wavelength evanescent fiber optic sensing method is employed for trace analysis of Ammonia, Phosphate and Iron in water.

3.1. Introduction

Accurate measurement of chemical species in water is of great practical significance in water treatment plants and other similar industries. The water quality analysis at different locations of the plant is usually carried out by spectrophotometric methods. Water samples from different locations are subjected to chemical reactions and are analysed for different chemical species like ammonia, phosphate, iron etc. The final analysis using spectrophotometer is costly and the device is bulky too. Use of optical fiber based sensors provides an easy, quick and accurate method to measure the water quality.

Interest in opto-chemical sensors has been growing rapidly in recent times. The direct spectroscopy measures the characteristic absorption spectra of the analyte, whereas chemically mediated spectroscopy indirectly measures the spectral changes of the solution when interacting with the analyte under investigation. Chemically mediated spectroscopy provides better sensitivity and selectivity than direct technique [1]. Using a fibre optic evanescent wave sensing technique the bulky spectrophotometers can be replaced with simpler interrogators with narrow band optical sources. Compared to other sensing methods, evanescent wave sensing technique provides several advantages [2, 3]. The evanescent wave fiber optic chemical sensors reported in literature mostly employ single wavelength probing [4-7]. In the present system with dual wavelength probing, the distortion of the signal, due to fiber bending and source fluctuations are reduced using a reference signal. A non-absorbing narrow band source is used for the compensation of other contributing losses like turbidity and refractive index which will enhance the repeatability aspect of the sensor [8].

We have used a fiber optic evanescent wave sensor with dual wavelength probing for better selectivity, sensitivity and repeatability in chemical sensing. The developed sensor is employed for the measurement of concentration of Iron, Ammonia and Phosphate in water.

3.2Theory

In evanescent wave based fiber optic sensors the sensing region is developed by either completely or partly removing the cladding for a short length. The light radiation that leaves the core at the sensing region can undergo several modifications. It can produce attenuated total internal reflection (ATIR) depending on the refractive index of the medium surrounding the exposed region. The radiation may get absorbed by the surrounding species if the operating wavelength is same as that of the peak absorption wavelength called analytical wavelength of the species. The absorption and scattering due to other contributing losses like interferences and turbidity. The effects mentioned above are responsible for the modulation of light intensity through an evanescent wave sensor. The first and third effect is present in all evanescent wave sensors and the second effect will come into play only if the operating wavelength is the analytical one for the given species.

So whenever an evanescent wave based fibre optic sensor is employed for chemical sensing, it is always advisable to use an analytical wavelength as the probing tool.

The power through the core of the fiber after the sensing region is [10, 11]

$$P_{core} = P_T - P_T \frac{0.3\ \lambda}{a(n_1^2 - n_2^2)} - P_T.A \qquad (3.1)$$

Where 'P_{core}' is the power through the core, 'P_T' is the total power injected into the fiber. 'λ' is the probing wavelength, 'a' is the core radius and 'n_1'and 'n_2' are the refractive indices of the core and cladding of the fiber used . 'A' is the absorbance of the species surrounding the exposed region of the sensor, which can be explained with the help of Beer's law for absorbing solutions. It states that the absorbance is directly proportional to concentration of the solution and the path length for light travel through the species is as given in equation:

$$A \propto b.C$$

Where 'b' is the path length of light travel and 'C' is the concentration of the species. Absorbance can be written as

$$A = \varepsilon.b.C\,, \qquad (3.2)$$

'ε' is the absorptivity, a constant that does not depend on concentration.

In a fibre optic sensor, if equal amount of samples are added for every measurement, the value of 'b' can be kept constant.

Hence $A \propto C$

Since we are taking the differential signal of the same source, source fluctuations can be eliminated. From expression (3.1), the second term corresponds to the contribution of index dependant power variation, which will be the same for absorbing and reference wavelength as explained in chapter 2. The contribution due to turbidity and interferences will also be the same for both wavelengths.

It is possible to select analytical wavelength and non-absorbing reference wavelength from the absorption spectrum of the solution under study. The analytical wavelength is selected in such a way that it corresponds to the absorption peak of the solution. The non-absorbing reference wavelength is chosen to be sufficiently away from the absorption peak, ensuring that it has very little absorption in comparison with analytical wavelength. In order to take the reference signal a 3db coupler is used.

To have a quantitative analysis of concentration / chemical content level, it is better to have a system capable of dual wavelength probing arrangement. In this scheme, one wavelength should be the analytical wavelength for the species under consideration and the second wavelength should be a non-absorbing one. The difference of output power in absorbing and non-absorbing wavelengths will be the contribution due to the absorption of the given chemical content in water. However in the case of mixtures with overlapping absorption bands the present approach cannot be used in a manner that will distinguish the contaminants.

3.3 Experimental Details

The experimental setup is as shown in figure 3.1, which consists of different LED sources, a 3dB fibre optic coupler and a pair of source to fibre coupler. The exposed area of the sensor (contact area) is 2 cm long. Light injected into the sensor is measured at the receiving end by two PIN photodiodes. The plastic multimode fibre used for the present study is a step index with core diameter of 980

μm and NA of 0.5. The refractive indices of the core and the cladding are 1.49 and 1.41 respectively. The core is made up of polymethacrylate and a thin layer of fluorinated polymer serves as the cladding material. A detailed discussion of experimental details is given in section 2.5.2.

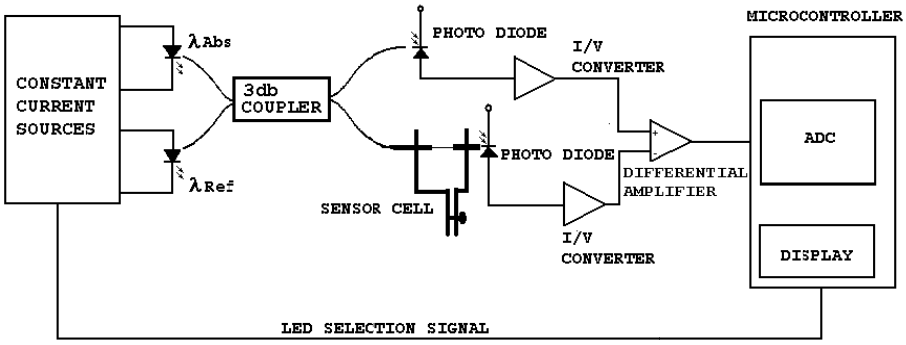

Figure 3.1 Experimental setup for dual wavelength probing to estimate the traces of ammonia, phosphate and iron in water.

3.3.1 Measurement Method

For the quantitative analysis, the source corresponding to analytical wavelength is switched on and the output of the analog to digital converter $(PD_1\text{-}PD_2)_1$ is recorded. This corresponds to the power loss due to refractive index, spectral absorption, and other contributing losses. This data is stored and the LED is switched off. The source corresponding to the non-absorbing reference wavelength is then switched on and the output data $(PD_1\text{-}PD_2)_2$ is taken. This reading will be the power loss due to refractive index variation, and other contributing losses. $(PD_1\text{-}PD_2)_1$ - $(PD_1\text{-}PD_2)_2$ is calculated to get the contribution due the absorbance of the given species in water. The power loss due to refractive index and other contributing losses like

interferences and turbidity will be almost same for both the wavelengths. Hence $(PD_1\text{-}PD_2)_1$ - $(PD1\text{-}PD2)_2$ will be proportional to the power due to spectral absorption of the given species in water.

3.3.2. Preparation of reagents and standard solutions

An intermediate reagent which reacts with the analyte forms an absorbing solution. The preparation of the reagents is detailed below.

Iron: Soluble iron in ground water is usually in the ferrous state. On exposure to air, ferrous iron is oxidised in to the ferric state (Fe^{3+}) and may hydrolyse to form red, insoluble hydrated oxide. Elevated iron levels in water can cause stains in plumbing, laundry and cooking utensils and can impart objectionable tastes and colour to food. The United Nations Food and Agriculture Organisation recommended the level for irrigation waters is 5mg/L. The U.S EPA drinking water standard MCL is 0.3mg/L.

To study the iron content, water sample is reduced with hydroxylamine hydrochloride and then reacted with bathophenanthroline (4.7-diphenyl-1, 10phenanthroline). The red ferrous complex is extracted with n-hexly or isoamly alcohol [12].

Reagent preparation for Iron

Bathophenanthroline Solution (0.835gm/L): Dissolve 0.835 gm of Bathophenanthroline in 100ml of ethyl alcohol.

Hydrochloric Acid: Mix equal volumes of hydrochloric acid (sp.gr.1.19) and water.

Iron standard solution: Dissolve 0.1 gm of pure iron in 10ml of hydrochloric acid and 1ml of bromine water. Boil to remove excess bromine. Add 200ml of hydrochloric acid, cool and dilute to 1 litre with water. Add 10 ml of this solution to 12ml of hydrochloric acid and dilute to 1 litre with water. In order to prepare standard solution of 1ppm, dissolve 0.1g of pure iron in10 ml of hydrochloric acid and 1 ml of bromine water. The solution is boiled to remove excess bromine and add 200 ml of hydrochloric acid. Allow the solution to cool and dilute to 1 litre with water. Take 10 ml of this solution and add 12 ml of hydrochloric acid and dilute to 1 litre with water. Add sufficient quantity of water to prepare solutions of desired concentrations.

Phosphate

Phosphorus occurs in natural waters and waste waters as phosphates. These are classified as orthophosphates, condensed phosphates, and organically bound phosphates. Here the concentration of dissolved orthophosphates in water is determined. To estimate the phosphate content Sample water is reacted with ammonium molybdate in an acidic medium and the resulting phosphomolybdate is reduced to molybdenum blue complex with amino- naphthol –sulphonic – acid [13].

Reagent Preparation for phosphate

ANSA solution: Dissolve 3.7 g of sodium sulphate (Na_2SO_3)in 100ml of water**.** Add 0.1 g of 1-amino-2-napthol-4 sulphonic acid and 6.2 g of sodium metabisulphite($Na_2S_2O_5$).

Ammonium Molybdate Solution: Dissolve 48g of ammonium molybdate in 800ml of water. Add 25ml of ammonium hydroxide (sp. Gr. O.9) and dilute to 1 litre with water. In order to prepare Phosphate stock solution of 100ppm, dissolve 0.1433 g of potassium dihydrogen phosphate (KH_2PO_4), dried at 105^0Cfor 1 hour, in water and dilute it to 1 litre. Dilute 10ml of this stock solution with 100 ml of water to prepare standard solution of 10ppm. The absorbing wavelength and the non-absorbing wavelength are determined to be 645 nm and 815 nm respectively from the absorption spectrum of sample solutions.

Ammonia

Ammonia is present naturally in surface and waste waters. The Nessler's reagent is employed for the determination of Ammonia in water [14]. To study the ammonia content, the water sample is reacted with Nessler's reagent (K_2HgI_4) to produce a reddish brown colloidal compound. In order to prepare the standard solution of 10 ppm, dissolve 4.718 g of ammonium sulphate [$(NH_4)_2SO_4$] in water and dilute to 1 litre. Dilute 10 ml of this solution to 1 litre. The absorbing wavelength and the non-absorbing wavelength are determined to be 425 nm and 640 nm respectively from the absorption spectrum of sample solutions.

Reagent Preparation Ammonia

Dissolve 100g of anhydrous mercuric iodide (HgI_2) and 70g of anhydrous potassium iodide (KI) in small volume of water. Add this mixture slowly with stirring, to a cooled solution of 160g of sodium hydroxide in 500ml of water. Dilute the mixture to 1 litre. Store the

solution in dark for 5 days and filter twice before using .This has a shelf life of one year.

3.4 Results and discussions

The reagents and standard solutions of iron, phosphate and ammonia are prepared and the dual wavelength evanescent wave sensor is utilised for sensing the traces of these components in standard solutions as well as in the boiler feed water of a power plant. The probing wavelengths are selected from the absorption spectrum of each species.

3.4.1 Iron

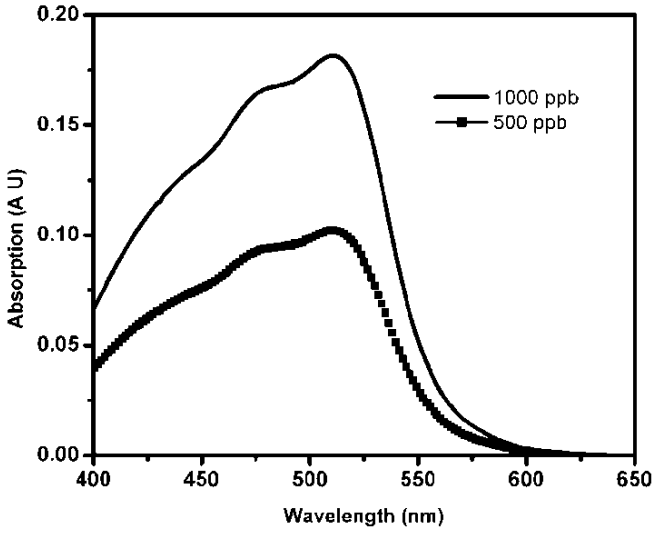

Figure 3.2 Absorption of Iron in water (1000 ppb and 500ppb)

The absorption spectrum of Iron is shown in figure. 3.2. The probing wavelengths are selected from the absorption spectrum. 510 nm corresponding to the absorption peak is selected as the analytical

wavelength and 640 nm is selected as the non-absorbing reference wavelength since the absorption at this particular wavelength is very small. The sensor output corresponding to Iron concentration in water from 100 ppb to 1000 ppb is given in the figure. 3.3. The respective result obtained using spectrophotometer is also shown in figure.The sensor showed good repeatable, linear results in the measurement of iron concentration in water from 100 ppb to 1000 ppb as shown and the sensitivity of measurement is 5.8 μV/ppb. Water samples from a power plant is collected and checked with the developed sensor. The results are found matching with the spectrophotometer results and it is depicted in table 3.1.

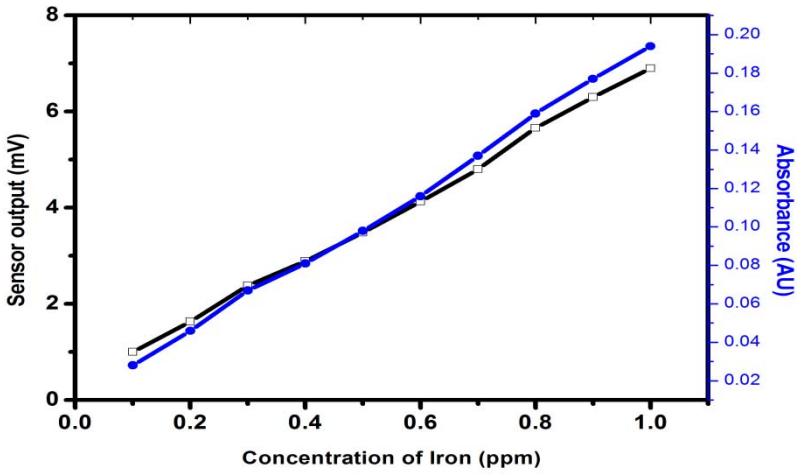

Figure 3.3 The response of spectrophotometer and sensor for different concentration of Iron in water

Table 3.1 The comparison of spectrophotometer and the concentration estimated from dual wavelength evanescent wave sensor for iron

Sample location	Concentration estimated with spectrophotometer (ppm)	Concentration estimated from the developed instrument (ppm)
LP Drum 1	0.18	0.18
LP Drum2	0.19	0.20
Hp Drum 1	0.22	0.23
Hp Drum 2	0.25	0.26

3.4.2 Phosphate

From the absorption spectrum of phosphate solution the absorbing wavelength is chosen as 645 nm and a non absorbing wavelength as 815 nm is selected.

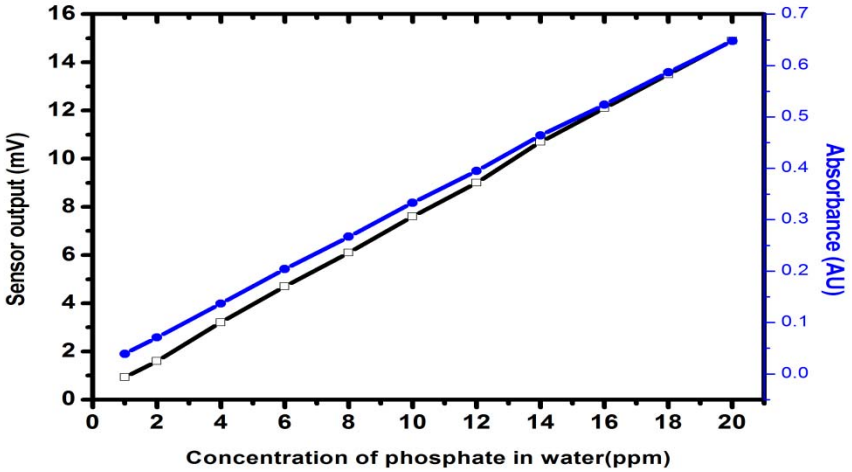

Figure 3.4 The response of spectrophotometer and sensor for different concentration of Phosphate in water.

Spectrophotometric and sensor response of Phosphate sample for a concentration range of 1ppm to 20ppm are given in figure. 3.4. Absorption of the sample increases from 0.039 to 0.65 as the

concentration varies from 1ppm to 20 ppm. At the same time as the concentration varies from 1ppm to 20 ppm, the sensor output increases from 1.37mV to 14.9mV. The sensitivity observed is 0.72 mV/ppm. The spectrophotometric results and the sensor output has one to one correspondence and they are linear within the range. The water samples from the different locations of a power plant are collected to evaluate the performance of the developed sensor and it is depicted in the table 3.2.

Table 3.2 The comparison of spectrophotometer and the concentration estimated from dual wavelength evanescent wave sensor for phosphate

Sample location	Concentration estimated with spectrophotometer (ppm)	Concentration estimated from the developed instrument (ppm)
LP Drum 1	17.5	17.48
LP Drum2	20	19.5
Hp Drum 1	6.5	6.52
Hp Drum 2	6.4	6.38

3.4.3 Ammonia

From the absorption spectrum of the ammonia solution, 425nm and 640 nm are selected as the absorbing and non absorbing wavelengths respectively. Figure. 3.5 represents the spectrophotometric and sensor response for Ammonia sample. Here as the concentration increases from 100 ppb to 600 ppb, the absorption of the sample increases from 0.025 to 0.090. Since the absorption is very low, the response of the fiber optic sensor is found to vary from 0.9mV to 3.2mV. From this graph it is evident that as the concentration of the sample increases from100

ppb to 600 ppb, the output of the sensor and the spectrophotometer is almost matching and shows linear response. The sensitivity of the sensor is 5.6 μV/ppb. The water samples from different locations of a power plant is collected and estimated the concentration of the sample using the spectrophotometer and the developed sensor. The results obtained are shown in table 3.3.

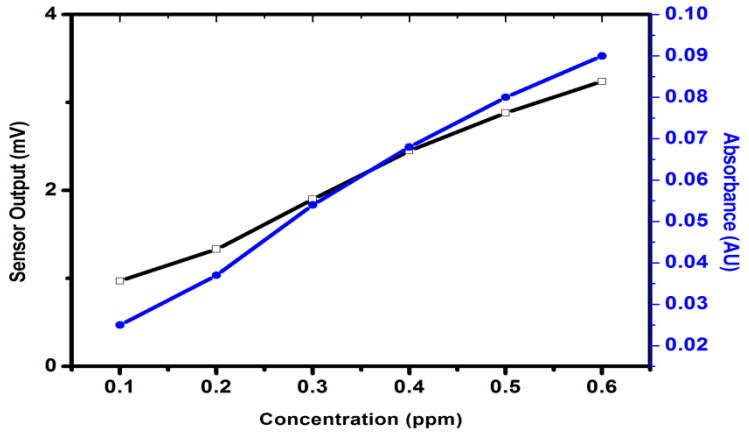

Figure 3.5 The response of spectrophotometer and Sensor for different concentration of Ammonia in water.

Table 3.3 The comparison of spectrophotometer and the concentration estimated from dual wavelength evanescent wave sensor for ammonia

Sample location	Concentration estimated with spectrophotometer (ppm)	Concentration estimated from the developed instrument (ppm)
LP Drum 1	0.45	0.455
LP Drum2	0.55	0.552
Hp Drum 1	0.32	0.324
Hp Drum 2	0.38	0.379

3.5 Conclusion

A sensitive and useful design of dual wavelength probing scheme for evanescent wave based FOS has been developed. The developed sensor is used for the measurement of traces of dissolved iron, ammonia and phosphate in water. The use of dual wavelength probing scheme for fiber optic evanescent wave sensor enhanced selectivity and repeatability. Moreover this design makes use of low cost components which makes the system cost effective, simple and portable. The comparative evaluation between the sensor output and spectrophotometric analysis bears a one to one correspondence. Hence this system can be employed for water sample analysis at a much simpler and cheaper manner in such needy environments.

References

[1] A. G. Mignani and A. A Mencaglia., Chemically mediated absorption spectroscopy using optical fiber instrumentation, IEEE Sens. J., **2**, 52, 2002.

[2] B. D. Gupta, Fiber optic sensors principles and applications, New India publications, New Delhi, Ch. 5,p 62 2006.

[3] J. Biirck, J. P. Conzen and H. J. Ache, A fiber optic evanescent field absorption sensor for monitoring organic contaminants in water, J. Anal. Chem., **342**, 394, 1992.

[4] S. Thomas Lee, P. Suresh Kumar, K. P Unnikrishnan, V. P. N. Nampoori and C. P. G. Vallabhan, Evanescent wave

fibre optic sensor for trace analysis of Fe^{3+} in water, Meas. Sci. and Technol., **14**, 858, 2003.

[5] T. Lee, A. G. Nibu, P. Suresh kumar, P. Radhakrishnan, C. P. G. Vallabhan and V. P. N. Nampoori, Chemical sensing with microbend optical fibers, Opt. Lett., **26**, 1541, 2001.

[6] M. Sheeba and P. Radhakrishnan, Fiber optic sensor for detection of adulterant traces in coconut oil, Meas. Sci. Technol., **16**, 2247, 2005.

[7] P. Suresh Kumar, C. P. G. Vallabhan, V. P. N. Nampoori, V. N. Sivasankara Pillai and P. Radhakrishnan, A fibre optic evanescent wave sensor used for the detection of tracenitrites in water, J. of Opt. A: Pure and Appl. Opt., **4**, 247, 2002.

[8] D. Izquierdo, M. Puyol, I. Salinas, R. Alonso, J. Alonso, C. Dominguez and I. Garces, Dual-wavelength measurement system for absorbance chemical sensing, Meas. Sci. Technol., **18**, 3443, 2007.

[9] J. Mendham, R. C. Denny, J. D. Barns andM. J. K. Thomas, VOGEL'S Text Book of Quantitative Chemical Analysis, Pearson Education, London, Sixth Edition, 2007.

[10] Gerd Keiser, Optical fiber Communications, McGraw Hill, New York, Ch. 2, p 33 2003.

[11] Benjamin Varghese P., Satish John and K.N. Madhusoodanan, Fiber optic Sensor for the measurement of

concentration of silica in water with dual wavelength probing, Rev. Sci. Instrum., **81**, 035111-1-5, 2010

[12] American Public Health Association, A W W A and W E F, Standard methods for the Examination of water and waste water, 21st Edition, Ch. 3, p 77, 2005.

[13] American Public Health Association, A W W A and W E F, Standard methods for the Examination of water and waste water, 21st Edition, Ch. 4, p 152, 2005.

[14] J. Mendham, R. C. Denny, J. D. Barns and M. J. K. Thomas, VOGEL'S Text Book of Quantitative Chemical Analysis, London, Pearson Education, Sixth Edition, Ch. 17, p 691, 2007.

****

Chapter 4

STRAIN AND TEMPERATURE MEASUREMENT USING FBG SENSOR

Contents

FBG sensors are characterized for strain and temperature measurements using simulations and experiments.

4.1 Introduction

The UV inscribed fiber gratings are widely used for Wavelength Division Multiplexing (WDM) filters, gain equalizers for erbium doped fiber amplifiers (EDFA) and dispersion compensators for high speed communications. The strain and temperature sensitivity of Fiber Bragg Grating (FBG) encouraged the growth of sensing applications based on grating sensor systems and devices. The FBG sensors are very useful sensing element for structural health monitoring [1, 2]. FOS have many advantages over conventional electrical sensors like resistance to corrosion and fatigue, small size

and light weight, immunity to electromagnetic disturbances [3-5] etc. Compared to other fiber optic sensors, FBG sensors have many advantages. The signal obtained from a FBG sensor is encoded directly in wavelength domain hence the source intensity fluctuations will not affect the measurements. Insensitivity to fluctuations, multiplexing, distributed sensing etc are the key advantages [6-8]. The FBG strain sensor arrangement is suitably modified to measure pressure [9, 10], displacement [11, 12], bend [13, 14], flow [15], level [16] etc.

This chapter deals with the measurement and study of FBG sensors for strain and temperature measurement. The MATLAB is used for simulating and optimising the performance of the measurements. In order to study strain, a cantilever structure made of spring steel is used. The FBG is pasted to the structure using a commercially available fast setting epoxy. Initially the temperature is maintained at 22^0C and the measurements are taken. In order to find the hysteresis of measurement the reflected spectrum is measured during unloading also. The experimental setup is housed in a chamber and the temperature is varied. The measurements are taken at 30, 35 and 40^0C.The drift of strain due to temperature is measured. A temperature controlled water bath is used for the temperature measurement. The FBG is immersed in the water bath and the reflected spectrum is noted for every 10^0 C rise in temperature. The variation of wavelength for every 1^0C rise in temperature is noted from 50 to 55^0C. The water bath was allowed to cool naturally and

reflected spectrum is measured to measure the hysteresis of the measurement.

4.2 Theory of FBG

Guided optical fiber modes can be classified into two types. One type belong to core modes, that are totally reflected at the core–cladding boundary (in terms of ray optics) and are bounded in the core region. The other is, cladding modes that are totally reflected at the cladding–air (surrounding medium) boundary and are bounded in cladding and core regions. The ray-optic illustration of the guided modes, which include the core and cladding modes, is shown in figure. 4.1.

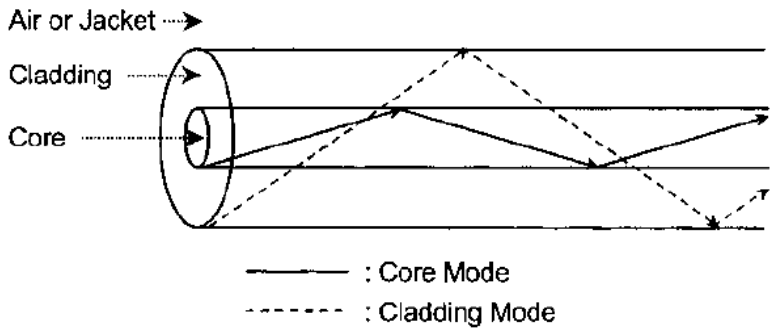

Figure 4.1 Ray-optic illustration of the guided modes

In fact, if there are some perturbations in the fiber, the modes can get coupled. The main coupling directions can be determined as contra directional or co directional based on whether the traveling directions of modes coupled to each other are opposite or the same. Based on the direction of the mode coupling, fiber gratings can be classified in two types. One type is a short-period or reflection grating,

where coupling occurs between modes traveling in opposite directions. The FBGs, chirped gratings, and tilted short-period gratings belong to this category. The other type is a transmission grating, represented by Long Period Fiber Bragg Gratings (LPFG), where coupling occurs between modes traveling in the same direction [17].

The intuitive illustration of mode couplings is shown in figure. 4.2, in which (a) illustrates a contra directional coupling for reflection-type gratings and (b) a co directional coupling for transmission-type gratings. By means of the refractive index perturbation, diffracted modes can be excited, as shown in figure. 4.2. For the diffracted mode to be accumulated constructively each diffracted radiation from the series of the perturbation should be in-phase; that is, the following equation should be satisfied:

$$\beta_i - (\pm\beta_d) = {}^{2\pi m}/_{\Lambda} \qquad (4.1)$$

Where β_i and β_d, respectively, are the propagation constants for the incident and diffracted modes, Λ is the period of the grating, and m stands for an integer number. It is noteworthy that a minus sign before the propagation constant describes the case wherein the mode propagates in the '-z' direction. The optical path difference between lights diffracted from the adjacent grating positions should be an integer multiple of the wavelength for a resonant coupling of modes, as in the case of a constructive interference in dielectric multilayer [18].

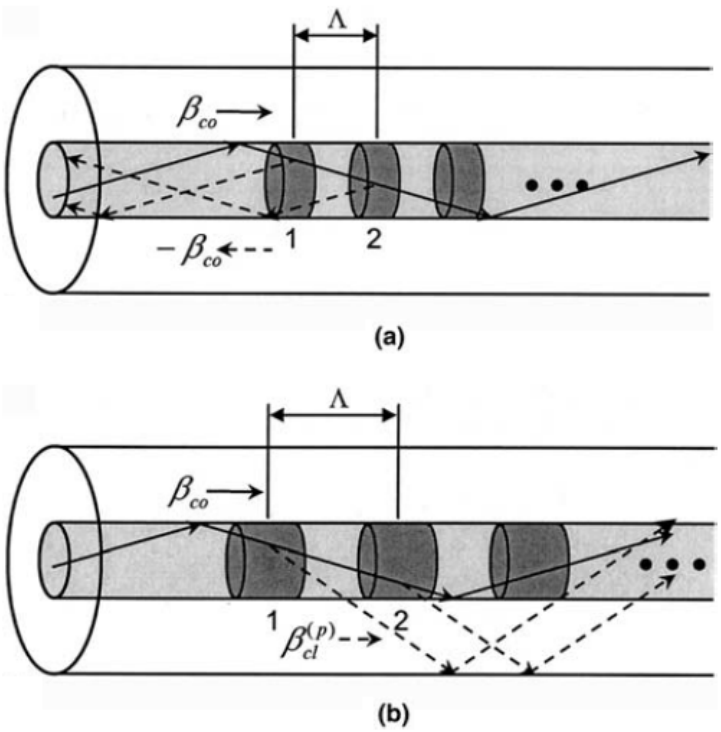

Figure 4.2 Illustration of mode couplings: (a) contra directional coupling; (b) co directional coupling

In most cases, first-order diffraction is dominant, and, hence, m is assumed to be unity [19]. Thus, the resonant wavelength can be obtained as follows:

$$\lambda = [n_{i,eff} - (\pm n_{d,eff})]\Lambda \tag{4.2}$$

In the case of a single-mode fiber, $n_{i,eff}$ and $n_{d,eff}$ can be the effective indices of both the core and cladding modes. In the case of contra directional coupling, the nominal Bragg wavelength of the core mode is given by

$$\lambda = 2\ n_{co,eff}\Lambda \tag{4.3}$$

where $n_{co,eff}$ is the effective index of the core mode. When the core mode becomes coupled to the counter propagating cladding mode, the $n_{d,eff}$ in Eq. (4.2) is given by the effective refractive index of a cladding mode with a minus sign, which is possible in the case of strong Bragg gratings and blazed gratings [20-22].

In the case of co directional coupling, the resonant wavelength for coupling between the core and cladding modes is given by [19]

$$\lambda = \left(n_{co,eff} - n_{cl,eff}^{p} \right)\Lambda \qquad (4.4)$$

where $n_{cl,eff}^{p}$ is the effective index of the pth cladding mode. The differences in effective indices between the core and cladding modes are much smaller than unity, and, hence, the grating period for co directional coupling at a given wavelength is much longer than that for contra directional coupling. Typically, the grating period for the co directional coupling is hundreds of micrometers in length [23].

4.3 Inscribing Bragg gratings in optical fibers

The phenomenon that enables the fabrication of FBG is ultraviolet (UV) photosensitivity, in which the index of refraction of germanium-silica core of an optical fiber is increased permanently through exposure to ultraviolet light. Photosensitivity of optical fibers is correlated with the concentration of GeO defects in the fiber core. The presence of this defect is responsible for the absorption at 240nm.The number of these defects increases with the concentration of Ge [24-27]. Increasing the concentration of defects increases the photosensitivity of optical fiber. The 240nm absorption is due to the

oxygen-deficient hole centre defect and indicates intrinsic photosensitivity. It is quantified as

$$K=\alpha_{242nm}/C \qquad (4.5)$$

where α_{242nm} is the absorption at 242nm and C is the molar concentration of GeO_2

Various techniques used in fabricating Bragg grating structures in optical fibers are discussed below. Depending on the fabrication technique Bragg gratings may be labelled as internally or externally written. Internal Bragg gratings are not considered very practical or useful. Externally written Bragg gratings inscribed using techniques such as Interferometric, point by point and phase mask overcome the limitations of internally written gratings and are considered far more useful. These inscription techniques were initially considered difficult, due to the sub-micron resolution and thus stability of the source. Today they are well controlled and the inscription of Bragg grating using these techniques is considered routine.

4.3.1 Interferometric method

The Interferometric fabrication technique which is an external writing approach for inscribing Bragg gratings in photosensitive fibers was first demonstrated by Meltz and co-workers [28]. In this experiment, an incident UV light beam was split into two beams that were subsequently recombined to form an interference pattern. The pattern is exposed to the photosensitive fiber, inducing a permanent refractive index modulation in the core.

The experimental set up of an interferometer is shown in figure 4.3. The UV radiation was split into two beams of equal intensity that were recombined to produce an interference pattern, normal to the fiber axis. A pair of cylindrical lenses focused light into the fiber.

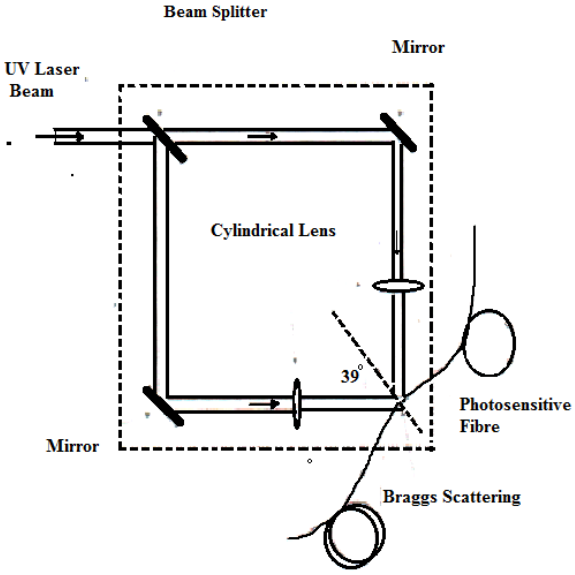

Figure 4.3 Interferometric method for inscribing grating

The most important advantage offered by this Interferometric technique is the ability to inscribe Bragg gratings at desired wavelength. This is accomplished by changing the intersecting angle between the UV beams. This method also offers complete flexibility for producing gratings of various lengths. The main disadvantage of this approach is the susceptibility to mechanical vibrations. Sub micron displacements in the position of the mirrors, beam splitter or other optical mounts in the interferometer during UV irradiation will cause the fringe pattern to drift and washing out the grating from the fiber. Furthermore, because the laser light travels along optical path

lengths, air currents which affect the refractive index locally. This can become problematic, degrading the formation of a stable fringe pattern. In addition to the above short comings, quality gratings can only be produced with laser source that has good coherence and excellent wavelength and output power stability.

4.3.2 Phase mask technique

One of the most effective methods for inscribing Bragg gratings in photosensitive fibers is the phase mask technique [29]. This method employs a diffractive optical element (phase mask) to spatially modulate the UV writing beam. Phase mask may be formed holographically or by electron – beam lithography. Holographically induced phase masks have no stitch error, which is normally present in the electron – beam phase mask. However, complicated patterns can be written into the electron-beam-fabricated masks. The phase mask grating has a one – dimension surface-relief structure fabricated in a high quality fused silica, transparent to the UV writing beam. The profile of periodic surface-relief grating is chosen such that when a UV beam is incident on the phase mask, the zero-order diffracted beam is suppressed to less than a few percent (typically less than 5%) of the transmitted power. In addition, the diffracted plus and minus first orders are maximized; each contain typically more than 35% of the transmitted power. A near field fringe pattern is produced by the interference of the plus and minus first order diffracted beams. The interference pattern photo-imprints a refractive index modulation in the core of a photosensitive optical fiber placed in contact with or in close proximity

to and immediately behind the phase mask. A cylindrical lens may be used to focus the fringe pattern along the fiber core.The Schematic is given in figure 4.4.

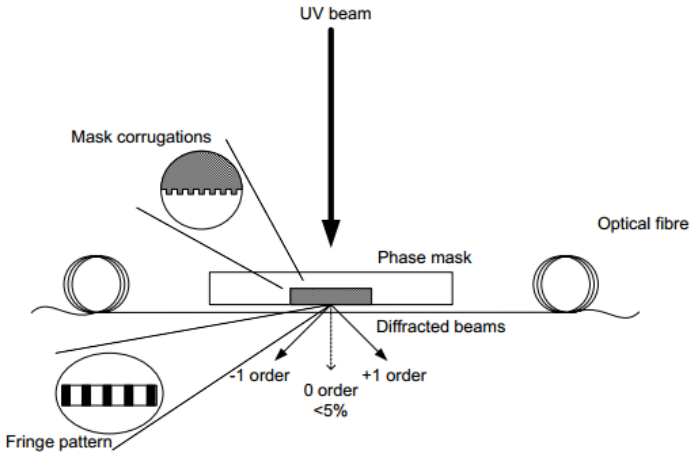

Figure 4.4 Production of FBG using phase mask method

The phase-mask greatly reduces the complexity of the fiber grating fabrication system. The simplicity of using only one optical element provides a robust and an inherently stable method for producing fiber Bragg gratings [30]. Since the fiber is usually placed directly behind the phase mask in the near field of the diffracting UV beams, sensitivity to mechanical vibrations and therefore stability problems are minimized. KrF Excimer lasers are most common UV sources used to fabricate Bragg gratings with a phase mask. The UV laser sources typically have low coherence. The low spatial coherence requires the fiber to be placed in the near contact to the grating corrugations on the phase mask in order to induce maximum modulation index of refraction. The farther the fiber is placed from the phase mask, the lower the induced index modulation, resulting in

lower reflectivity Bragg gratings. Clearly the separation of the fiber from the phase mask and the spatial coherence are critical parameters in producing quality gratings [31, 32]. However placing the fiber in contact with the fine grating corrugations is not desirable due to possible damage to the phase mask. Improving the spatial coherence of the UV writing beam not only improves the strength and quality of gratings inscribed by the phase mask technique, it also relaxes the requirement that the fiber has to be in contact with the phase mask.

4.3.3 Point-by-point fabrication of Bragg gratings

The point by point technique [33] for fabricating Bragg gratings is accomplished by inducing a change in the index of refraction one step at a time along the core of the fiber. Each grating plane is produced separately by a focused single pulse from an excimer laser. A single pulse of UV light from an Eximer laser passes through a mask containing a slit. A focussing lens images the slit onto the core of the optical fiber from the side and the refractive index of the core in the irradiated fiber section increases locally. It is then translated through a distance Λ corresponding to the grating pitch in a direction parallel to the fiber axis and the process is repeated to form the grating structure in the fiber core. Essential to the point-by-point fabrication technique is a very stable and precise submicron translational system. The point by point method of inscribing FBG is illustrated in figure 4.5.

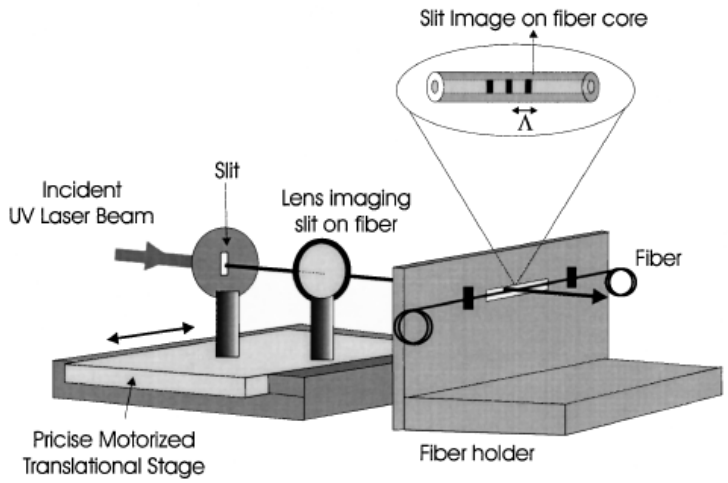

Figure 4.5 Point-by-point method for inscribing grating

The main advantage of the point –by-point writing technique lies in its flexibility to alter the Bragg grating parameters. Because the grating structure is built up a point at a time, variations in grating length, grating pitch and spectral response can easily be incorporated. Chirped gratings can be produced accurately simply by increasing the amount of fiber translation each time the fiber is irradiated. Because the UV pulse energy can be varied between point of induced index change, the refractive index profile of the grating can be tailored to provide any desired spectral response.

One disadvantage of the point-by-point technique is that it is a tedious process. Because it is a step-by-step procedure, this method requires a relatively long process time. Errors in the grating spacing due to thermal effect and/or small variations in the fiber strain can occur. This limits the grating to very short lengths. This method is suited for fabricating Long Period Fiber Gratings.

4.4 FBG sensing principles

According to Bragg's law

$$\lambda_B = 2n_{eff}\Lambda \tag{4.6}$$

Where λ_B is the Bragg wavelength n_{eff} is the effective refractive index of the fiber core and Λ is the Bragg grating period. The Bragg wavelength of fiber shifts due to strain and temperature .The shift is given by [34]

$$\Delta\lambda_B = (1 - p_e)\lambda_B\epsilon + [\frac{1}{\Lambda}(\frac{\delta\Lambda}{\delta T}) + \frac{1}{n}(\frac{\delta n}{\delta T})]\lambda_B\Delta T \tag{4.7}$$

The shift in wavelength '$\Delta\lambda_B$' is due to strain and temperature. The first part of the equation is for strain, 'p_e' is the photo elastic coefficient, 'ε' is the dynamic strain of the fiber. Where 'p_e' is

$$p_e = \left(\frac{n^2}{2}\right)[P_{12} - \mu(P_{11} + P_{12})] \tag{4.8}$$

Where P_{ij} are the Pockel's coefficients of the strain optic tensor and μ is the Poisson ratio of the optical fiber. Second part of the equation is the contribution due to temperature. At constant temperature second part of equation becomes zero. So the expression for wavelength shift at constant temperature due to strain is

$$\Delta\lambda_B = (1 - p_e)\lambda_B\epsilon \tag{4.9}$$

But when we study the temperature drift of strain second part is also significant.

The reflected spectrum of FBG is as follows [35].

$$R(\lambda) = R_B \exp\left[-4ln2\left(\frac{\lambda - \lambda_B}{\sigma_B}\right)^2\right] \tag{4.10}$$

where R_B is the reflectivity, σ_B is Full Width at Half Maximum (FWHM) of the FBG.

4.5 Strain Measurement

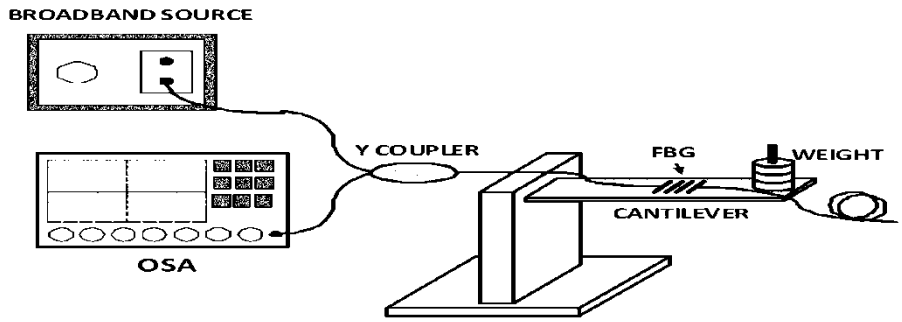

Figure 4.6 Experimental set-up for the measurement of strain

The experimental set-up for strain measurement is shown in Figure 4.6. The setup consists of a white light source ([Yokogawa] AQ 4305), and an optical spectrum analyzer ([Yokogawa] AQ 6319), and FBG with Bragg wavelength 1550 nm with a grating length of 13mm and reflectivity of 90 %. One input of 'Y' coupler is connected to the broad band source and other input is connected to the optical spectrum analyser (OSA) for monitoring the reflected spectrum. The FBG is connected to the other end of the fiber. All FC/APC connectors are used for the measurement. The cantilever structure is made of spring steel of 4mm thick and 5cm width with a length of 20cm. the cantilever is bolted to strong pillar with good base. The base is again bolted to a vibration free optical table. FBG is bonded to the cantilever using a fast setting epoxy. The curing time is 30 minutes at room temperature. Provisions are made on the cantilever structure so that the standard weights are added at the same location to provide repeatability. Sufficient time is provided for settling the strain, to avoid loading transients. The experiment is carried out at 22^0C. Reflected spectrum is monitored during loading and unloading of the structure to check the hysteresis of measurement.

In order to study the temperature variation of strain, the cantilever structure is kept inside a chamber and an IR lamp is used for heating. An auto transformer is used to control the power given to the IR lamb. The temperature inside the chamber is monitored using a digital thermometer. A small window is provided for loading and unloading of the structure.

4.5.1 Results and Discussions

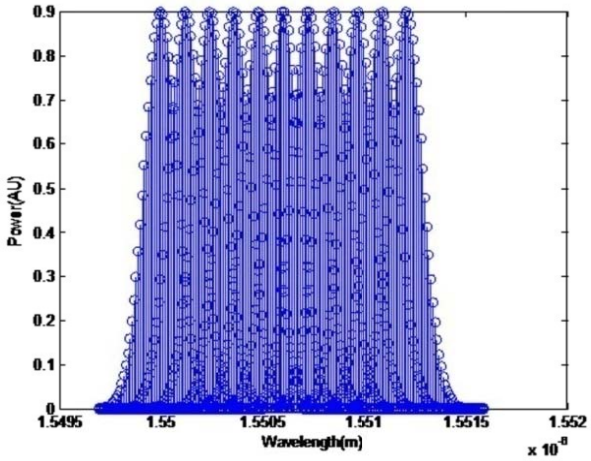

Figure 4.7 Simulated Reflected spectrum for the FBG

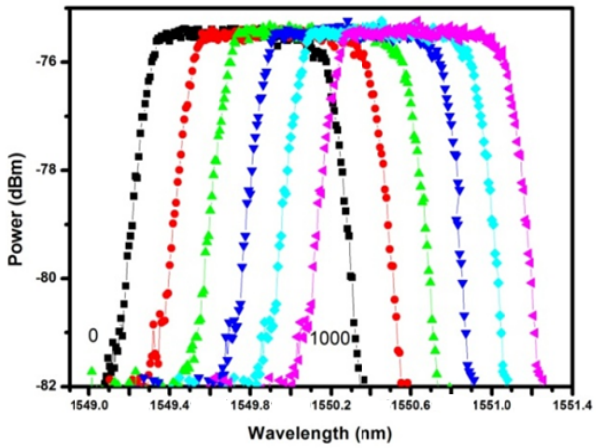

Figure 4.8 Reflected spectrum during strain measurement

The MATLAB is used for simulating the strain on the structure. The reflected spectrum obtained from the simulation of strain from 0 to 1000 μstrain is plotted in figure 4.7. For the strain measurement the structure is loaded with standard weights and the reflected spectrum is measured for every 100μ strains. The electrical strain gauges connected to a digital display is also employed for monitoring the strain. The structure is loaded up to 1000μ strains. The experiment is conducted at 22^0C. The reflected spectrum obtained from Optical Spectrum Analyser (OSA) is plotted in figure 4.8. The simulation of strain measurement using FBG is carried out using standard parameters, hence the response is found different during experiment. Actual response of the measurement system and detector are not reflected in simulation results. The shift in wavelength is considered from the leading edge of the reflected spectrum. It is observed that for 0-1000μ strains the wavelength shifted from 1549.21 to 1550.14 at the leading edge of the reflected spectrum. The structure is loaded many times and checked the reflected spectrum to ensure the repeatability. The reflected spectrum is observed during loading and unloading of the structure. The traces were found coinciding, which shows that the hysteresis is negligible. The transmitted spectrum is observed during loading and it given in figure 4.9.

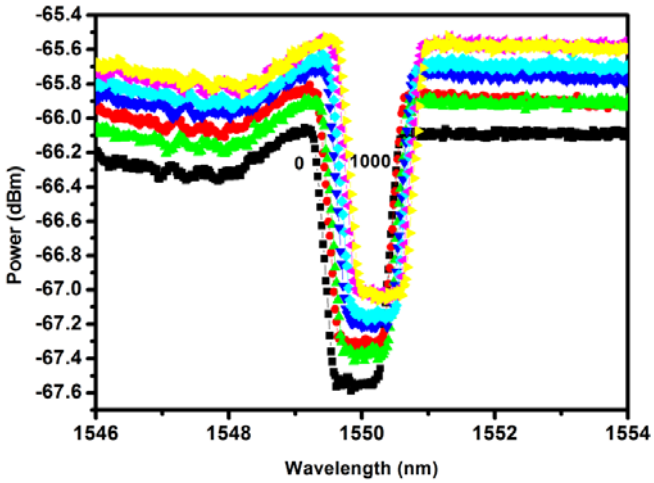

Figure 4.9 Transmitted spectrum

The wavelength variation in reflected spectrum at 79dBm is plotted in figure 4.10. The response shows that the wavelength variation is linear. Then the setup is housed in a wooden chamber. An Infrared lamp is used for heating the chamber. The temperature is monitored using a digital thermometer. A small window is provided for loading the structure. The strain measurements are repeated for the temperatures 30, 35, and 40^0C. The MATLAB is used for simulating the strain at different temperatures. The shift in simulated peak wavelength is plotted against wavelength in figure 4.10. The reflected spectrum obtained from OSA is analyzed and wavelength shift at the leading edge of the spectrum is also plotted in figure 4.10.

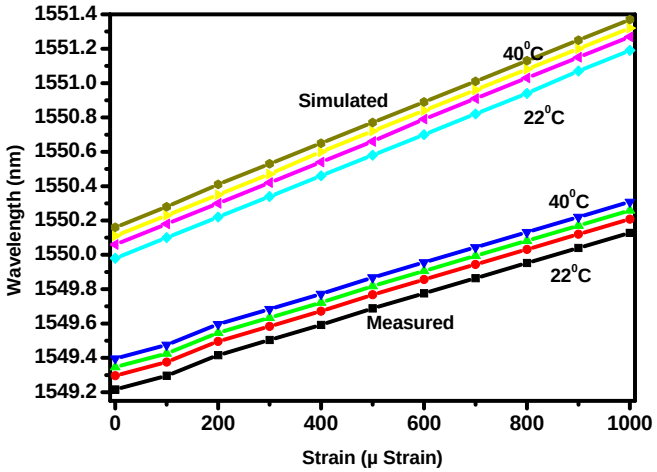

Figure 4.10 Simulated and measured Wavelength variation at different temperature

4.6 Temperature measurement

Bragg wavelength shift due to temperature accounts to temperature dependence of the refractive index of silica and thermal Expansion of glass. Major contribution is due to the temperature dependence of refractive index of silica. The shift in Bragg wavelength can be expressed as [9]

$$\Delta\lambda_B = [\frac{1}{\Lambda}(\frac{\delta\Lambda}{\delta t}) + \frac{1}{n}(\frac{\delta n}{\delta t})]\lambda_B \Delta T \qquad (4.11)$$

The first term relates to thermal expansion of fiber and second term to the temperature dependence of refractive index.

4.6.1 Experimental details

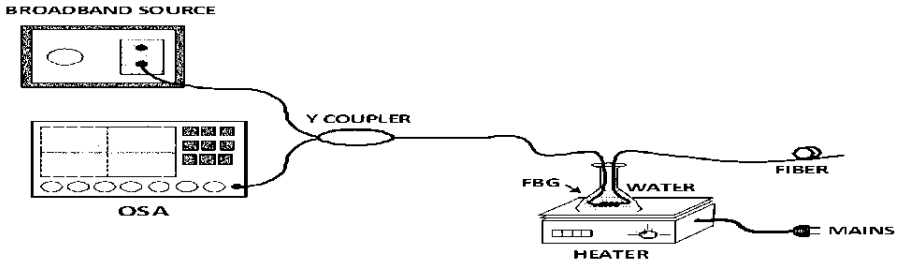

Figure 4.11 Experimental set up for temperature measurement.

The experimental set-up (Fig. 4.11) has white light source ([Yokogawa] AQ 4305), and an optical spectrum analyzer ([Yokogawa] AQ 6319). The fiber has a diameter of 125 micron and a numerical aperture of 0.14. The core and the cladding refractive indices are 1.463 and 1.456 respectively. FBG central wavelength is 1555.05nm with a grating length of 10mm. and reflectivity is 80%. The light is connected to one input of a 'Y' coupler. Other input of the coupler is connected to the OSA for the Bragg reflected signal. On the other end of the coupler the FBG is connected. Reflected spectrum is recorded at different temperatures in the range 22^0C-100^0C. To check the hysteresis of the measurement the temperature bath is allowed to cool naturally and the measurements are repeated. In order to get more précise results the reflected spectrum is measured from 50 to 55^0C for every 1^0C rise.

4.6.2 Results and discussion

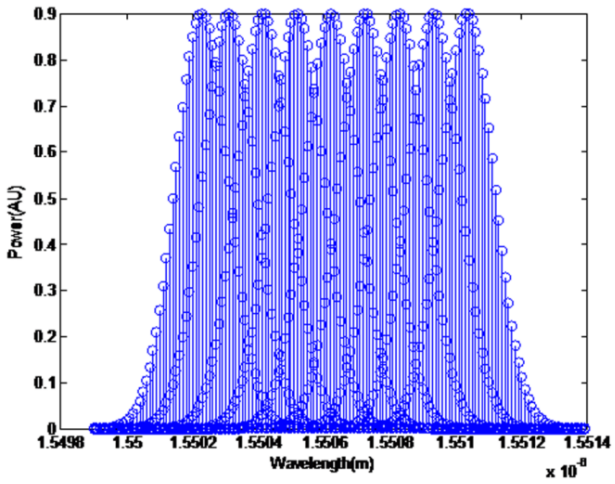

Figure 4.12 Simulated Reflected spectrum for a temperature variation of 22 to 100 ^{0}C

The simulated reflected spectrum using MATLAB is shown in figure 4.12. During the measurement the temperature of the water bath is varied from 22^0 to100^0C. The temperature of the bath is monitored using PT-100 and controlled using a PID controller. The readings are noted for every 10^0C rise in temperature. The experimental reflected spectrum at different temperature is plotted in figure 4.13.

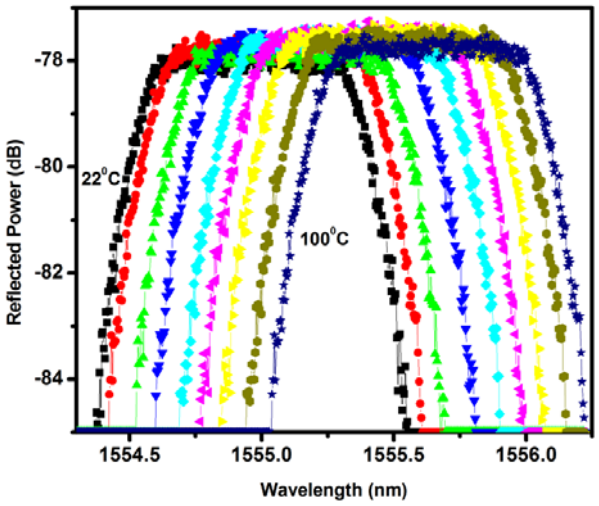

Figure 4.13 Reflected power for a temperature variation of 22-100 ^{0} C

At the leading edge the wavelength is varying from 1554.4 to 1555.1 for 22^{0} to 100^{0}C. The simulated and measured wavelength variation at different temperature is plotted in figure 4.14.

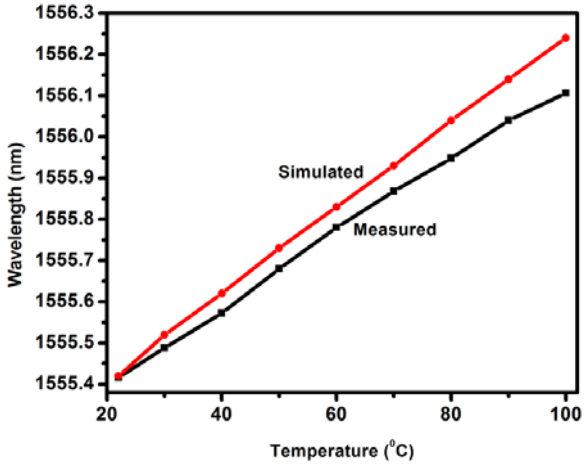

Figure 4.14 Wavelength shift for temperature variation from 22 to 100^{0} C

In order to check measurement resolution readings are taken closely in the range of 50-55^{0}C with 1^{0}C step. The results are as shown in figure 4.15& 4.16. The variation is found linear in this range.

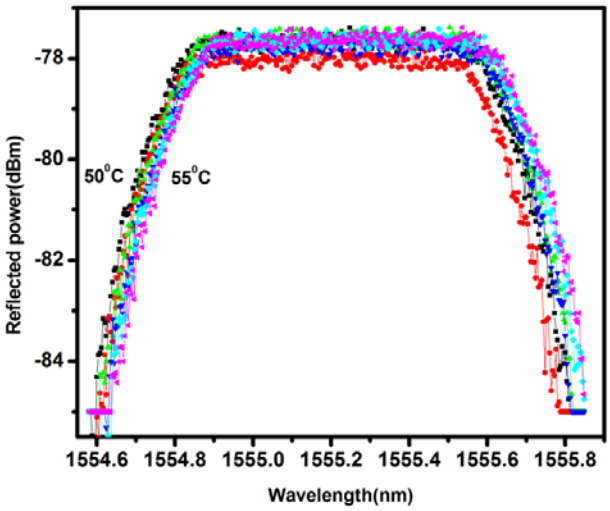

Figure 4.15 reflected power for temperature in the range 50-55^{0}C

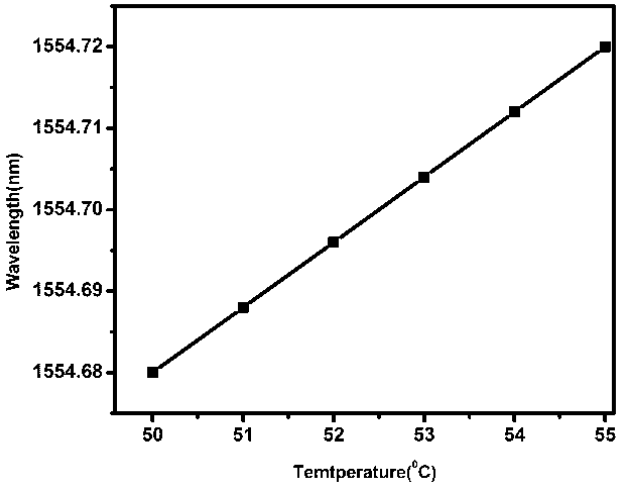

Figure 4.16 Variation of wavelength for temperature 50-55^{0}C

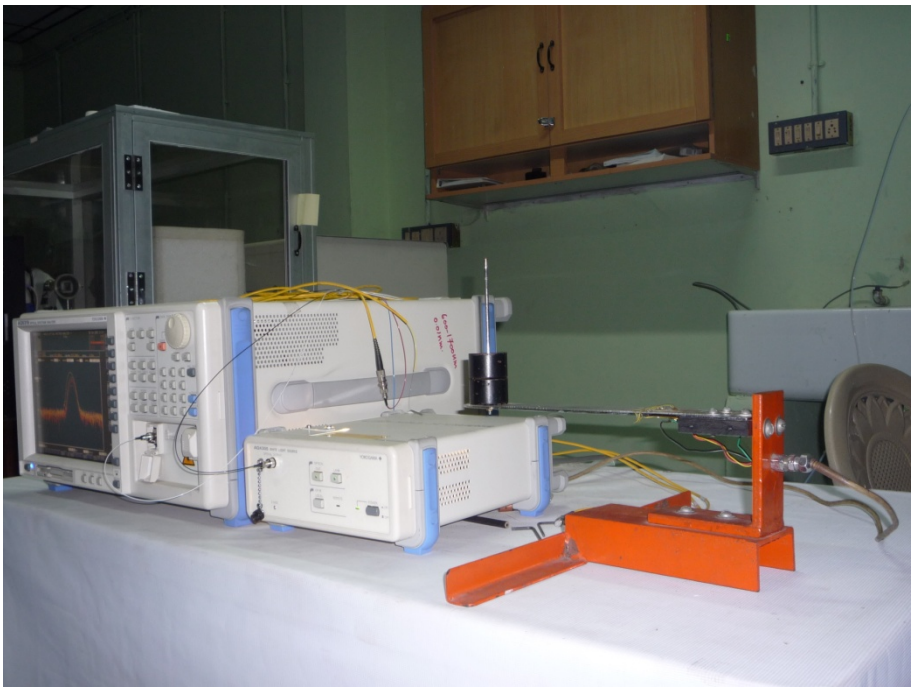

Figure 4.17 Photograph of the experimental set up for characterising FBG sensors

4.7 Conclusion

Fiber Bragg grating based strain and temperature sensor is realised**.** The simulated and measured results are found matching. Bragg reflected spectrum of FBG is measured for 0-1000 μ strains. The results are verified with electrical strain gauges. The structure is loaded many times to ensure repeatability. The wavelength shift due to the applied strain is linear and repeatable. The sensitivity of measurement is 0.9 pm/μ strain. The temperature drift of strain at 30, 35 and 40^0C is measured. The drift due to temperature is estimated to be 9.6nm/^{0}C. During temperature measurement the wavelength shift is found linear and repeatable within the range of 22-100^0C. The simulated and measured results are found matching. The wavelength

shifted from 1555.41 nm to 1556.1 nm. The sensitivity of measurement is 9.4 pm/^{0}C. Temperature variation up to 1^{0}C can be detected with this arrangement. An OSA with higher resolution is required for improving the measurement accuracy and resolution. An interrogator may also give better resolution.

References

[1] A. Kerrouche, W. J. O. Boyle, T. Sun and K. T. V. Grattan, Design and in the field performance evaluation of compact FBG sensor system for structural health monitoring applications, Sensor. Actuat. A., **151**, 107, 2009.

[2] Benjamin Torres, Ignacio Paya-Zaforteza, Pedro A. Calderon and Jose M. Adam, Analysis of the strain transfer in a new FBG sensor for structural Health Monitoring, J. Engg. Struc., **33**, 539, 2011.

[3] Shizhuo Yin, B. Paul, Ruffin Francis and T. S. Yu, Fiber Optic Sensors, CRC Press, New York, Ch.1, p 2, 2008.

[4] Bishnu P. Pal, Fundamentals of fiber optics in Telecommunication and Sensor systems, New age International, New Delhi, ch 22, p 548, 1997.

[5] B. D. Gupta, Fiber optic sensors principles and applications, New India publications, New Delhi, Ch.1, p 2, 2006.

[6] Shizhuo Yin, B. Paul, Ruffin Francis and T. S. Yu, Fiber optic Sensors, Second edition, CRC Press Taylor & Francis Group, Ch. 4, p 104, 2008.

[7] Y. J Rao, In fiber Bragg grating sensors, Meas. Sci. Technol., **15**, 8, 1442, 1997.

[8] A. D. Kersey, M. A. Davis, H. J. Patrik, M. LeBlanc, K. P. Koo, C. G. Askins, M. A. Putnam and E. J. Friebele, Fiber grating sensors, J. Lightwave Technol., **15**, 1442, 1997.

[9] Xu, M. G., Reekie, L., Chow, Y.T., Dakin and J.P., Optical in-fiber grating high pressure sensor, Electron. Lett., **29**, 398, 1993.

[10] A. D. Kersey, Optical fiber sensors for permanent down well monitoring applications in the oil and gas industry, IEICE Trans. Electron., **83**, 400, 2000.

[11] T. A. Berkoff and A. D. Kersey, Experimental demonstration of a fiber Bragg grating accelerometer, IEEE Photonic Tech. L., **8**, 1677, 1996.

[12] M. D. Todd, G. A. Johnson, B. A. Althouse and S. T. Vohra, Flexural beam-based fiber Bragg grating accelerometers, IEEE Photonic Tech. L., **10**, 1605, 1998.

[13] X. Dong, Y. Liu and Z. Liu, Simultaneous displacement and temperature measurement with cantilever- based fiber Bragg grating sensor, Opt. Commun., **192**, 213, 2001.

[14] L. A. Ferreira., A. B. Lobo Ribeiro, J. L. Santos and F. Farahi, Simultaneous measurement of displacement and temperature using low finesse cavity and a fiber Bragg grating, IEEE Photonic Tech. L., **8**, 1519, 1996.

[15] J. Lim, Q. P Yang, B. E Johns, P. R. Jackson and D. P., Flow sensor using optical fiber Bragg grating, Sensor. Actuat. A, **92**, 102, 2001.

[16] Dongcao Song, Jilin Zou, Hongliang Cui, Zhanxiong Wei and Zubin Chen, Liquid-level sensor using a fiber Bragg grating and carbon fiber composite diaphragm, Opt. Eng., **50**, 014401, 2011.

[17] H. J. Patrick, A. D. Kersey and F. Bucholtz, Analysis of the response of long period fiber gratings to external index of refraction, J. of Lightwave Technol., **16**, 9, 1606, 1998.

[18] R. Guenther, Modern Optics, John Wiley & Sons, New York, 1990.

[19] Shizhuo Yin, B. Paul, Ruffin Francis and T. S. Yu, Fiber Optic Sensors, CRC Press, New York, Ch.7, 301, 2008.

[20] T. Erdogan, Fiber grating spectra, J. Lightwave Technol., **15**, 1277, 1997.

[21] T. Erdogan, Cladding-mode resonances in short- and long-period fiber grating filters, J. Optical Soc. Amer. A, **14**, 1760, 1997.

[22] Y. Zhao and J. C. Palais, Fiber Bragg grating coherence spectrum modelling simulation and characteristics, J. Lightwave Technol., **15**, 154, 1997.

[23] A. M. Vengsarkar, P. J. Lemaire, J. B. Judkins, V. Bhatia, T. Erdogan and J. E. Sipe, Long-period fiber gratings as band-rejection filters, J. Lightwave Technol., **14**, 58, 1996.

[24] H. Hosono, Y. Abe, D. L. Kinser, R. A. Weeks, K. Muta and H. Kawazoe, Nature and origin of the 5-eV band in SiO2:GeO2 glasses, Phys. Rev. B., **46**, 11445, 1992.

[25] Nishii, J., Fukumi, K., Yamanaka, H., Kawamura, K., Hosono, H. Kawazoe and H., Photochemical reactions in GeO_2 –SiO_2 glasses induced by ultraviolet irradiation: Comparison between Hg lamp and excimer laser, Phys. Rev. B., **52**, 1661, 1995.

[26] H. G. Limberger, P. Y. Fonjallaz, R. P. Salathe and F. Cochet, Compaction-and photo elastic induced index changes in fiber Bragg gratings, Appl. Phys. Lett., **68**, 3069, 1996.

[27] B. Poumellec, The UV induced refractive index gratings in Ge: SiO2preforms: additional CW experiments and the microscopic origin of the change in index, J. Phys. D: Appl. Phys., **29**, 1842, 1996.

[28] G. Meltz, Formation of Bragg gratings in optical fibers by a transverse holographic method, Opt. Lett., **14**, 823, 1989.

[29] K. O. Hill, B. Malo, F. Bilodeau, D. C. Johnson and J. Albert, Bragg gratings fabricated in monomode photosensitive optical fiber by UV exposure thorough a phasemask, Appl. Phy. Lett., **62**,1035, 1993.

[30] K. T. V. Grattan and B. T. Meggitt, Optical Fiber Sensor technology, Kluwer Academic Publishers, London, Ch. 2, p 140, 2000.

[31] Othonos A. and Lee X., Novel and improved methods of writing Bragg gratings with phase- masks, IEEE Photonic Tech. L., **7**, 1183, 1995.

[32] P. E. Dyer, Farley R. J. and Giedl R., Analysis and application of a 0/1 order Talbot interferometer for 193nm laser grating formation, Opt. Commun., **129**, 98, 1996.

[33] B. Malo, K. O. Hill, F. Bilodeau, D. C. Johnson and J. Albert., Point by point fabrication of micro-Bragg gratings in photosensitive fiber using single excimer pulse refractive index modification techniques, Electron. Lett., **29**,1668, 1993.

[34] B. D. Gupta, Fiber optic sensors principles and applications, New India publications, New Delhi, Ch. 11, 212, 2006.

[35] Kuo-Chih Chuang and Chien-Ching Ma, Multidimensional Dynamic Displacement and Strain Meaurements using an intensity demodulation-based fiber-bragg grating sensing system, J. Lightwave Technol., **28**, 13,1897, 2010.

****

Chapter 5

DEVELOPMENT OF INTERROGATION SYSTEMS FOR FIBER BRAGG GRATING SENSORS

Contents

This chapter presents two simple methods for interrogating the FBG sensors. The response of the system is evaluated by measuring strain and temperature.

5.1 Introduction

FBGs have proved its potential in measuring strain, temperature, pressure, displacement, refractive index, humidity etc [1-8]. FBGs also find application in structural health monitoring as well in medical field [9-11]. Small size, real time measurement, fast response, immunity to electromagnetic waves, are the advantages of general fiber optic sensors [12]. Among the fiber optic sensors, FBG sensors have advantages, such as high multiplexing capabilities, distributed sensing, as well as localised sensing region and elimination of frequent calibration [13-15]. The signal obtained from FBG sensor

is usually encoded directly in wavelength domain and hence it is insensitive to source fluctuations. The main bottle neck in the use of FBG sensors for different applications are the costly demodulation techniques. Even costly spectrum analyser can detect up to 4 pico meter and the resolution in strain measurement is approximately 20 μStrain. Dynamic response of the measurement is also poor since every time the spectral components need to be analysed. In the literature, many optical wavelength-intensity demodulation techniques based on long period grating, FBG filter, chirped fiber grating etc. have been discussed [16-18]. In the present study we suggest two simple methods for wavelength to intensity conversion.

The first method is by selecting a narrow band source, and a FBG with Bragg reflection at trailing edge of the source spectrum. So, as the Bragg reflected wavelength shifts due to strain or temperature variations, the reflected power vary depending on the selection of Bragg wavelength. Few components are used hence the cost of measurement is less in this method. The main limitation in this study is that, the emission of the source and the FBG reflection need to be critically matched. In the second method two matched FBGs are used. The Bragg reflected signal from the reference FBG is fed in to the FBG in which the measurements are carried out. During the measurement the reflected power varies as the Bragg reflected wavelength shifts. This can be monitored using a power meter. The dynamic response of the measurement will be better, since the intensity is measured. If the source used is a broad band source with a

flat spectrum then the impact due to temperature variations will not affect the strain measurements in the second arrangement.

5.2 Interrogators overview

FBG optical sensing is based on the principle that the measured information is wavelength encoded in the Bragg reflection of the grating. The wavelength shift can be related to the variations in measurand at the sensor position. Therefore the primary work for the FBG sensor lies in the wavelength interrogation of the Bragg reflection. Interrogators or demodulators in a fiber grating sensor system are the measurand-reading units that extract measurand information from the light signals coming from the sensor heads. Since the measurand is encoded spectrally, the interrogators are usually meant to measure the Bragg wavelength shifts and convert the results to measurand data.

The reflected spectrum and the Bragg wavelength shift from the sensor arrangement can be observed using an Optical Spectrum Analyzer [19]. But Optical Spectrum Analyzer is costly and bulky. It is generally suitable only for laboratory measurements. Analysing the spectral components of the reflected spectrum is time consuming and the dynamic response of measurement is also poor when strain or temperature is measured from the wavelength shift observed in OSA.

Many interrogation systems are in use for FBG sensors. Depending upon the application, sensitivity and accuracy required, different types of interrogators are designed. Joel Villatoro et.al [20] proposed an interrogation system with a Photonic Crystal Fiber (PCF)

based interferometer. The splicing of this interferometer with the fiber is tedious and the tuning of the interferometer response to meet the required range and linearity is complicated. Construction of PCF interferometer is difficult and it is expensive too. Moghadas et al. have proposed an interrogator for fault detection in high voltage transformers using FBG, which utilises a tunable filter along with a data acquisition system [21]. The proposed system utilises a tunable filter with considerable linearity which is expensive and the power level after the filtering will be very low. A similar system is proposed for fault detection in radial power systems [22]. Kuo-Chih Chuang and Chien-Ching Ma have measured dynamic strain and displacement by utilizing a filter made of long period fiber grating [23]. The response of the LPFG and the fiber grating need to be critically matched in order to get linear response. Considering the limitations of the above interrogation systems we are proposing two simple interrogation systems with less number of components and less complexity.

5.3 Theory

According to Bragg's law

$$\lambda_B = 2n_{eff}\Lambda \tag{5.1}$$

where 'λ_B'is the Bragg wavelength, 'n_{eff}' is the refractive index of the fiber core and 'Λ' Bragg grating period [24]. The strain measurement is based on the physical elongation of optical fiber which corresponds to change in grating pitch and refractive index of

the fiber due to photo elastic effect. At constant temperature, shift in Bragg wavelength can be expressed as

$$\Delta\lambda_B = (1 - p_e)\lambda_B\epsilon \tag{5.2}$$

where 'ε' is the applied strain and 'p_e' is the effective photo elastic coefficient and it is expressed as

$$p_e = \left(\frac{n^2}{2}\right)[P_{12} - \nu(P_{11} + P_{12})] \tag{5.3}$$

'P_{ij}' is the Pockel's coefficients of the strain optic tensor and 'ν' is the Poisson's ratio of the optical fiber.

Bragg wavelength shift due to temperature accounts for, the temperature dependence of the refractive index of silica and thermal expansion of glass. Major contribution is due to temperature dependence of the refractive index of silica.The shift in Bragg wavelength can be expressed as [25]

$$\Delta\lambda_B = [\frac{1}{\Lambda}(\frac{\delta\Lambda}{\delta T}) + \frac{1}{n}(\frac{\delta n}{\delta T})]\lambda_B\Delta T \tag{5.4}$$

The first term relates to thermal expansion of the fiber and second term to the temperature dependence of refractive index.

The reflected spectrum of the FBG is given by [23]

$$R_{r1}(\lambda) = R_{r1}\exp\left[-4ln2\left(\frac{\lambda-\lambda_{r1}}{\sigma_{r1}}\right)^2\right] \tag{5.5}$$

Where R_{r1} is the reflectivity, σ_{r1} is Full Width at Half Maximum (FWHM) of the FBG. The intensity at the power meter is given by

$$I = \int_0^\infty L(\lambda)R_{r1}(\lambda)d\lambda \tag{5.6}$$

Where L (λ) is the source spectrum and it is

$$L(\lambda) = P \exp\left(\frac{-(\lambda-\lambda_p)^2}{0.362*\sigma_s{}^2}\right) \quad (5.7)$$

P is the peak power, λp is peak emission wavelength, σ_s is FWHM of the source. Hence in the first study the power reaching at the detector is given by equation (5.6).

In the second study this power is given to the measuring FBG. Since the FBGs are matched, this signal is again reflected by the second FBG. The reflected spectrum is given by [23]

$$R_{r2}(\lambda) = R_{r2}\exp\left[-4ln2\left(\frac{\lambda-(\lambda_{r2}+\Delta\lambda)}{\sigma_{r2}}\right)^2\right] \quad (5.8)$$

where $\lambda_{r2} = \lambda_{r1} + \Delta\lambda_x$ where $\Delta\lambda_x$ is accountable for slight mismatch between two FBGs, R_{r2} is the reflectivity of the measuring FBG, σ_{r2} is the FWHM of measuring FBG and Δλ is Bragg wavelength shift due to applied strain. Initially for matched FBGs, $R_{r1} = R_{r2}$,$\sigma_{r1} = \sigma_{r2}$. Hence without strain in second FBG,'Δλ' is zero and $R_{r1}(\lambda) \approx R_{r2}(\lambda)$.

Intensity 'I' is given by

$$I=\int_0^\infty L(\lambda)\, R_{r1}(\lambda)R_{r2}(\lambda)d\lambda \quad (5.9)$$

On substitution, the reflected power at the power meter is given by

$$\int_0^\infty L(\lambda)\, R_{r1}R_{r2} \exp\left[-4ln2\left\{\left(\frac{\lambda-\lambda_{r1}}{\sigma_{r1}}\right)^2 + \left(\frac{\lambda-(\lambda_{r2}+\Delta\lambda)}{\sigma_{r2}}\right)^2\right\}\right] \quad (5.10)$$

5.4 Experimental details

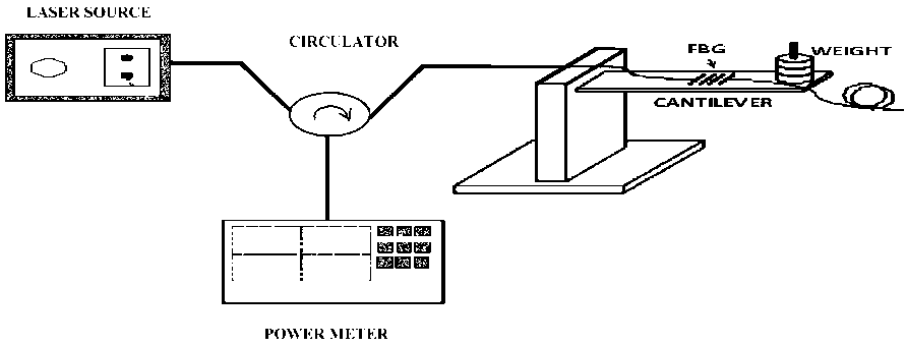

Figure 5.1 Experimental set up for strain measurement.

The experimental set-up for implementing the first method described above is shown in figure 5.1.The setup has a Laser source, [ILX Light wave 7900B], an optical circulator having 3-ports, FBG pasted to a cantilever setup and a power meter. The laser source has an emission peak at 1550nm. FBG have a Bragg wavelength of 1550 nm with a grating length of 13mm and the reflectivity offered is 90%. The laser source is connected to port 1 of the circulator. FBG bonded to the cantilever structure is connected to the port 2 of the circulator. A power meter [Hewlett- Packard, 8153A] is connected at port 3 of circulator to measure the Bragg reflected power. Cantilever for the strain measurement has length of 20 cm, breadth of 5cm and is made in a spring steel of 2mm thick. Using a fast setting epoxy the FBG is pasted to the cantilever structure. The strain in the cantilever structure is monitored using electrical strain gauges also. The standard weights were added to the structure and the reflected spectrum is measured for every 100 μ strain. Experimental set up was placed in a vibration free

table and allowed sufficient time before every measurements to avoid loading transients.

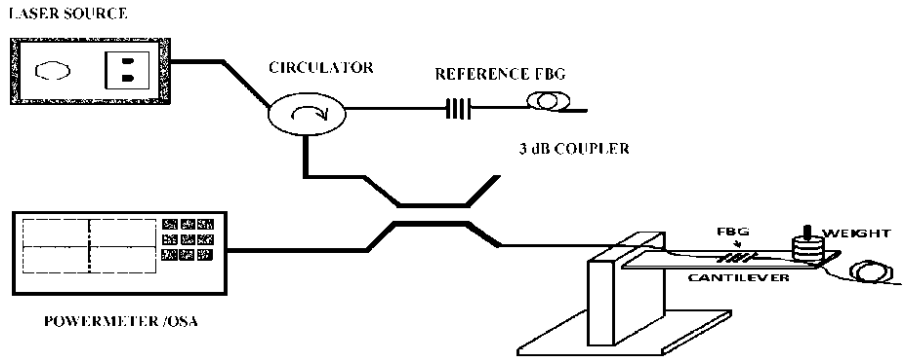

Figure 5.2 Experimental setup for strain measurement with reference FBG

The experimental setup for implementing the second method described above is given in figure 5.2. In the setup shown in figure 5.2, the first port of the optical circulator is connected to laser source and second port to the reference FBG, which is matched with the measuring FBG. The third port is connected to a 3dB coupler. The FBG is pasted to the cantilever structure for the strain measurement and power meter is connected as shown in figure 5.2. The reflected signal from the strain measuring set up is monitored using an optical spectrum analyzer [Yokogawa, AQ 6319], as well as the power meter.

To measure temperature, the FBG is immersed in water bath and temperature is varied from 22^0C to 100^0C. A digital thermometer is also used for monitoring temperature of water bath. The reflected spectrum is monitored for a temperature rise of 10^0C. Hysteresis is measured by monitoring the reflected power by allowing the water bath to cool naturally.

5.5 Results and Discussion

The source spectrum is monitored and it is depicted in figure 5.3. The emission peak is observed at 1550nm and then the power level drops linearly making it suitable for the measurements without a reference FBG. The spectral stability of the source is very critical in this study. The source used is very stable and temperature is maintained at 22^0C. The experiment was carried out for both the interrogation methods.

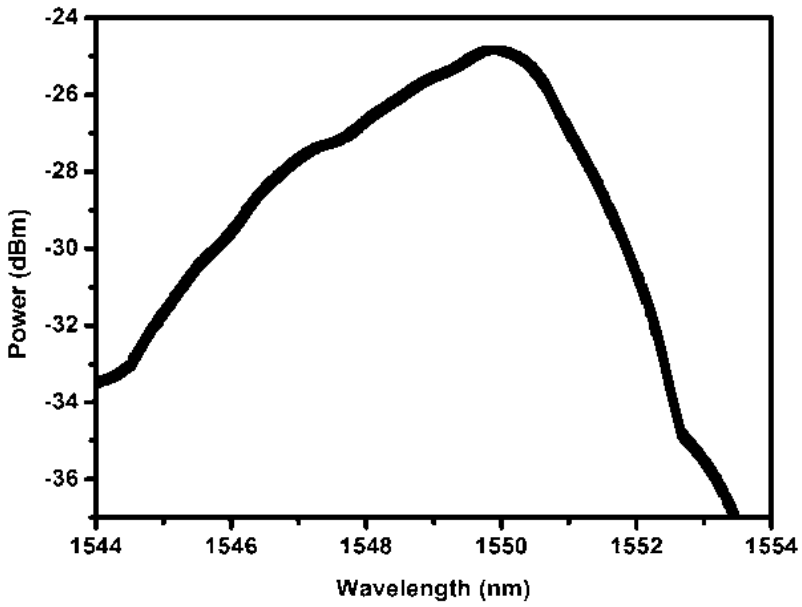

Figure 5.3 Source spectrum

5.5.1 Interrogation with narrowband source

The reflected spectrum for strain measurement is simulated using MATLAB for an ideal laser source with an emission peak at 1550nm. The FBG used has an emission peak at 1550nm. The

simulation results in figure 5.4 shows that as the strain increases the Bragg wavelength shifts and the power reduces correspondingly. Hence the set up can be used as an interrogator for FBG sensors.

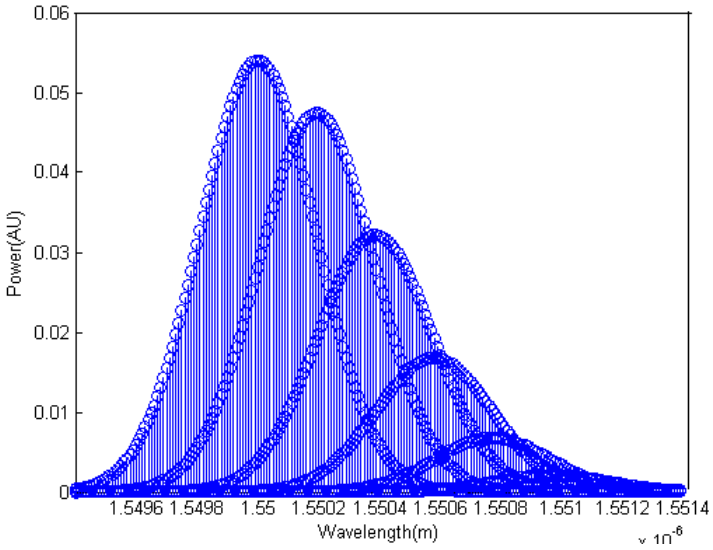

Figure 5.4 Simulated reflected spectrum during strain measurement without reference FBG.

The reflected spectrum from the FBG available at port 3 of circulator is monitored using OSA for strain measurement and it is shown in figure 5.5. The peak power level is ranging from -30 dBm to - 60dBm for a strain of 0-1000 μ strains. The power variation is almost linear in this range. FBG Bragg reflection is at trailing edge of the source spectrum and as the Bragg reflected wavelength red shifts due to the strain or temperature, the reflected power also decreases. The selection of Bragg wavelength of FBG and the source emission peak is very critical in this configuration. The simulations are carried out considering the ideal source spectrum with FWHM of the

narrowband source. Actual response of the measurement system and detector are not reflected in simulation results.

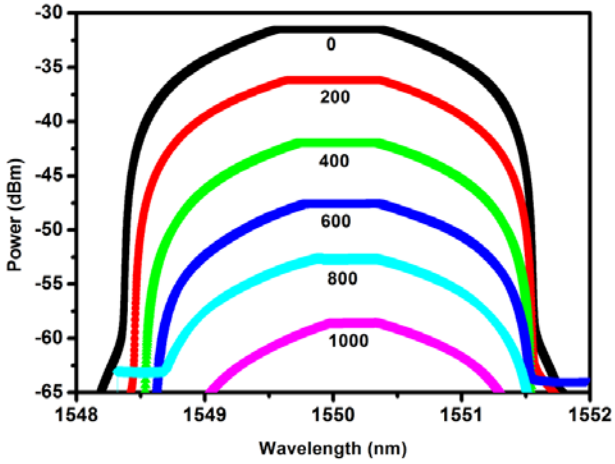

Figure 5.5 Reflected spectrum during strain measurement without reference FBG

The port 3 of circulator is connected to the power meter and output is monitored for a strain of 0 to 1000 μ strain. The output is varying from -20 dBm to -40 dBm. The results are found linear in this range. The hysteresis of the measurement is also determined during unloading of the structure and plotted in figure 5.6 and it shows that the measurement has negligible hysteresis.

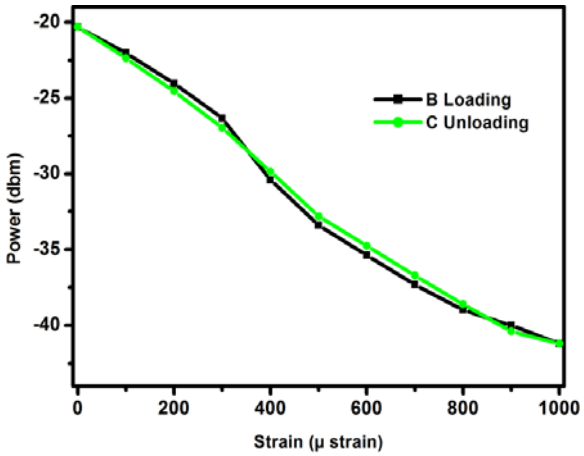

Figure 5.6 Reflected power for the interrogation system using a narrow band source during strain measurement

Measurements are also carried out for temperature sensing using the setup. The temperature is measured from 22^0C to 100^0C. The reflected power variation for temperature measurement at port 3 without reference is plotted in figure 5.7. The water bath is allowed to cool naturally and the power is measured for every 10^0C decrement. The result shows that measurement has negligible hysteresis.

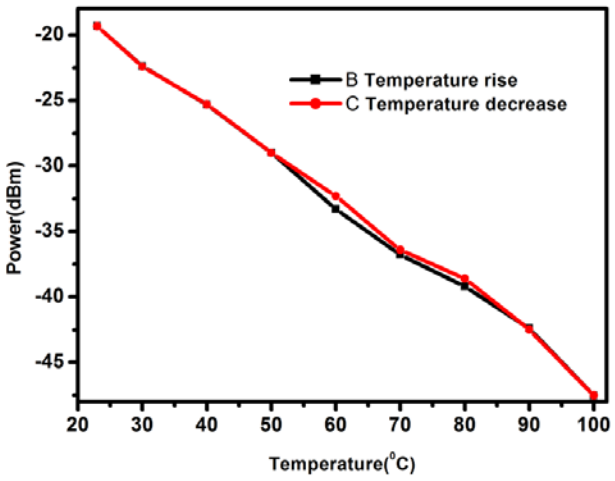

Figure 5.7 Reflected power for the interrogation system without reference during temperature measurement

The sensitivity for the strain and temperature measurements with narrowband source is found to be 0.0283dBm/μ strain and 0.4dBm/^{0}C respectively.

5.5.2 Interrogation with narrowband source and reference FBG

The measurements of strain and temperature are continued with a reference FBG as discussed in the second method. Reflected signal from the reference FBG is sourced to the second one and the reflected spectrum from the second FBG is measured for different strain and the simulated results for different applied strains are shown in figure 5.8. The measured spectrum is shown in figure 5.9 for 0 to1000 μstrains. Since the FBGs are matched the same reflected spectral components from the reference FBG is reflected from the second FBG initially. It is observed that as the strain increases the reflected power from sensing FBG decreases.

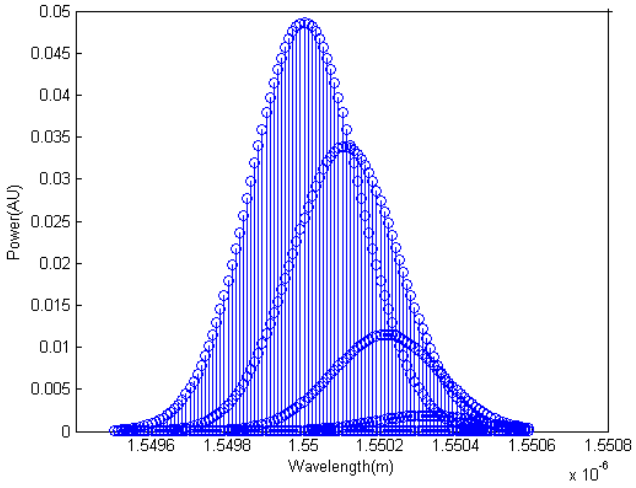

Figure 5.8 Simulated reflected spectrum with reference FBG

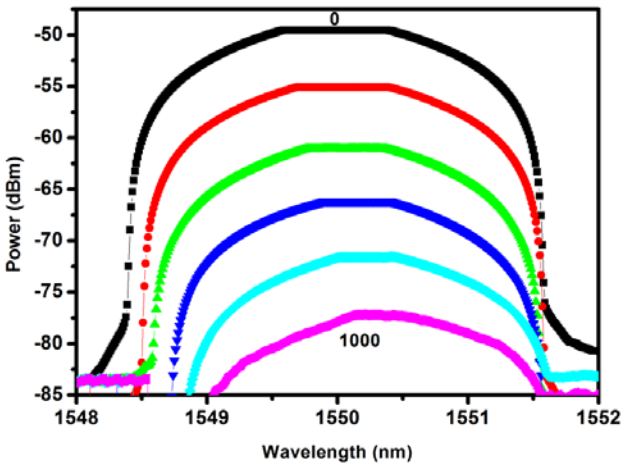

Figure 5 .9 Reflected spectrum during strain measurement with reference FBG

The reflected power variation for strain measurement with reference is shown in figure 5.10. The reflected power varies linearly from -37.39 dBm to -65.21 dBm for 0 to 1000 µstrains. The hysteresis of the measurement is also plotted in figure 5.10 and it is observed that hysteresis is negligibly small.

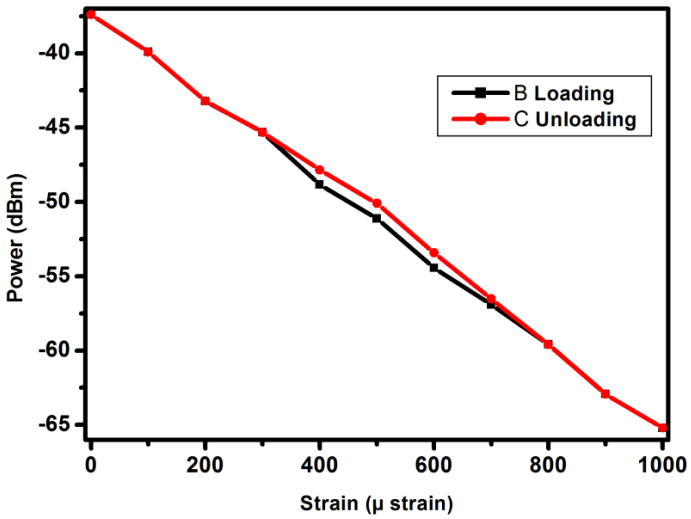

Figure 5.10 Reflected power variation & hysteresis for the interrogation system with reference

The arrangement can be made temperature insensitive during strain measurement using a powerful broad band source. As the temperature shifts the reflected spectrum from both the FBGs will shift evenly. But the decrease in power is only due to applied strain in the second FBG. Hence strain measurement can be made temperature insensitive.

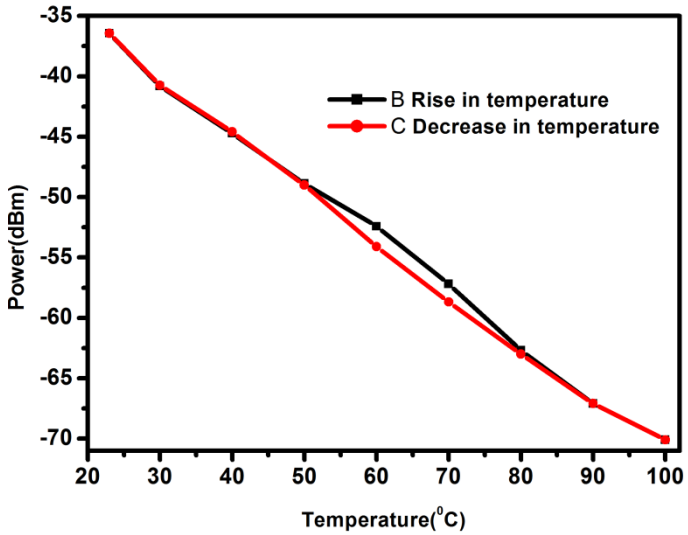

Figure 5.11 Reflected power variation & hysteresis for the interrogation system with reference

The temperature measurement is also carried out with reference FBG for 22 to 100 ^{0}C. From the figure 5.11 it is evident that power variation is linear within this range. The temperature of water bath is allowed to cool naturally and the reflected power is monitored. The hysteresis of the measurement is found negligible. The sensitivity of strain and temperature measurements with reference FBG is found to be 0.028dBm/μstrain and 0.38dBm/^{0}C respectively.

5.6 Conclusion

Two interrogation methods for FBG sensors are developed. If the emission spectrum of the narrow band source and FBG are matched perfectly then the first method is appropriate, since it can provide better power levels with less number of components. But the stability and spectral response of the source is critical. In the second design which makes use of a reference FBG, the source response is not very critical as in the earlier case. This method is gives more linear results than the first method. It can be made temperature insensitive by using a powerful broadband source with flat spectrum in the measurement range. Using a 4pico m resolution OSA we can measure a minimum strain of 24 μstrains and temperature of 0.1^0C. Whereas using this arrangement, measurement up to 0.5μstrain and $0\ .01^0$C is possible with a power meter resolution of 0.01dBm, provided the source power is constant. The highlights of this design are portability, cost effectiveness and better resolution and the dynamic response is also expected to be better.

Reference

[1] E. Udd, C. Lawrence and D. Nelson, Development of a three axis strain and temperature fiber optic grating sensor, Proc. SPIE , **3042**, 229, 1997.

[2] Cherl-Hee Lee, Min-Kuk Kim, Kwang Tack Kim and Jonghun Lee, Enhanced temperature sensitivity of fiber

Bragg grating temperature sensor using thermal expansion of copper tube, Microw. Opt. Techn. Lett., **53**, 7, 1669, 2011.

[3] A. D. Kersey, M. A. Davis, H. J. Patrick, M. LeBlanc, K. P. Koo, C. G. Askins, M. A. Putnam and E. J. Friebele, Fiber grating sensors, J. Lightwave Technol., **15**, 1442, 1997.

[4] X. Shu, K. Sugden and I. Bennion, Sensitivity characteristics of long-period fiber gratings, J. Lightwave Technol., **20**, 255, 2002.

[5] M. G. Xu, L. Reekie, Y. T. Chow and J. P. Dakin, Optical in-fibre grating high pressure Sensor, Electron. Lett., **29**, 398, 1993.

[6] I. Yong Zhao, He Huang and Qi Wang, Interrogation technique using a novel spectra bandwidth measurement method with a blazed FBG and a fiber-optic array for an FBG displacement sensor, Sensor. Actuat. A, **165**, (2), 185, 2011.

[7] Wei Liang, Yanyi Huang, Yong Xu, Reginald K Lee and Amnon Yariv, Highly sensitive fiber Bragg grating refractive index sensors, Appl. Phys. Lett., **86**, 151122, 2005.

[8] T. L. Yeo, T. Sun, K. T. V. Grattan, D. Parry, R. Lade and B. D. Powell, Characterisation of a polymer-coated fibre Bragg grating sensor for relative humidity sensing, Sensor. Actuat. B, **110**, 148, 2005.

[9] R. M. Measures, Smart composite structures with embedded sensors, Compos. Eng., **2**, 1992 .

[10] G. Zhou and L. M. Sim, Damage detection and assessment in fibre-reinforced composite structures with embedded fibre optic sensors-review, Smart Mater. Struct., **11**, 925, 2002.

[11] A. F. Silva, J. P. Carmo, P. M. Mendes and J. H. Correia, Simultaneous cardiac and respiratory frequency measurement based on a single fiber Bragg grating sensor, Meas. Sci. Technol., **22**, (075801), 5, 2011.

[12] Shizhuo Yin, Paul B. Ruffin and Francis T. S. Yu, Fiber optic Sensors, Second edition, CRC Press Taylor & Francis Group, Ch. 2 , 2008.

[13] S. Kutaran and M. S. Kilickaya, The modeling of fiber bragg grating, Opt. Quantum Electron., **39**, 643, 2007.

[14] H. N. Li, D. S. Li and G. B. Song, Recent applications of fiber optic sensors to health monitoring in civil engineering, Eng. Struct., **26**, 1647, 2004.

[15] M. Majumder, T. K. Gangopaadhyay, A. K. Chakraborty, K. Dasgupta and D. K. Bhattacharya, Fiber Bragg gratings in structural health monitoring—present status and Applications, Sensor. Actuat. A, **147**, 150, 2008.

[16] R. W. Fallon, L. Zhang, L. A. Everall, J. A. R .Williams and I. Bennion, All-fiber optical sensing system: Bragg grating sensor interrogated by a long period grating, Meas. Sci. Technol., **9**, (12), 1969, 1998.

[17] I. C. Song, S. K. Lee, S. H. Jeong and B. H. Lee, Absolute strain measurement made with fiber Bragg grating sensors, Appl.Opt., **43**, (6), 1337, 2004.

[18] S. Kim, S. Kim, J. Kwon and B. Lee, Fiber Bragg grating strain sensor demodulator using a chirped fiber grating, IEEE Photon. Technol. Lett., **13**, 8, 839, 2001.

[19] Alain Trouillet, Emmanuel Marin and Colette Veillas, Fibre gratings for hydrogen sensing, Meas. Sci. Technol., **17**, 1124, 2006.

[20] Joel Villatoro, Vittoria Finazzi, Vladimir P. Minkovic and Goncal Badenes, Compact All-Fiber Interrogation Unit for FBG sensors, Optical Fiber Communication Conference, IEEE Xplore, DOI: 10. 1109/OFC.2008. 4528750, 2008.

[21] Amin Moghadas and Mehdi Shadaram, Novel Fiber Bragg Grating Sensor Applicable for Fault Detection in High Voltage Transformers, Innovative Technologies for an Efficient and Reliable Electricity Supply, CITRES, IEEE Xplore, DOI:10. 1109/CITRES. 2010. 5619778., 2010.

[22] Amin Moghadas, Ronald Barnes and Mehdi Shadaram, An Innovative Fiber Bragg Grating Sensor Capable of Fault Detection in Radial Power Systems, Annual IEEE systems conference, IEEE Xplore, DOI:10. 1109/SYSTEMS. 2010. 5482459, 2010.

[23] Kuo-Chih Chuang and Chien-Ching Ma, Multidimensional Dynamic Displacement and Strain Meaurements using an intensity demodulation-based fibre- bragg grating sensing system, J. Lightw. Technol., **28**, 1897, 2010.

[24] Kashyap R., Fiber Bragg Grating, London: Academic, 153, 1999.

[25] B. D. Gupta, Fiber optic sensors principles and applications, New India publications, New Delhi, 212, 2006.

****

Chapter 6

OPTICAL TIME REFLECTROMETRY FOR DISTRIBUTED SENSING OF WEIGHT AND DISPLACEMENT.

Contents

This chapter deals with the distributed sensing using optical time domain reflectometers. A quasi distributed fiber optic macro bend weight - displacement sensor using Optical Time Domain Reflectometer (OTDR) is presented.

6.1 Introduction

The multiplexing of Fiber Optic Sensors (FOS) offers the possibility of large number of sensors supported by a single fiber optic line [1]. The main advantages of a distributed fiber sensor are less number of components and hence reduced cost, weight and cabling [2]. The most commonly employed techniques are time [3], frequency [4-6], wavelength [7, 8], and polarisation multiplexing [9]. Time division multiplexing employs a pulsed light source, launching light in to an optical fiber and analysing the time delay to discriminate

between sensors. This technique is generally employed for distributed sensing of strain, displacement, and temperature. In a frequency division multiplexed sensor a laser diode is frequency chirped by driving it with a saw tooth current drive. The carrier frequency output of the successive Mach-Zehnder interferometers is separated to monitor the measurands. In wavelength division multiplexing a broad band light is sourced in to the fiber which is coupled to a series of fiber sensors that reflects or modulates the light of different wavelengths. An OSA or dispersive elements like grating or prism is used to separate the signals. In the case of polarisation multiplexing sensor, launch light with a particular polarisation in each sensor separately and extract the light with the same polarisation and the measurand is determined.

The properties like fiber loss and attenuation are prone to environmental effects like humidity, temperature, physical stress, bend etc. The OTDR backscatter measurement is a non destructive testing capable of doing *in situ* monitoring by accessing only one end of the fiber. Measurements provide information about length dependence of attenuation, insertion loss of defects, splices, bends, and connectors.

Many studies have been reported on single mode/ multimode step index fiber for the on line monitoring of civil structures[10-12], slide damage monitoring[13], temperature sensors[14], crack sensors[15], strain and displacement sensors[16], marine structures[17] etc using Optical Time Domain Reflectometry. Among the different type of sensors the FOS have advantages like immunity

to electromagnetic interference, chemical reactions etc. This makes FOS employable in the natural environments. Another attractive feature of Distributed FOS is that they are able to serve as both the sensing element and the signal transmission medium, allowing the electronic instrumentation to be located remotely from the measurement site [18].

In this investigation, we present a detailed study on weight-displacement sensing using optical time domain reflectometry. OTDR has the advantage that the measuring parameter can be monitored continuously along the fiber. But in a distributed sensor arrangement, the spatial resolution is an important parameter. So quasi distributed sensing is carried out in which the parameter is measured only at specific locations. Studies discussed earlier [10-13] have few drawbacks like the destructive nature of testing and the lack of repeatability. Various measurements in this study are much more reliable and repeatability is also observed. The weight-displacement sensing arrangement is standardized with specially made triangular corrugations with springs and guides, which give excellent repeatability. The restoring force exerted by the springs ensures non-destructive measurement. Moreover the size and shape of macro bends can be easily reproduced at a later time, which is a desirable quality when measuring a quantity for a long period of time, like health monitoring of structures. All other related parameters like velocity, strain, acceleration, pressure etc. can be derived from this.

In a quasi distributed sensor, the spatial resolution is not very important. The important thing is to clearly resolve the individual sensing points. We have selected the measurement points sufficiently apart so that they are clearly resolvable. The optical reflectometry is to measure optical reflectivity as a function of distance [19]. An optical pulsed probe signal is sent to the fiber. The reflected signals from the fiber return after various time delays depending on the location of the reflecting sites. This signal is processed to determine the magnitude and associated time delay. Knowing the speed of light through the fiber, the time delay can be converted into the distance of the fiber.

In this study we used an OTDR (JDSU MTS 8000) with SMF 28 fiber. Controlled macro bending is provided using triangular corrugations of different pitches. Standard weights are applied on the spring loaded arrangement. This arrangement creates a controlled repeatable macro bends in the fiber. Displacement caused by strain and deformation in the bridges, dams and other civil engineering structures can be monitored by suitably modifying and selecting the appropriate sensor parameters. We have studied the effect of pitch of corrugation on the loss mechanism and it is found that maximum loss/ sensitivity occurs at a particular pitch, in the case of SMF 28 fiber, which also depends on the diameter of the measuring fiber. The number of corrugations is also changed to evaluate its dependence on measurement.

6.2 Principle of OTDR operation

Optical Time Domain Reflectometer launch short duration pulses in to a fiber and then measure, as a function of time, the reflected signals. During the propagation of pulses they encounter many reflecting and scattering sites resulting a fraction of light reflected back in opposite direction. Rayleigh scattering and Fresnel reflections are the reasons for this. By measuring the arrival time of the reflected light, the location and magnitudes of faults can be estimated. The block diagram of a generic OTDR is as shown in figure 6.1

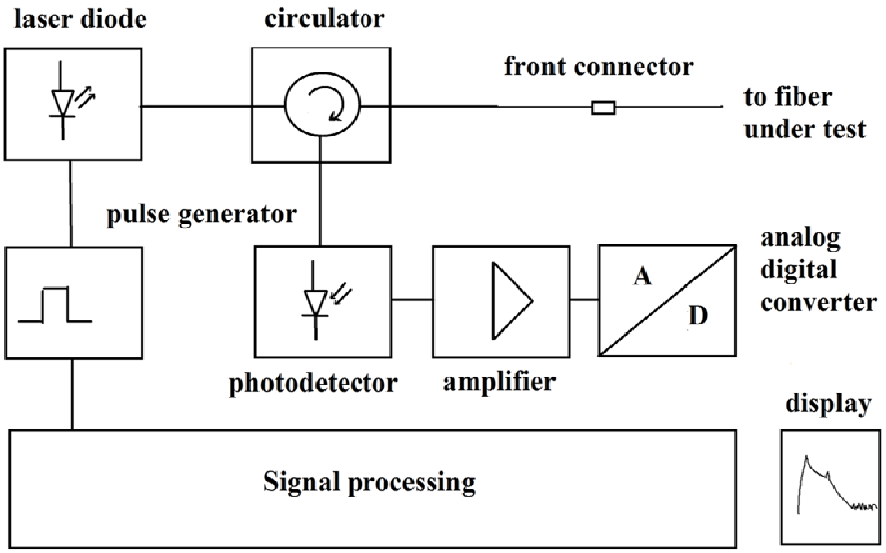

Figure 6.1 Block diagram of an OTDR

A pulse generator triggered by a signal processing unit is used to modulate the intensity of the laser diode. Pulse widths between 5ns to 10μs are used depending on the spatial resolution and sensitivity

requirements of measurement. An optical circulator is used at the output of the laser diode so that the source is connected to the fiber under test and the reflected signal is connected to the detector. An avalanche photo diode is used as the detector, and it is connected to a low noise transimpedance amplifier with high linearity. Signals covering several orders of magnitude are incident on the photo detector. This requires the receiver to have a high dynamic range together with sensitivity. A flash type Analog to Digital Converter (ADC) is used to convert the analog signal to digital. Sampling rate of ADC determines the spatial resolution. A sampling rate of 50MHz corresponds to a spatial resolution of 2m. Since the Backscattered signal is very weak, the process of sending pulses and receiving echo is repeated to improve the signal to noise ratio by averaging.

6.2.1 Dead zones

Dead zones occur when the reflected signal saturates the OTDR receiver. The receiver is slow to recover its sensitivity after saturation resulting in loss of information. If the receiver saturates due to strong signals, it will take some time to recover from this over load condition. So the measured fiber response is affected by this overload behaviour, causing a fiber segment covered by exponentially diminishing tail. The OTDRs event dead zone is the distance between the beginning of a reflection and the -1.5 dB on the falling edge of the reflection. In this experiment we have used 100 meters of fiber at the beginning as the event dead zone.

6.2.2 Sensing Principle

The spatial resolution and pulse width of the probing signal are related to each other. The spatial resolution can be single point or two-point spatial resolution. Two point spatial resolution refers to the minimum distance between two reflectors that can still be resolved by the measurement system. The single point spatial resolution refers to the accuracy for determining the location of a single reflector. In time domain reflectometry, spatial resolution is limited by the pulse width of the source. Shorter pulse width results in finer spatial resolution. The relationship between spatial resolution, ΔZ_r, and pulse width is [20]

$$\Delta Z_r = \frac{V_g}{2} \Delta t_s \qquad (6.1)$$

Δt_s is the system response time/ pulse width, v_g is the group velocity; speed of pulse along the fiber and is expressed as $v_g = c/n_g$, where 'c' is the velocity of light in vacuum and 'n_g' is the group refractive index of the medium. In equation (6.1) 'Δt_s' can be approximated as $(\tau_p^2 + \tau_r^2)^{½}$ where 'τ_p' is the optical pulse width and 'τ_r' is the response time of the receiver. This gives the dynamic response time of the measurement.

Micro bending is due to small imperfections in the geometry of the fiber caused either by manufacturing process or by mechanical stress such as pressure, tension and twist. Whereas macro bending occurs when fiber is bend to curvature with diameters of the order of centimeters. The bending reduces the angle of ray with the normal at the interface in the bent region. If the angle becomes smaller than the

critical angle, the ray leaves the core and hence loss occurs .We make use this loss in the fiber for the measurement.

The backscattered power from a distance L is given by [20]

$$P_s(L) = S.\ \alpha_s.W.\ P_0.\ e^{-2\alpha L} \quad (6.2)$$

$$P_s(L) = (NA/n_0)^2.1/m.\alpha_s.\tau v_{gr}.P_0.e^{-2\alpha L} \quad (6.3)$$

Where NA= numerical aperture

n_0= core refractive index

m = depends on refractive index profile

$$\alpha = \alpha_a + \alpha_s \quad (6.4)$$

α_a = absorption coefficient ; α_s = scattering coefficient

τ = temporal pulse duration

v_{gr} = group velocity

P_0 = launched Power

'S' is the fraction of light scattered in all directions that is captured by the fiber core and guided back to the OTDR. The backscattering capture coefficient is given by,

$$S = (NA/n_0)^2.1/m \quad (6.5)$$

$$W = \tau\, v_{gr} \quad (6.6)$$

is the length of fiber element within which light is scattered.

As the wavelength is increased the mode becomes less confined to the core. The lower confinement can lead to higher

radiation loss for bends induced in the fiber. Hence it is obvious that longer measurement wavelengths allow sensitive and easier detection of small bends.

6.3 Experimental Details

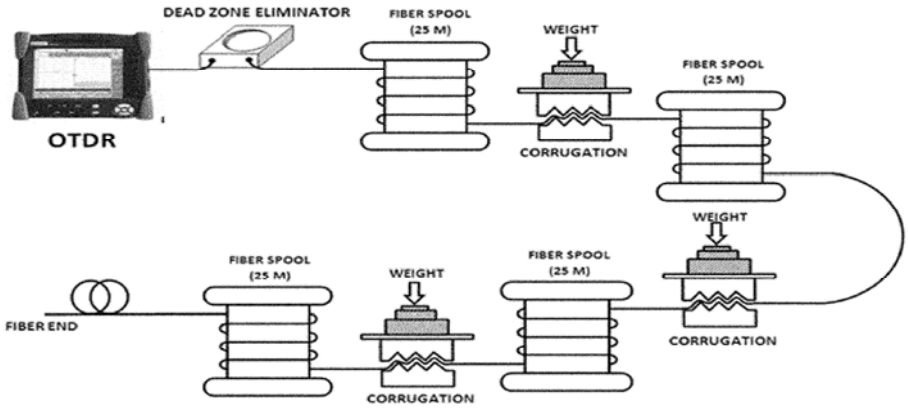

Figure 6.2 Experimental setup for Quasi Distributed sensing

The experimental set up for quasi distributed weight and displacement sensing is shown in figure 6.2. JDSU MTS 8000 OTDR is used for the reflection measurements. A dead zone eliminator with 100m fiber is used to improve the spatial resolution of the measurement. Additional 100m is wounded on four spools, leaving 2 m of fiber in between for the measurement. Single mode fiber SMF 28 is used for this purpose. Figure 6.3 shows triangular corrugations of 5mm pitch, made in aluminum block, used for introducing macro bends in the fiber. In order to ensure repeatability, proper guides and springs are provided along with the corrugations. Stainless steel springs with spring constant of 0.296 N/mm is used. Standard weights are added on the corrugations in different combinations.

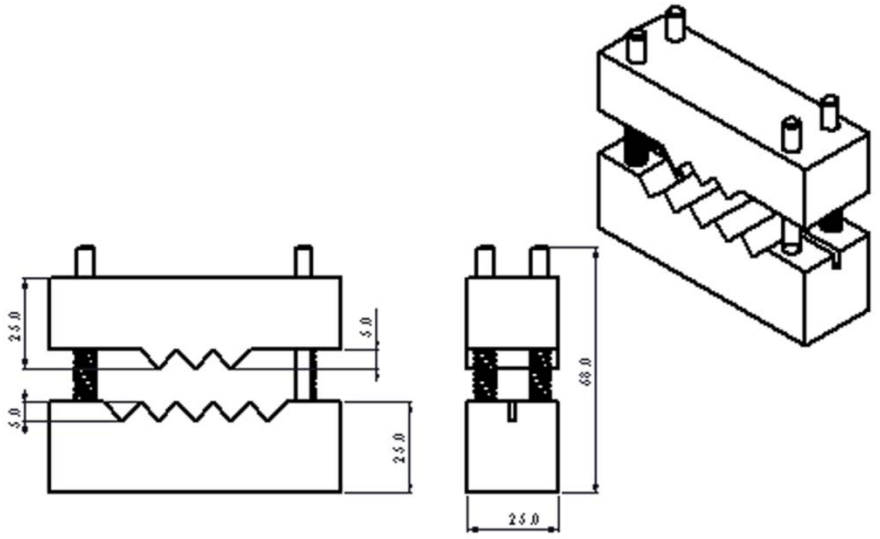

Figure 6.3 Triangular corrugations made on aluminium block (All dimensions are in 'mm'.)

Triangular corrugations having pitches of 5mm, 10mm and 15 mm are used for the measurement. Initially three numbers of 5mm pitch corrugations are used to study the distributed sensing. Other corrugations are used to evaluate the effect of number of pitch on sensing activity. So we used them as a single point sensor. Wavelength of 1550nm with a pulse width of 30 ns is used for all the measurements. 1310nm is also used for the studies to show the insensitivity of fiber loss at this wavelength. The impact due to number of corrugation on measurement is also carried out. We used aluminium blocks of 5mm pitch with 1, 2, 3 and 4 corrugations. The photograph of the experimental set up for distributed sensing is shown in figure 6.4.

Figure 6.4 Photograph of the experimental set up for the distributed sensing

6.4 Results and Discussions

Initially the measurements are carried out with single point configuration at 132 m using 5 mm pitch corrugation. The loss in the fiber due to addition of weights and corresponding displacements are measured. For the distributed measurements, corrugations of 5mm pitches are placed at 132, 157 and 172m. The sensitivity of the measurement is monitored by changing the probing wavelengths. The single point measurement is carried out to find the response of corrugations for different pitches. Finally the numbers of corrugations are also varied to find the response of the measurements. The results are detailed below.

6.4.1 Measurement at a point

Optimisation of distributed sensing is carried out by, single point measurements at 132 m of the fiber. The standard weight of 5gm is added to the triangular pitch of 5mm and the reflected trace from the OTDR is recorded. The trace of the OTDR is as shown in figure 6.5. In the graph as the weight increases the loss also increases. The reflected power (loss) in dBm Vs weight is plotted and is shown in figure 6.6, which reveals that the loss increases linearly with the applied load. The sensitivity of the measurement is found to be 0.053 dBm/g. Sensitivity and dynamic range of the sensor may be adjusted to the requirements of the measurement by properly choosing the various parameters like spring constant, pitch of the corrugation etc. From the experimental data it is also observed that as the load increases the power transmitted decreases hence the back scattered power also decreases which accounts for the oscillations in the trace data.

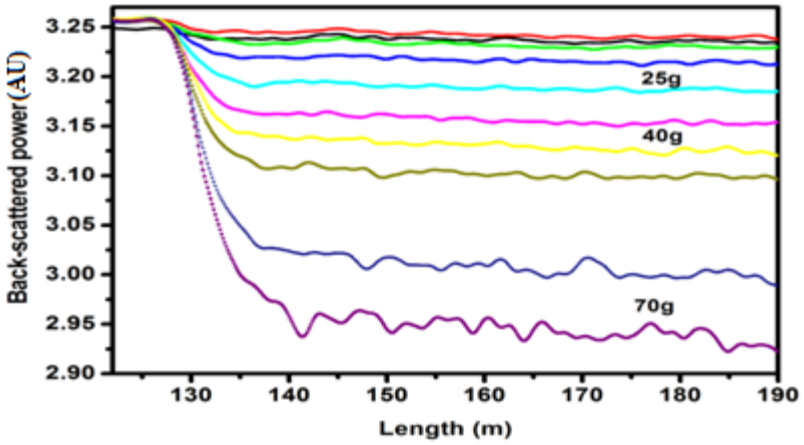

Figure 6.5 Back-scattered power due to the applied load at 132 m with 5mm pitch

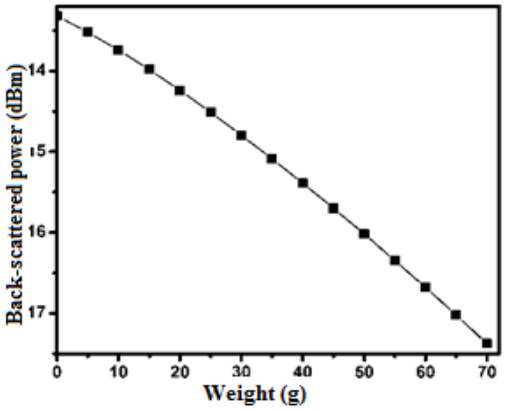

Figure 6.6 Power loss due to applied load at 132 m

In order to measure the displacement corresponding to load, a dial gauge is used. The dial gauge has a resolution of 0.002mm and can measure upto 5mm. The displacement varies linearly with applied load, as shown in figure 6.7. Therefore we can easily measure the displacement also, using the same setup.

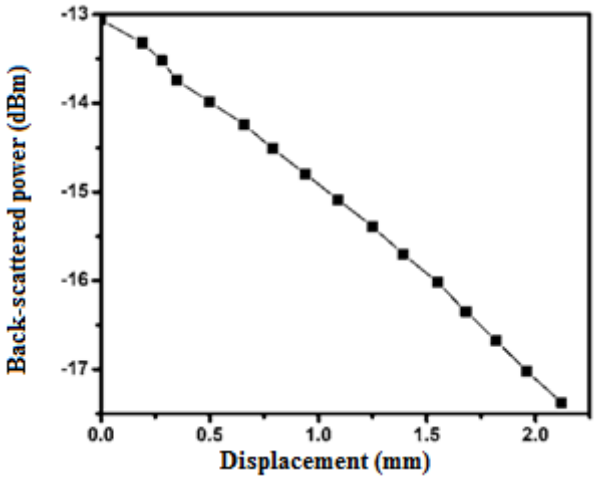

Figure 6.7 Displacement corresponding to the applied load at 132 m

6.4.2 Distributed sensing

In order to study the distributed sensing, weights are applied at three different locations (132 m, 157 m and 172 m) of the fiber using 5mm pitch corrugations. Keeping the weights on the 2nd and 3rd measurement points constant, weight on the 1st measurement point is varied. The results are shown in figure 6.8. The losses at 2nd and 3rd measurement points are also found to increase uniformly with the increase in weight at the 1st point. The variation of loss at different sensing points is as shown in figure 6.9. This is due to the fact that power transmitted to the 2nd and 3rd point decreases with the bend loss at the first point.

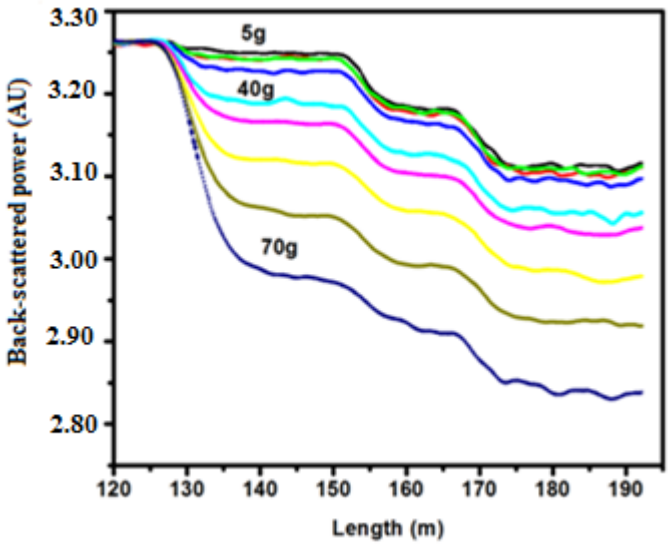

Figure 6.8 Back-scattered power due to the applied load at 1st measurement point

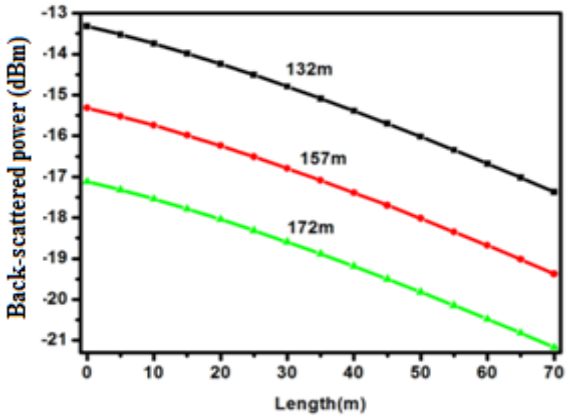

Figure 6.9. Back-scattered power at 1st, 2nd, 3rd measurement points due to the applied load at 1st point

Keeping the weights of the 1st and 3rd point constant, weight on 2nd measurement point is varied. The results are shown in figure 6.10. The loss at 1st point remains constant but the loss at 3rd measurement point is found to increase with the increase in weight at the 2nd point. This is because the transmitted power to 3rd measurement point is reduced by the loss at 2nd point.

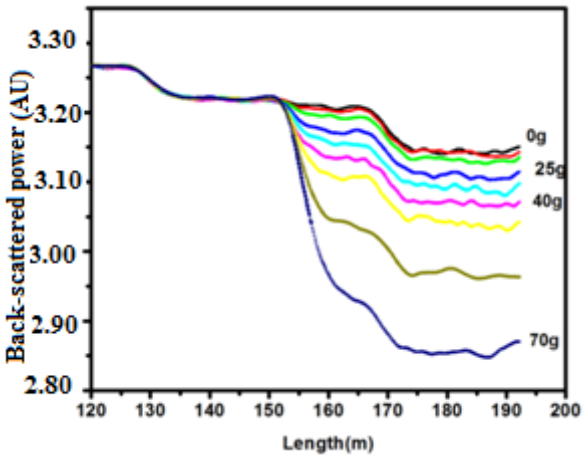

Figure 6.10. Variation of loss at 1st& 3rd measurement points due to the applied load at 2nd point

Keeping the weights of the 1st and 2nd points constant, weight on the 3rd measurement point is varied. The results are shown in figure 6.11. The loss at 1st and 2nd points remains constant and only the loss at 3rd point increases with the applied weight. Both 1st and 2nd points are unaffected by the bend at 3rd measurement point.

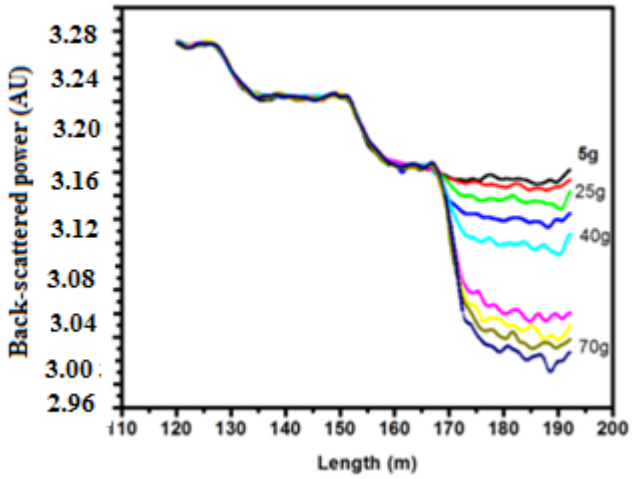

Figure 6.11. Variation of loss at 3rd measurement point due to the applied load at 3rd point.

From the above observations it is clear that the loss indicated by the OTDR at a point, includes the sum of all losses before that particular point. In order to get the loss at a particular point we have to subtract the offset loss, i.e. the total loss by the previous events, from the total indicated loss in the OTDR corresponding to that point.

6.4.3 Measurement sensitivity to wavelength

The bend sensitivity to different wavelength is shown in figure 6.12. 1550nm and 1350nm radiations are employed for the measurements under the same condition. The sensitivity at 1550 nm is far better than that at 1310nm. This is because of the fact that when the wavelength is increased, the mode becomes less confined to the core, which leads to higher losses, hence better sensitivity.

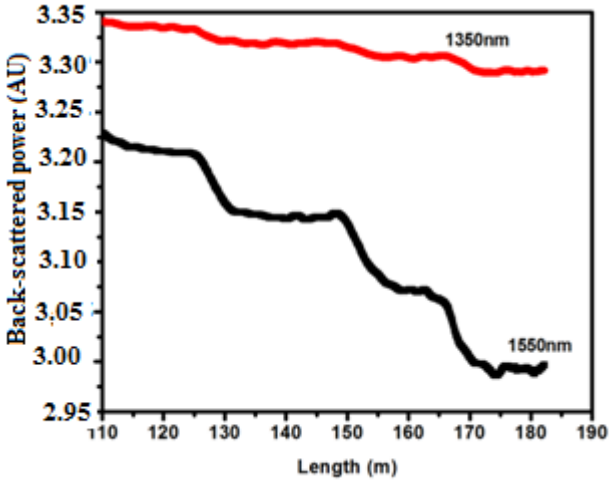

Figure 6.12 Back-scattered power with 1350nm and 1550 nm.

6.4.4 Measurement sensitivity to size of corrugation

Study of measurement sensitivity to size of corrugation is carried at 132m.Triangular corrugation of 5, 10, 15mm are used for the measurements. The reflected power for different corrugations is as shown in figure 6.13. Loss due to 5mm and 15mm pitch are comparable, where as 10 mm is more sensitive. This is because 5 mm pitch introduces less macro bend in the fiber and hence the loss is low.

The 15 mm pitch loss is more significant than that of 5mm, but less sensitive compared to 10mm because of the radius of curvature of bend introduced by the corrugation is large to introduce sufficient loss. 10 mm pitch loss is more because it is making sufficient macro bend. Corrugations with pitch less than 5mm cause damage to the fiber and hence undesirable for controlled bending in SMF 28. The sensitivities of 5 mm, 10 mm and 15 mm pitches are 0.07, 0.166, 0.078 dBm/g respectively. This shows that there is an optimum pitch which introduces the maximum loss and hence sensitivity.

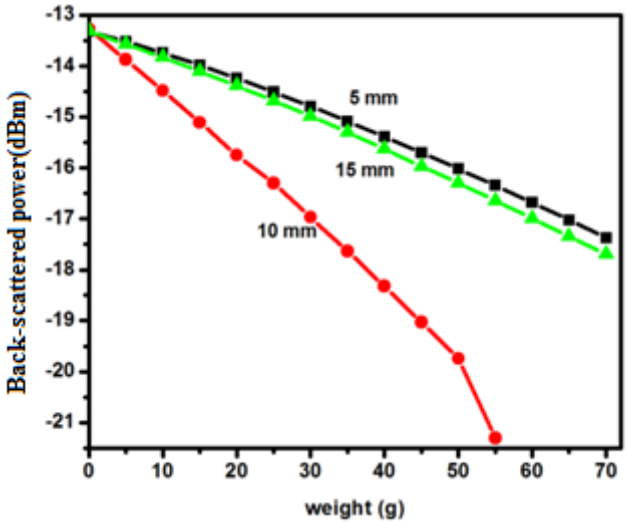

Figure 6.13. Back-scattered power with triangular pitches of 5mm, 10mm & 15mm

6.4.5 Measurement sensitivity to number of corrugations

Sensitivity to the number of corrugations is also determined by choosing 5 mm pitch corrugation. The reflected OTDR trace is observed by placing the different corrugations at 132m. Under the same conditions, the loss is plotted for different number of corrugations in the figure 6.14. The figure shows that as the number of

corrugation increases the loss also increases leading to an increase in the sensitivity of the sensor.

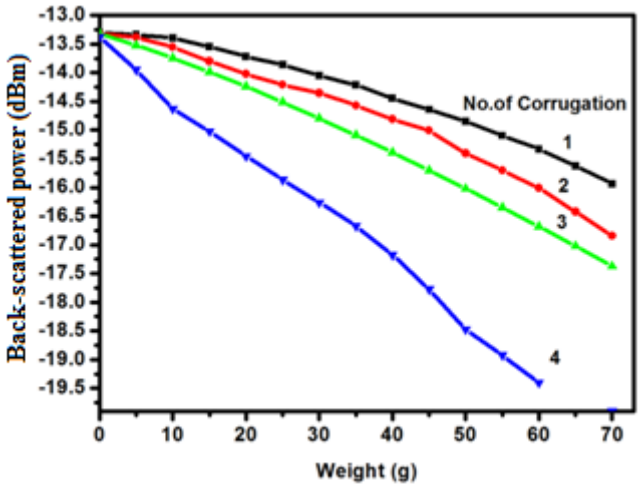

Figure 6.14 Study of variation in number of corrugations

6.5 Conclusion

The spring loaded triangular corrugation of 5mm pitch is used at a location and the loss is measured from the OTDR reflected trace. The reflected power varies linearly with the applied weight. Displacement can also be measured using the same arrangement as the displacement varies with applied weight linearly. Spring loaded triangular corrugations with a pitch of 5mm are used for distributed sensing at three points. It is observed that the loss at a particular point is transmissive and will add up with the successive events. The loss due to controlled macro bend at different point is resolvable. Hence such an arrangement can be used for the quasi distributed sensing of weight or displacement. Triangular pitches of 5mm, 10mm and 15mm are compared and found that 10mm pitch shows a sharper decrease in the reflected power and hence higher

sensitivity but decreased dynamic range. It is observed that there is a particular period/pitch of corrugation for a fiber which gives maximum sensitivity. The wavelength used is also important since it is found that 1550nm is much more sensitive than 1310nm. The power loss and sensitivity increases with number of corrugation. Using the measurement of displacement, other related parameters like velocity, strain, acceleration, pressure etc. can be derived. As it can monitor various parameters at multiple locations for a longer period of time this study find applications in the field of health monitoring of structures, remote measurements etc.

Reference

[1] Shizhuo Yin, Paul B Ruffin and Francis T.S. Yu, Fiber Optic sensors, CRC Press, New York, Ch. 1, p 24, 2008.

[2] B. D. Gupta, Fiber Optic Sensors principles and applications, New India publishing agency, New Delhi, Ch. 13, p 231, 2006.

[3] S. F. Knowles, B. E. Jones, S. Purdy and C. M. France, Multiple micro bending optical fiber sensors for the measurement of fuel quantity in air craft fuel tanks, Sensor. Actuat. A., **68**, 320, 1998.

[4] Der- Tsair Jong and Kazuo Hotate , Frequency division multiplexing of optical fiber sensors using an optical delay loop with a frequency shifter, Appl Opt., **28**, (7), 1289,1989.

[5] T. Liu and G. F. Fernando, A frequency division multiplexed low-finesse fiber optic Fabry–Perot sensor system for strain and displacement measurements, Rev. Sci. Instrum., 71, 1275, 2000.

[6] Wei Jin and Brian Culshaw, Frequency Division Multiplexing of Fiber-optic Gyroscopes, J. Lightwave Technol., **10**, 10, 1992.

[7] Luiz Carlos Guedes Valente, A. M. B. Braga, Alexandre Sant'Anna Ribeiro, Rogerio Dias Regazzi, Wolfgang Ecke,

[8] Christoph Chojetzki, and Reinhardt Willsch, Combined Time and Wavelength Multiplexing Technique of Optical Fiber Grating Sensor Arrays Using Commercial OTDR Equipment, IEEE Sens. J., **3**, 1, 2003.

[9] J. M. Senior and S. D. Cusworth, Wavelength division multiplexing in optical fibre sensor systems and networks: a review, Optic. Laser Technol., **22**, 2, 1990.

[10] Z. B. Ren and Ph. Robert, Polarization multiplexing applied to a fiber current sensor, Opt. Lett., **14**, (21), 1, 1989.

[11] Fei Luo, Jingyuan Liu, Naibing Ma and T. F. Morse, A fiber optic microbend sensor for distributed sensing application in the structural strain monitoring, Sensor. Actuat., **75**, 41, 1999.

[12] Xie Guangping, Seah Leong Keey and Anand Asundi, Optical time-domain reflectometry for distributed sensing of structural strain and deformation, Opt. Laser. Eng., **32**, 437, 2000.

[13] N. M. P. Pinto, O. Frazao, J. M. Baptista and J. L. Santos, Quasi-Distributed displacement sensor for structural monitoring using a commercial OTDR, Opt. Laser. Eng., **44**, 771**,** 2006.

[14] Tang Tian Guo, Wang Qing Yuan and Liu Hao Wu, Experimental Research on distributed fiber sensor for sliding damage monitoring, Opt. Laser. Eng., **47**, 156, 2009.

[15] Gunes Yilmaz and Sait Eser Karlik, A distributed optical fiber sensor for temperature detection in power cables, Sensor. Actuat. A., **125**, 148, 2006.

[16] Kai Tai Wan and Christopher K. Y. Leung, Applications of a distributed fiber optic crack sensor for concrete structures, Sensor. Actuat. A., **135**, 458, 2007.

[17] Chuan Li, Yi-MoZhang, Hui Liu, Sheng Wu and Cai-Wen Huang, Distributed fiber optic bidirectional strain-displacement sensor modulated by fiber bending loss, Sensor. Actuat. A., **111**, 236**,** 2004.

[18] Kazuro Kageyama, Isao Kimpara, Toshio Suzuki, Isamu Ohsawa, Hideaki Murayama and Kengo Ito, Smart marine structures: an approach to the monitoring of ship structures with fiber optic sensors, Smart Mater. Struct., **7**, 472, 1998.

[19] P. Benjamin Varghese, Satish John and K. N. Madhusoodanan, Fiber optic sensor for the measurement of concentration of silica in water with dual wavelength probing, Rev. Sci. Instrum., **81,** 035111, 2010.

[20] B. D. Gupta, Fiber Optic Sensors principles and applications, New India publishing agency, New Delhi, Ch. 13, 232, 2006.

[21] Dennis Derickson, Fiber Optic Test and measurement, Prentice Hall, New Jersey, Ch. 11, 1998.

****

Chapter 7

WAVELENGTH DIVISION MULTIPLEXED FBG SENSORS FOR THE SIMULTANEOUS MEASUREMENT OF STRAIN, WEIGHT AND TEMPERATURE

Contents

Wavelength division multiplexed quasi distributed Fiber Bragg Grating sensors for the simultaneous measurement of strain, weight and temperature is discussed in this chapter.

7.1 Introduction

FBGs have great potential for a wide range of sensing applications. They are widely used for measurements of different physical quantities like strain, temperature, pressure, flow, displacement etc. [1-6]. FBG sensors are also used in structural health monitoring [7-9]. Compared to other fiber sensors, FBG sensors have many advantages like insensitivity to fluctuations, multiplexing, distributed sensing etc. [10]. The signal obtained from a FBG sensor is encoded

directly in wavelength domain hence the source intensity fluctuations will not affect the measurements. The FBG sensors are widely used in distributed measurements of different parameters [11-14].

In the present investigation, we demonstrate a wavelength division multiplexed FBG sensor for the simultaneous measurement of strain, weight and temperature. Three FBG sensors are connected in series on a standard SMF 28 communication fiber leaving about 25 meters of fiber in between. The FBG is glued on to a cantilever structure using a fast setting epoxy for measuring strain. Standard weights are loaded on the structure for creating strain. The electrical strain gauges are also employed to monitor the strain on the structure. For mass measurement, a 2000g load cell structure is used. The FBG is pasted on the structure using a fast setting epoxy. The standard weights of 100g are added and the reflected spectrum is observed. A temperature controlled water bath is used for the measurement of temperature. The FBG is immersed in the water bath and the temperature is monitored using a digital thermometer. In order to study the temperature drift of strain, the cantilever structure is kept in a chamber and an IR lamb is used for heating. Initially the study of strain and mass are carried out at 22^0C. The study demonstrates the capability of simultaneous measurement of strain, mass and temperature. The study of drift in strain measurement at different temperatures is also carried out.

7.2 FBG sensor Multiplexing Techniques

In many applications a large numbers of sensors have to be used for distributed measurement of parameters. The FBG sensors are simple, intrinsic sensing elements that can be written to a single fiber and also the output can be monitored through a single fiber. Hence it can find many applications in distributed sensing. Both Time division multiplexing (TDM) [15, 16] and wavelength division multiplexing (WDM) [17] can be used for distributed sensing.

7.2.1 Time division multiplexing (TDM)

In time division multiplexing of FBG sensors the return pulses between the adjacent FBGs are recovered, with the two pulses separated by a distance equal to the round trip time between the gratings. Using a phase sensitive detection scheme, FBG sensors can be multiplexed using time division addressing. Pulses are launched from a broad band source into a fiber having the FBG sensor array, with different peak reflection wavelengths along the fiber length. The input pulse width has to be equal to or less than the round trip time between the two gratings. The return pulse reflections from each grating are then separated in time at the output. The reflected pulses are fed through a Mach- Zehnder interferometer that acts as the wavelength shift detector. Individual sensor pulses can be demultiplexed using an electronic circuit capable of gating out a single pulse within the pulse train signal, allowing the phase detection methods to be used to recover sensor information from each sensor channel.

7.2.2 Wavelength Division Multiplexing (WDM)

The straight forward multiplexing techniques for FBG sensors is WDM. More over it uses optical power more efficiently [18]. The WDM technique is based on the spectral slicing of an available source spectrum. Each FBG sensor is encoded with a unique wavelength along a single fiber. Since the FBGs are operating in the wavelength domain, the physical spacing between FBG sensors can be as short as desired to give accurate distributed information of measurands. FBG arrays written along a single fiber are illuminated by a broadband source and the optical signals reflected from the FBG sensor array are fed in to a wavelength detection scheme. A parallel topology is also used for connecting the sensors in WDM. A 1X N fiber power splitter and couplers are used for probing the sensors from the broad band source. More FBG sensors can lead to a larger power penalty. In the present study 3 FBGs are written on a single fiber illuminated by a broad band source. Reflected spectrum is analysed using OSA. The resonant wavelengths of FBGs are selected in such a way that they do not interfere.

7.3 Theory

Bragg wavelength shift due to temperature accounts for temperature dependence of the refractive index of silica and thermal expansion of glass. Major contribution is due to temperature dependence of the refractive index of silica. The shift in Bragg wavelength can be expressed as [19]

$$\Delta\lambda_B = [\frac{1}{\Lambda}(\frac{\delta\Lambda}{\delta T}) + \frac{1}{n}(\frac{\delta n}{\delta T})]\lambda_B \Delta T \quad (7.4)$$

The first term relates to thermal expansion of fiber and second term to the temperature dependence of refractive index.

The reflected spectrum of a FBG is given by [20].

$$R(\lambda) = R_B \exp\left[-4ln2\left(\frac{\lambda-\lambda_B}{\sigma_B}\right)^2\right] \quad (7.5)$$

where R_B is the reflectivity, σ_B is FWHM of the FBG.

The reflected spectrum from 'N' FBG sensor array is given by

$$R_n(\lambda) = R_{B0}\exp\left[-4l\,n\,2\left(\frac{\lambda-\lambda_{B0}}{\sigma_{B0}}\right)^2\right] + R_{B1}\exp\left[-4l\,n\,2\left(\frac{\lambda-\lambda_{B1}}{\sigma_{B1}}\right)^2\right] + R_{B2}\exp\left[-4l\,n\,2\left(\frac{\lambda-\lambda_{B2}}{\sigma_{B2}}\right)^2\right] + \ldots\ldots\ldots\ldots R_{BN}\exp\left[-4l\,n\,2\left(\frac{\lambda-\lambda_{BN}}{\sigma_{BN}}\right)^2\right]$$

7.4 Experimental details

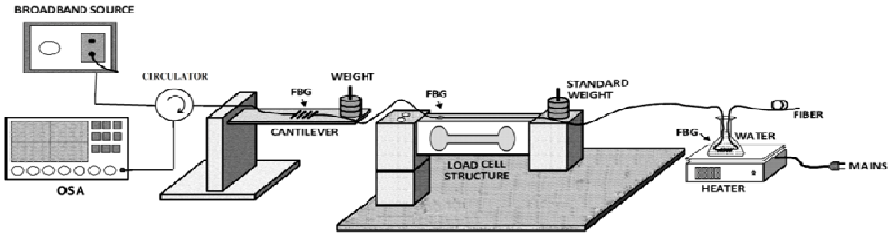

Figure 7.1 Experimental set up for distributed sensing

The experimental set-up shown in Figure 7.1 has a white light source ([Yokogawa] AQ 4305), and an optical spectrum analyzer ([Yokogawa] AQ 6319). The fiber has a diameter of 125 micron and a numerical aperture of 0.14. The core and the cladding refractive indices are 1.463 and 1.456 respectively. FBGs with center wavelengths at 1549.75nm and 1551.75nm are used for strain and weight measurements respectively. The FBG employed has a grating length of 13 mm with a reflectivity of 90%. For temperature measurement, central wavelength is 1555nm with a grating length of 10mm and reflectivity of 80%. The white light source is connected to the port 1 of circulator and port 2 of circulator is connected to the FBGs which are connected in series leaving 25m fiber in between. Port 3 of circulator is connected to OSA for the Bragg reflected signal associated with strain, weight, and temperature.

In order to study strain, a cantilever structure is made using a spring steel of 4mm thickness and length and breadth of 20cm and 5cm respectively. The FBG of 1549.75nm is pasted to the cantilever structure with a fast setting epoxy. The electrical strain gauges are also pasted to the structure for monitoring the strain. The strain is applied in the range of 0-1000μstrains. The reflected spectrum is observed for every 100μstrain. The structure is placed on a vibration- free table and sufficient time is given to avoid the loading transients. The reflected spectrum is also monitored during unloading for checking hysteresis of measurement.

For measuring weight, the FBG is pasted to a 2000g double beam cantilever load cell. The standard weights of 100g are added and the reflected spectrum is noted. In order to check the hysteresis of measurement the reflected spectrum is also observed during unloading. Temperature controlled water bath is used for measuring the temperature. The temperature is also monitored using a digital thermometer. The FBG is immersed in the water bath. The temperature is varied from 22^0C to 100^0C. The reflected spectrum is monitored for every 10^0 C rise. The water bath is allowed to cool naturally and reflected spectra are recorded to check the hysteresis of the measurement.

7.5 Results and Discussion

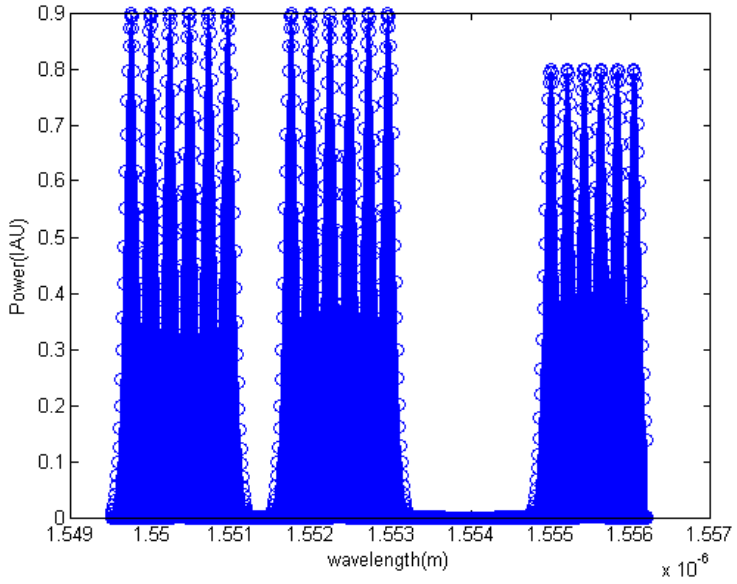

Figure7.2 Simulated Reflected spectrum of distributed sensing.

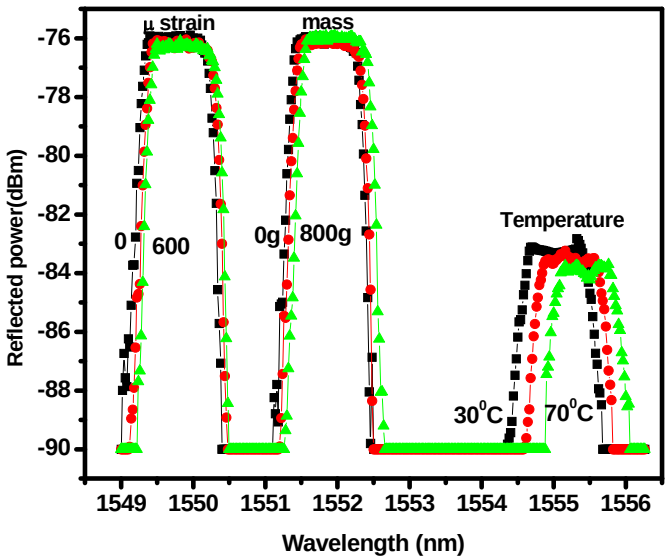

Figure 7.3 Reflected spectrum of distributed sensing

Figure 7.2 shows the reflected spectrum obtained by simulating the distributed study. The simulation was carried out with a broadband source and giving the FBG parameters discussed in section 7.5. The measured results are depicted in figure7. 3. The centre wavelengths of the FBG are selected in such a way that they do not interfere. The 1549.75nm is used for the strain measurement and 1551.75nm is employed for mass measurement. These two FBGs are identical except for the Bragg reflected wavelength as shown. The FBG with 1555nm as the centre wavelength has a reflectivity of 80%. Hence the power reflected is less. The detailed study of strain, mass and temperature are presented below.

7.5.1 Strain

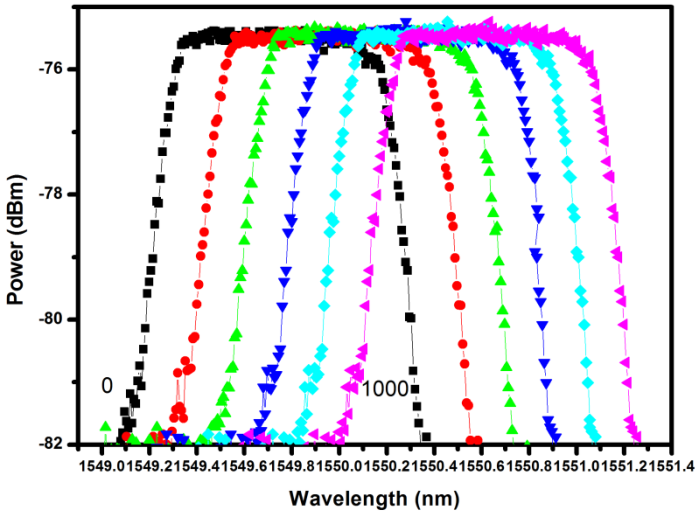

Figure 7.4 Back reflected spectrum corresponding strain measurement.

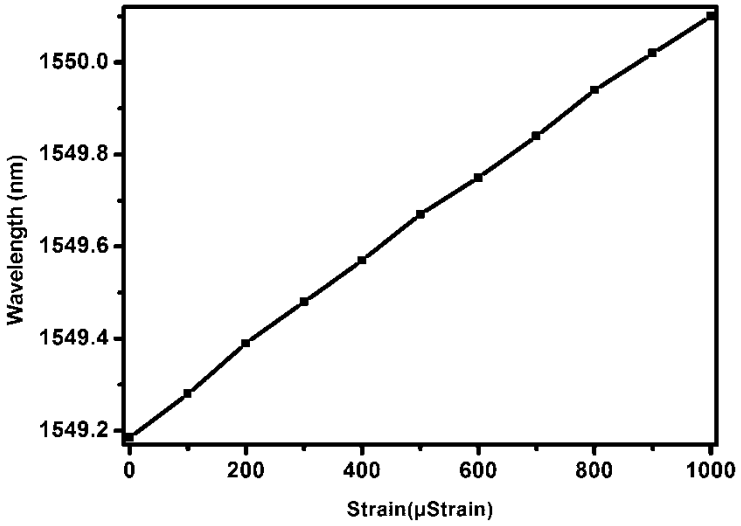

Figure 7.5 Wavelength shift for 0 to 1000μ strain

The standard weights are added to study the strain on the cantilever structure. The strain is monitored using electrical strain gauges as well. 0 to1000μstrain is applied on the structure at a step of 100μ strain

each. The temperature during the experiment is maintained at 22^0C. The reflected spectrum corresponding to strain measurement is as shown in figure 7.4. It is observed that the wavelength is shifted from1549.2nm to1551.1nm at leading edge of the reflected spectrum. The wavelength variation for 0 to 1000μstrain is plotted in figure 7.5.

7.5.2 Weight

The reflected spectrum for the weight measurement is shown in figure 7.6. Standard weights of 100 grams are added and the reflected spectrum is observed. The temperature during the experiment is maintained at 22^0C. In the reflected spectrum, the wavelength varied from1551.392nm to 1551.808nm for 0g to 2000g at the leading edge of the spectrum. The shift in wavelength with respect to mass is linear and it is plotted in figure 7.7. The reflected spectrum is monitored during the unloading of the structure and hysteresis is found negligible.

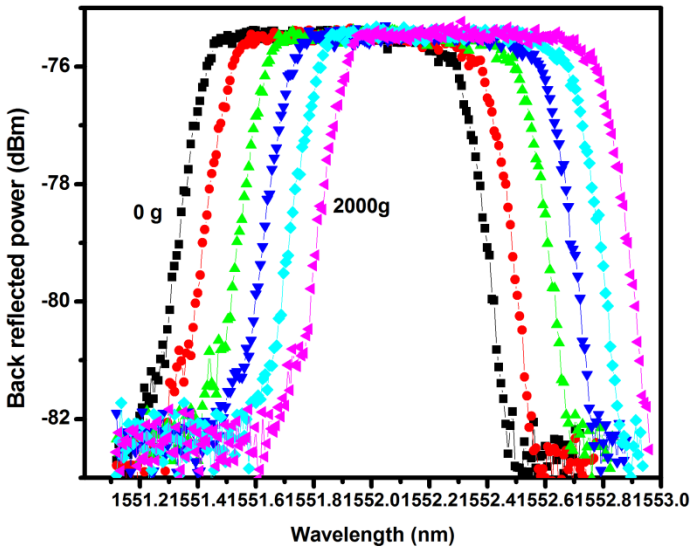

Figure 7.6 Reflected spectrum for 0 to 2000g

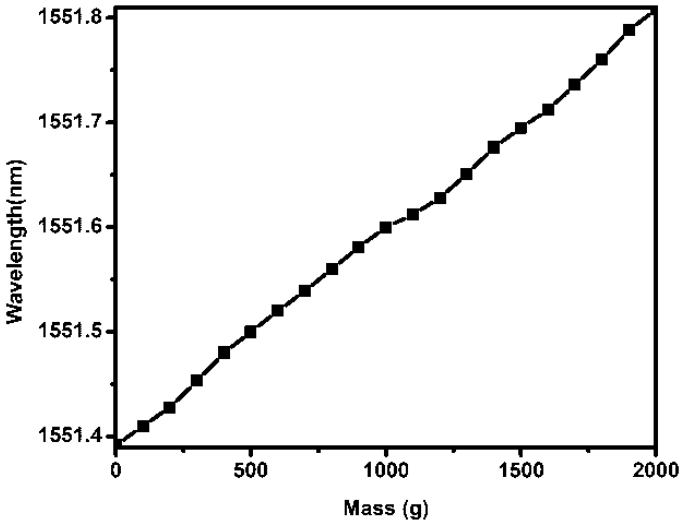

Figure 7.7 Wavelength shift for the mass 0 to 2000g

7.5.3 Temperature

For the temperature measurement, the FBG is immersed in a water bath. The temperature is controlled and varied from 22 to 100^0C. During measurement the temperature is monitored using a digital thermometer and reflected spectrum is monitored for every 10^0C rise in temperature. The reflected spectrum of FBG for 22-100^0C is shown in figure 7.8. The wavelength is shifted from 1555.416nm to 1556.106nm at the leading edge of the spectrum. The wavelength shift with respect to temperature is found linear and it is plotted in figure 7.9.

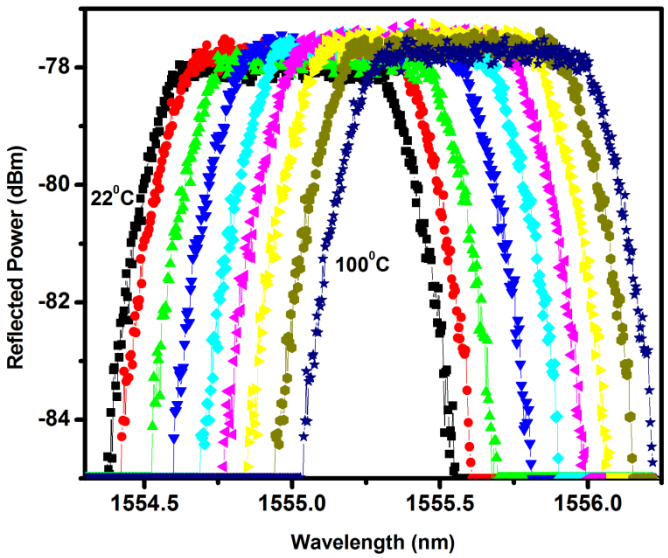

Figure 7.8 Back reflected power for 22 to 100^{0}C

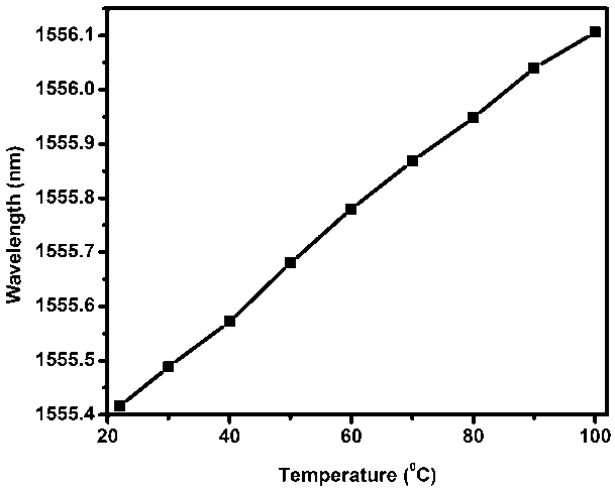

Figure 7.9 Wavelength shift for a temperature of 22 to 100^{0}C.

7.6 Conclusion

A distributed sensor capable of simultaneous measurement of strain, weight, and temperature is developed. The strain measurement

is carried out in the range of 0 to 1000 μ strains. From the reflected spectrum, wavelength shift is found linear. The sensitivity of strain measurement is 0.83 pm/μ strain. The mass measurement is carried out for 0 to 2000g at 22^0C. In the reflected spectrum, wavelength shift is found linear and free of hysteresis. The sensitivity of measurement is 0.2pm/g. The measurement of temperature is carried out from 22 to100^0C. The sensitivity is found to be 10 pm/^{0}C. The temperature sensing FBG can be used as a reference for other measurements to compensate for temperature drift.

Reference

[1] Samir K. Mondal, Umesh Tiwari, Gopal C. Poddar, Vandana Mishra, Nahar Singh, Subhash C. Jain, S. N. Sarkar, K. D. Chattoypadhya and Pawan Kapur, Single fiber Bragg grating sensor with two sections of different diameters for longitudinal strain and temperature discrimination with enhanced strain sensitivity, Rev. Sci. Instrum., **80**, 103106, 2009.

[2] Cherl-Hee Lee, Min-Kuk Kim, Kwang Tack Kim and Jonghun Lee, Enhanced temperature sensitivity of fiber Bragg grating temperature sensor using thermal expansion Of copper tube, Micro. Optic. Tech. Let., **53**, (7), 1669, 2011.

[3] Tuan Guo, Xueguang Qiao, Zhenan Jia, QidaZhao and Xiaoyi Dong, Simultaneous measurement of temperature and pressure by a single FBG with a broadened reflection spectrum, Appl. Opt., **45**, (13), 2935, 2006.

[4] I. Yong Zhao, He Huang and Qi Wang, Interrogation technique using a novel spectra bandwidth measurement method with a blazed FBG and a fiber-optic array for an FBG displacement sensor, **165,** (2), 185, 2011.

[5] Wei Liang, Yanyi Huang, Yong Xu, Reginald K Lee and Amnon Yariv, Highly sensitive fiber Bragg grating refractive index sensors, Appl. Phys. Lett., **86**, 151122, 2005

[6] Long Jin, Weigang Zhang, Jing Li, Hao Zhang, Bo Liu, Qinchang Tu, Guiyun Kai and Xiaoyi Dong, Two-dimensional bend sensing with a cantilever-mounted FBG, Meas. Sci. Technol., **17**, 168, 2006.

[7] A . Kerrouche, W. J. O. Boyle, T. Sun and K.T.V. Grattan, Design and in the field performance evaluation of compact FBG sensor system for structural health monitoring applications, Sens. Actuators A., **151**, 107, 2009.

[8] Benjamin Torres, Ignacio Paya - Zaforteza, Pedro A. Calderon and Jose M. Adam, Analysis of the strain transfer in a new FBG sensor for structural Health Monitoring, J. engstruct., **33**, 539, 2011.

[9] Shizhuo Yin, Paul B. Ruffin and Francis T. S. Yu, Fiber optic Sensors, Second edition, CRC Press Taylor & Francis Group, New York, Ch. 4, p 109, 2008.

[10] Qiang Wu, Yuliya Semenova, An Sun, Pengfei Wang and Gerald Farrell, High resolution temperature insensitive

interrogation technique for FBG sensors, Optic. Laser Technol., **42**, 4, 2010.

[11] Iacopo Toccafondo, Mohammad Taki, Alessandro Signorini, Farhan Zaidi, Tiziano Nannipieri, Stefano Faralli, and Fabrizio Di Pasquale, Hybrid Raman/fiber Bragg grating sensor for distributed temperature and discrete dynamic strain measurements, Opt. Lett., **37**, 21 , 2012.

[12] Alan D. Kersey, Michael A. Davis, Heather J. Patrick, Michel LeBlanc, K. P. Koo, C. G. Askins, M. A. Putnam, and E. Joseph Friebele, Fiber Grating Sensors, J. Lightwave Technol., **15**, 8, august 1997.

[13] Mark Froggatt and Jason Moore, Distributed measurement of static strain in an optical fiber with multiple Bragg gratings at nominally equal wavelengths, Appl. Opt., **37**, 10, 1998.

[14] George T. Kanellos, George Papaioannou, DimitrisTsiokos Christos Mitrogiannis, George Nianios and Nikos Pleros, Two dimensional polymer-embedded quasi distributed FBG pressure sensor for biomedical applications, Opt. Express, **18**, 1 2010.

[15] Yongbo Dai, Yanju Liu, Jinsong Leng, Gang Deng and Anand Asundi, A novel time-division multiplexing fiber Bragg grating sensor interrogator for structural health monitoring, Opt. Laser Eng., **47**, 1028, 2009.

[16] Bo Dong, Shiya He, Shuyang Hu, DaweiTian, Junfeng Lv, and Qida Zhao, Time-Division Multiplexing Fiber Grating

Sensor With a Tunable Pulsed Laser, IEEE Photonic. Tech. L., **18**, (24), 2006.

[17] Peng-chunpeng, Jia-he lin, Hong-yihtseng, and Sien Chi, Intensity and wavelength-division multiplexing FBG sensor system using a tunable multiport fiber ring laser, IEEE Photonic Tech. L., **16**, (1), 2004.

[18] Shizhuo Yin, Paul B Ruffin and Francis T.S. Yu, Fiber Optic sensors, CRC Press, New York, Ch. 1, p 25,2008.

[19] B. D. Gupta, Fiber optic sensors principles and applications, New India publications, New Delhi,ch.11 p 213 2006.

[20] Kuo-Chih Chuang and Chien-Ching Ma, Multidimensional Dynamic Displacement and Strain Meaurements using an intensity demodulation-based fiber-bragg grating sensing system, J. Lightwave Technol., **28**, (13), 1897, 2010.

****

Chapter 8

SUMMARY AND SCOPE FOR FURTHER STUDY

The objective of the preset work is to develop optical fiber sensors for various physical and chemical parameters. As a part of this we initially investigated trace analysis of silica, ammonia, iron and phosphate in water. For this purpose we have implemented a dual wavelength probing scheme which has many advantages over conventional evanescent wave sensors. Dual wavelength probing makes the design more reliable and repeatable and this design makes the sensor employable for concentration, chemical content, adulteration level, monitoring and control in industries or any such needy environments. Use of low cost components makes the system cost effective and simple. The Dual wavelength probing scheme is employed for the trace analysis of silica, iron, phosphate, and ammonia in water. Such sensors can be employed for the steam and water quality analysers in power plants. Few samples from a power plant are collected and checked the performance of developed system for practical applications.

Several physical parameters are measured using FBG sensors. The responses of the FBG sensor for different physical parameters are simulated with the help of MATLAB. FBG sensor is mounted to a

cantilever structure and a strain measurement is carried out for 0 to 1000 μ strain. The simulated and measured results were found matching. Reflected spectrum is measured during unloading to ensure that the measurement is free of hysteresis. The temperature measurement is carried out in a temperature controlled water bath. The water bath was allowed to cool naturally and the measurements were taken in order to ensure that the hysteresis is negligibly small.

FBG sensors require simple interrogation system in order to make measurements easier and portable. Two methods are identified for interrogating FBG sensors. In the first method FBG is probed with a narrow band source and the response of the FBG is simulated and measured. The responses were found linear but the source response is very critical in this study. In the second method the sensing FBG is probed with the output of reference FBG. The response of the interrogator is simulated and measured. Measurements and simulations are carried out for both strain and temperature sensing. It can be made temperature insensitive by using a powerful broadband source with flat spectrum in the measurement range. Using a 4pm resolution OSA it is possible to measure a minimum strain of 24μstrains and temperature of 0.1^0C at the same time with present arrangement, measurement up to 0.5 μstrain and 0 $.01^0$C is possible with a power meter resolution of 0.01dBm, provided the source power is constant. The highlights of this design are portability, cost effectiveness and better resolution and the dynamic response is also expected to be better.

Distributed sensing using a quasi-distributed fiber optic macro bend weight - displacement sensor using Optical Time Domain Reflectometer (OTDR) is realised. The weight-displacement sensing arrangement is standardized with specially made triangular corrugations with springs and guides, which give excellent repeatability. The restoring force exerted by the springs ensures non-destructive measurement. As the sensors can monitor various parameters at multiple locations for a longer period of time this study can find applications in the field of health monitoring of structures, remote measurement etc.

A wavelength division multiplexed quasi-distributed Fiber Bragg Grating sensors for the simultaneous measurement of strain, weight and temperature is also implemented. The experimental results show the capability of the proposed system to perform the simultaneous measurement of strain, weight and temperature.

Further studies can be extended to the development of evanescent wave fiber optic sensors for gas sensing and identification of coating materials for enhancing the selectivity and sensitivity of such sensors.

Interrogator for FBG sensors has to be developed as a standalone unit and performance need to be optimised. The dynamic response of the interrogator is to be investigated. Measurement of different physical and chemical quantities has to be carried out using FBG with interrogators.

****